REPUBLIQUE ALGERIENNE DEMOCRATIQUE ET POPULAIRE

MINISTERE DE L'ENSEIGNEMENT SUPERIEUR ET DE LA RECHERCHE SCIENTIFIQUE

UNIVERSITE SAAD DAHLEB DE BLIDA

Institut d'Aéronautique et des Etudes Spatiales

MEMOIRE DE FIN D'ETUDES

Pour l'Obtention du Diplôme Master en Aéronautique

Option : Propulsion

THEME :

Conception d'un Mini-Drone à Voilure Fixe

Présenté par

- KADA BENCHAIB Ali

Devant le jury composé de :

- Mr. RENANE Rachid	Président
- Mr. CHOUGRANI	Examinateur
- Mr. ABADA	Examinateur
- Mr. BENTRADE Hocine	Encadreur

Novembre 2018

PEOPLE'S DEMOCRATIC REPUBLIC OF ALGERIA

MINISTRY OF HIGHER EDUCATION AND SCIENTIFIC RESEARCH

SAÂD DAHLEB UNIVERSITY OF Blida

Institute of Aeronautics and Space Studies

MEMORY of End Studies
For the Degree Master in Aeronautics

Specialty: Propulsion

Design of Mini Unmanned Aerial Vehicle (Fixed-Wing)

<u>By</u>:
- KADA BENCHAIB Ali

<u>Supervisors</u>:
- Mr. RENANE Rachid   President
-Mr. CHOUGRANI   Examiner
-Mr.ABADA   Examiner
- Mr. BENTRADE Hocine   Advisor

November 2018

Acknowledgment

We thank Allah, the all powerful and merciful, who has given us the strength and patience to accomplish this modest work

We express our sincere thanks to all faculty members for accepting our return to the university.

We extend our gratitude to our teacher, Mr. Bentrad Hocine, to thank him for having proposed the subject and for having supervised us. His follow-up, encouragement and guidance were of great comfort and help.

From heart to heart to Hachaene Hacene, Arbia Houcem eddine and the entire aerospace clubs of Blida for their support

We also thank the president of the jury and the members of the jury for the honor they have shown us for having studied this work and judging it.

DEDICATION

I have the immense pleasure of dedicating this modest work:

To my family, to all my colleagues one by one.

_____

In memory of Dr.TAHI.Ali

<u>*Ahmed.*</u>

DEDICATION

I have the immense pleasure of dedicating this modest work:

To my little family, my whole family and all my friends.

A. Kada Benchaib

تلخيص

تتمحور رسالة التخرج هذه حول دراسة وتصميم طائرة بدون طيار من الفئة الصغيرة ذات شراع ثابت ، مهمتها حمل حمولات مختلفة من تجهيزات خاصة بالاستطلاع والاستكشاف ، تتميز هذه الطائرة بهيكل خفيف من المواد المركبة أقل من 5 كيلوغرام، زودت بحمولة قدرها 400 غرام أساسها كاميرا معدة للبث المباشر للصور والفيديوهات للمنطقة المراد إستطلاعها و بمحركين كهربائيين لدفعها وكذا عجلات كوسيلة للهبوط والاقلاع كما يمكن استبدالها بنظام اقلاع مطاطي والتقاطها اثناء الهبوط بشبكة.

كلمات مفتاحية

طائرة بدون طيار، الاستطلاع والاستكشاف، تصميم وبناء طائرة، تصميم طائرة

Abstract

This graduation thesis is on the study and approach design of a fixed-wing mini unmanned aerial vehicle, carrying various payloads of reconnaissance and exploration, with a composite layout of less than 5 kg. Equipped with a avionic system of 400 grams based on a camera designed for direct transmission of the area to be surveyed, And two electric motors to push it as well a standard landing gear with wheels is mounted can be replaced by a rubber take-off system and capture during the landing with network.

Key words:

Mini-drone, unmanned, mini UAV, Aircraft design, UAV design, airplane simulation, UAV stability and control

Résumé

Cette thèse porte sur l'étude et la démarche de conception d'un mini drone à voilure fixes, portant diverses charges utiles de reconnaissance et d'exploration, avec une structure en composite de moins de 5 kg. Un choix établi d'un système avionique de 400 grammes basé sur une caméra conçue pour la transmission directe de la zone de surveillance, ainsi que de deux moteurs électriques pour le pousser et un train d'atterrissage standard à roues peut être remplacé par un système de décollage en caoutchouc et capturer pendant l'atterrissage avec un filet.

Les mots clés :

Mini-drone, reconnaissance, étude de configuration. Conception avion

TABLE OF CONTENTS

CHAPTER I Introduction To Unmanned Aircraft

CHAPTER II Preliminary Conception and Aerodynamic Design

CHAPTER III Numerical Simulation

CHAPTER IV Performance Evaluation

GENERAL CONCLUSION
APPENDIXES
REFERENCES

LIST OF TABLES

CHAPTER III

CHAPTER IV

LIST OF FIGURES

CHAPTER III

CHAPTER IV

LIST OF SYMBOLS

Symbole	Description
A	
a	Lift curve slope
ac	Aerodynamic center
AR	Aspect ratio
AR_h	Horizontal tail aspect ratio
AR_v	Vertical tail aspect ratio
B	
b	Wing span
b_a	Aileron span
b_{ia}	Aileron inner distance
b_{oa}	Aileron outer distance
C	
C, C_w	Wing chord
$\bar{c}$, mac	Main aerodynamic chord
C_d	Drag coefficient (profile)
C_D	Drag coefficient (aircraft)
C_{D_0}	Drag coefficient (aircraft) zero lift
C_f	Friction coefficient
C_l	Lift coefficient (profile)
C_{l_α}	Lift curve slope (profile)
C_L	Lift coefficient (aircraft)
C_{L_α}	Lift curve slope (Aircraft)
C_m	Moment coefficient
C_{m_0}	Moment coefficient at zero lift
C_T	Propeller thrust coefficient
C_P	Propeller power coefficient
D	
m	masse
D	Propeller diameter
CG	Aircraft center of gravity
E	
G	
$G(s)$	Fonction de transfert de boucle ouverte
g	Gravity
H	

h_x , h_y , h_z	$\vec{h}$ Components with XYZ
I	
i	Incidence angle
i_h	Horizontal tail construction angle
I_{xx}, I_{yy}, I_{zz}	Inertial moments with XYZ
L	
L	Lift
L_h	Distance from aircraft CG to horizontal tail ac
M	
M	Mach number
N	
$\bar{q}$	Dynamic pressure
S	
S, S_w	Wing surface
S_h	Horizontal tail surface
S_v	Vertical tail surface
S_a	Aileron surface
S_e	Elevator surface
S_r	Rudder surface
T	Thrust
W	Aircraft weight
Z	
Grec	
α	Angle of attack
β	Descent angle
δ	Control surface deflection angle

LIST OF ABBREVIATION

Symbol	Description
IAES	Institut d'aéronautique et des études spatiales (institute of aeronautics and astronautics)
UAV	Unmanned aerial vehicle
UAS	Unmanned aircraft system
RPV	Remotely piloted vehicles
MTOW	Maximum takeoff weight
CAD	Computer-aided design
CFD	Computational fluid dynamic
RC	Remote control
AOA	Angle of attack
3D	Three dimensions
2D	Two dimensions
DMU	Digital mockup
CG	Center of gravity

A irplane design means the intellectual engineering process of creating on paper a flying machine to meet certain specifications and requirements, Pioneer innovative new idea and technology. **In our thesis** is preferred to design an **unmanned Aerial Vehicle.**

Developing an unmanned aerial vehicle has been one of the main points of concern by many counties all over the world; about 70 different countries have some sort of UAV technology. UAV expenditures reached more than US$ 3 billion and constituted a growth of more than 12% in 2010. Approximately 70% of global growth and market share is in the US. UAVs are used to gather information from the air in hostile areas. They can also be used in devastated areas where man support may not be available. These types of UAVs must be portable by ground and very reliable for recurrent use. With these types of uses by the military the UAVs designed are very costly and have very specific uses designed for each.

The goal for this UAV design is to provide an optional alternative to these very specific uses products. The model will be classed as **mini UAV** equipped with 400 grams unfixed avionics system package, our choice is based on a CCD camera and mainly composite UAV with a gross weight under 5 kg.

In order to decide upon a design for this UAV, certain limiting factors had to be taken into consideration, namely the payload of electronic equipment that would need to be incased and secured somewhere within the fuselage. Also by taking into account the necessary minimum flight time this plane would need to see, while carrying this payload, the possibilities were narrowed down further. After conducting a little research into the designs of commonly used UAVs and comparing their uses with those that this plane would see, it was decided that a mini unmanned aerial carrier design would be used. Being that this aircraft would need to see at least fifteen minutes of flight time seemed like the most feasible option.

A very interesting use of CAD software to catch the different similar UAVs components size and parameters has been prepared. Simulation of the configuration is a method to extract and confirm the results; furthermore, performance capacity of the design is estimated also.

Chapter I

Introduction to unmanned aircraft

Chapter II

Preliminary Conception And Aerodynamic Design
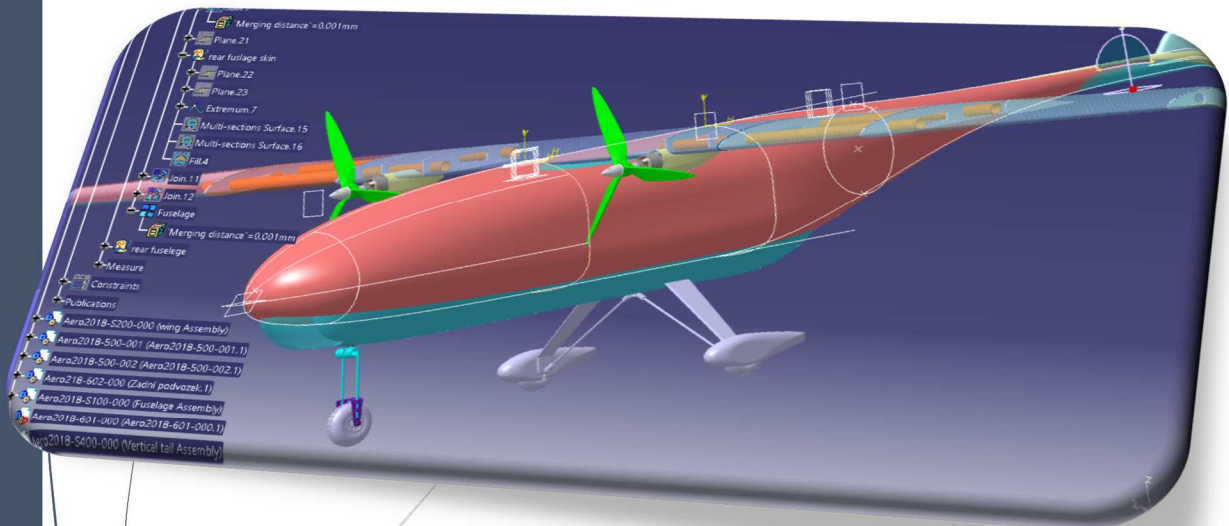
Chapter III

Numerical Simulation
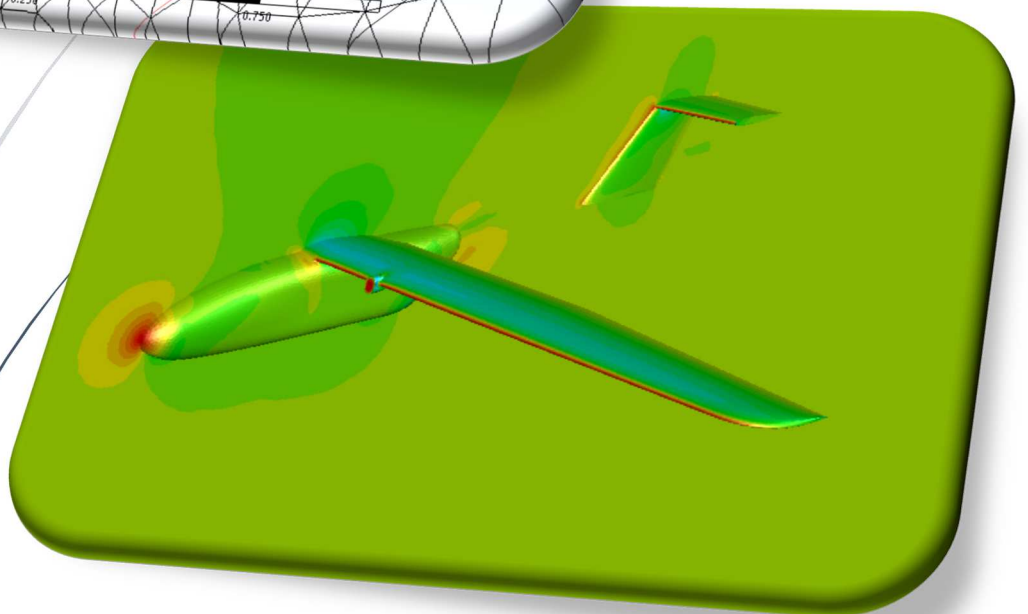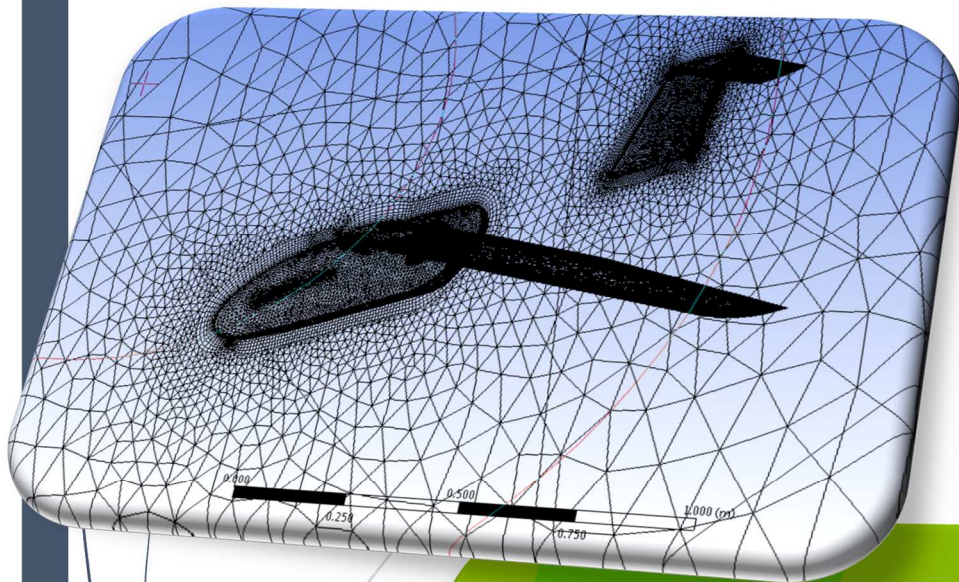
Chapter IV

Performance Evaluation

I.   INTRODUCTION

The unmanned aerial vehicle (UAV) is a remotely piloted or self-piloted aircraft that can carry cameras, sensors, communications equipment or other payloads. The most of the world's modern armed forces are recognizing the tremendous advantage of using UAV in military operations. UAV is easier to build and less expensive to acquire than manned vehicles.

Since many names have been to describe unmanned aircraft, this chapter begins with an overview of these terms and their raison as well. It then continues with some other commonly used over time, concluding with a list of some applications that are in use in the field [5].

II.   AVIATION HISTORY AND UNMANNED FLIGHT

There are many who believe that UAVs are a recent invention going back at most two or three decades, unmanned flight has a rich history that goes back all the way to ancient times. Of course, the first systems that can qualify with the modern definition of UAVs are quite recent and mainly involve the reconnaissance drones developed and deployed during the cold war. Today, UAV systems have evolved and expanded into widely different designs like quadrotors, ducted fan, and blimps [5].

II.1   Precursors of Flight and Unmanned Aircraft:

In modern times, manned aviation appeared in the late 1700s, and it took another century for heavier than air machines to take to the skies. Unmanned aircraft followed soon after the advent of the airplane, appearing around the time of the First World War (1916). However, the idea of building "flying machines" was first conceived close to 2,500 years ago, in ancient Greece and China Pythagoras, Archimedes, and others studied the use of autonomous mechanisms for a variety of applications. The first known autonomous flying machine has been credited to Archytas from the city of Tarantas or Tarentum in South Italy, known as Archytas the Tarantine. Archytas has been referred to as Leonardo da Vinci of the ancient World and was also the father of number one in number theory (Valavanis et al. 2007) and the solution for doubling the cube. He was also possibly the first engineer, designing and building various mechanisms. In 425 BC he built a mechanical bird, which he called "the pigeon" [5].

During the same era in a different part of the Ancient World – China – at about 400 BC, the Chinese were the first to document the idea of a vertical flight aircraft. The earliest version of the Chinese top consisted of feathers at the end of a stick. The stick was spun between the hands to generate enough lift before released into free flight. Over the years, the Chinese experimented with other types of flying machines such as hot air balloons, rockets, or kites [5].
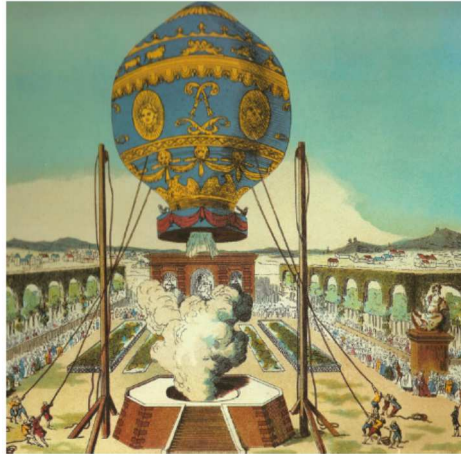
Figure I. 1 The first manned flight using a hot air balloon

II.2   Around Wright brothers historical flight:

1916, less than 15 years after the Wright brothers historical flight, the first modern unmanned aircraft was demonstrated. It was the Hewitt–Sperry Automatic Airplane, named after the two inventors that designed it. This aircraft could not have become a reality without the previous work of Sperry on gyroscopic devices that were needed to provide flight stabilization. Sperry managed to attract the interest of the U.S [5].

Navy resulting in the development of the Curtiss–Sperry Aerial Torpedo, while at the same time the U.S. Army Air Force sponsored the Liberty Eagle Aerial Torpedo of Charles Kettering shown in (**Figure. I.2**) (Zaloga 2008) [5].

**Figure I. 2 The USAF Liberty Eagle Aerial Torpedo, also known as
the Kettering Bug after**

In Britain, experiments with unmanned aircraft took place throughout the 1920s with the RAE 1921 Target. In 1933, the Royal Navy used the Queen Bee target drone for the first time (Newcome 2004) [5].

II.3   The Machines of the ColdWar:

Soon after the end of WWII, interest in reconnaissance missions increased. The descendants of Reginald Denny's target drones became the basis of the first reconnaissance drone, the SD-1 (Newcome 2004). Also known as the MQM-57 Falconer, it was developed in the mid-1950s, and by the end of its career, close to 1,500 had been built (National Museum of the USAF 2009). The SD-1 (**Figure.I.3**) was remotely operated, carried a camera, and after a 30min flight returned to base and was recovered with parachute (Zaloga 2008) [5].

The USAF supported the Ryan Model 147 drone that evolved into a series of models with different capabilities (**figure I.4**). In fact, modernized versions of this drone are still being built and used to carry out missions to this day [5].

Figure I. 3 The SD-1, also known as the MQM-57 Falconer   **Figure I. 4 AQM-34Q (the Ryan Model 147)**

II.4   Modern Systems:

Modern systems are much more diverse than their precursors. Although one can readily identify the heritage of the reconnaissance drones in the popular Pioneer (Figure. I.5) of the 1980s or the French-built SPERWER (Figure. I.6), we have moved towards larger, more capable, and higher endurance systems like the RQ-4 Global Hawk (Figure. I.7). Systems that can take multiple roles are also available like the MQ-9 Reaper (Fig.I.8), which besides reconnaissance can also be used as a hunterkiller, and the Neptune that is used for water operations [5].

Although some of the aforementioned UAVs like the MQ-9 Reaper can be armed, there is now an entire class of systems being developed with combat operations as their primary mission, known as Unmanned Combat Aircraft Systems (UCAS) [5].

Figure I. 5 An RQ-2 Pioneer

Figure I. 6 The French SPERWER

Figure I. 7 The RQ-4 Global Hawk

Figure I. 8 The MQ-9 Reaper

Although many of these systems are still in experimental stages, there are several that are already operational. Examples of UCAS include the Neuron, the Barracuda, the Italian Sky-X the MiG Skat, and the BAE Mantis. Almost all of the aforementioned systems utilize a fixed-wing design. However, there is a number of helicopter UAVs available, several of which are currently operational in military and civil applications. Some examples of helicopter UAVs [5].

Figure I. 9 The A-160 Hummingbird

Figure I. 10 The MQ-8 Fire Scout

Small UAVs have also garnered significant interest, especially since they are considered by many as entry points to the civilian market. Although their smaller size invariably leads to reduced payload capacities, a large number of small and miniature UAVs are in operation or active development [5].

Figure I. 11 The WASP is a MAV

Figure I. 12 The Raven

In addition to the popular fixed-wing and helicopter systems, other designs are also used for UAVs (**Figure. I.11**). These include duct-fan design (e.g., the iStar MAV, the Sikorsky Cypher, and the SELEX Galileo Spyball), counterrotating rotors (e.g., the IT-180 and the KOAX X-240), as well as mixed designs like the Eagle Eye (**Figure. I.12**) that combine some of the advantages of fixed-wing and helicopter designs. Finally, the CyberQuad and the AirRobot AR 100-B (**Figure. I.13**) are both examples of the quad-rotor design that is especially popular in academic environments [5].

Figure I. 13 The Sikorksy Cypher

Figure I. 14 The Eagle Eye

Figure I. 15 The AirRobot AR 100-B

Figure I. 16 The Persistent Threat Detection System (PTDS)

III.   UAV or UAS ?

Several names have already been used to describe unmanned aircraft. UAVs became UAS, the preferred term used by the Federal Aviation Administration (FAA). Other names included Remotely Piloted Vehicles (RPVs), a term that was used in the Vietnam War. Today the USAF has mainly substituted RPV for Remotely Piloted aircraft or RPA, a term used to include both the aircraft and the pilot, while the United Kingdom has designated them as Remotely Piloted Air System (RPAS), to demonstrate the presence of the man in the loop to control them [5].

An unmanned aerial vehicle (also known as a drone) refers to a pilotless aircraft, a flying machine without an onboard human pilot or passengers. As such, "unmanned" implies total absence of a human who directs and actively pilots the aircraft. Control functions for unmanned aircraft may be either onboard or off-board (remote control) [5].

The term UAV or unmanned aerial vehicle has been used for several years to describe unmanned aerial systems. Various definitions have been proposed for this term, like a reusable aircraft designed to operate without an onboard pilot. It does not carry passengers and can be either remotely piloted or preprogrammed to fly autonomously [5].

In the definition above, the characterization reusable is used to differentiate unmanned aircraft from guided weapons and other munition delivery systems. [5]

A few years ago, the U.S. Department of Defense (DoD), followed by the FAA and the European Aviation Safety Agency (EASA), adopted the term UAS or Unmanned Aircraft System. This was meant to signify that UAS are aircraft and as such airworthiness will need to be demonstrated, and they are also systems consisting of ground control stations, communication links, and launch and retrieval systems in addition to the aircraft itself [5].

In practice, UAS and UAV are often used interchangeably, and only when the system aspect is important (mainly for legal/regulatory reasons) does UAS have preference [5].

IV.   UAV CLASSIFICATION

There is a large number of metrics that have been used for UAV classification, including mean takeoff weight (MTOW), size, operating conditions, capabilities, or any combination of these and other characteristics. It should be noted that while some of these metrics have minimal effect on the safety performance requirements of the system, they are still important from an operational, commercial, legal, and possibly other points of view. Rather than an exhaustive list which would be of little value, this section presents characteristic examples of different types of classifications from the literature [5].

A comprehensive classification of UAV demonstrating both the wide variety of UAV systems and capabilities as well as the multiple dimensions of differentiation is presented in **Table I.1**.

Table I. 1 NATO UAV classification guide from the Sep. 2009 JCGUAV meeting [5]

Class	Category	Normal operating altitude	Normal mission radius	Example platforms
Class I (less than 150 kg)	Small > 20 kg	Up to 5,000 ft AGL	50 km (LOS)	Luna, Hermes 90
	Mini 2–20 kg	Up to 3,000 ft AGL	25 km (LOS)	Scan Eagle, Skylark, Raven, DH3, Aladin, Strix
	Micro < 2 kg	Up to 200 ft AGL	5 km (LOS)	Black Widow
Class II (150–600 kg)	Tactical	Up to 10,000 ft AGL	200 km (LOS)	Sperwer, Iview 250, Hermes 450, Aerostar, Ranger
Class III (>600 kg)	Strike combat	Up to 65,000 ft AGL	Unlimited (BLOS)	
	HALE	Up to 65,000 ft AGL	Unlimited (BLOS)	Global Hawk
	MALE	Up to 45,000 ft AGL	Unlimited (BLOS)	Predator B, Predator A, Heron, Heron TP, Hermes 900

IV.1 Classification Based on MTOW :

MTOW is a good metric to classify aircraft for regulatory purposes since it correlates well. A simple classification scheme based on MTOW is presented in **Table I.2**; this scheme also shows the expected range and maximum operating altitude of the UAVs of each class which is also a function of MTOW [5].

Table I. 1 Classification of UAVs based on MTOW [5]

Class	MTOW (kg)	Range category	Typical max altitude (ft)
0	≤25	Close range	1,000 ft
1	25–500	Short range	15,000 ft
2	501–2,000	Medium range	30,000 ft
3	>2,000	Long range	Above 30,000 ft

IV.2 Classification Based on Operational Altitude and Midair Collision Risk

Although MTOW provides a good basis to classify aircraft based on the risk they present to people and property after a ground impact, UAV classes based on altitude may also be of interest since they will dictate to a degree collision avoidance

requirements (see Zeitlin 2009). A simple classification was proposed in Dalamagkidis et al. (2012) and is outlined below and presented in **Table I.3**: [5]

1. *Very low altitude (VLA/LOS)* operating in Class G airspace and typically in altitudes less than 400–500 ft with the operator always in visual contact with the aircraft.
2. *Very low altitude (VLA/BLOS)* as above but with the possibility that the aircraft is flown beyond the line of sight of the operator.
3. ***Medium altitude (MA)*** operating in Class A through E airspace.
4. *Very high altitude (VHA)* operating in Class E airspace above FL600.

Table I. 2 Proposed classification based on class of airspace used [5]

Class	Airspace class	S&A	Transponder	2-way ATC communication
VLA/LOS	Class G	Not required	Not required	Not required[a]
VLA/BLOS	Class G	Required[b]	Required[b]	Not required[a]
MA	Class A–E	Required	Required	Required
MA/A	Class A	Required[b]	Required	Required
VHA	Above Fl600	Required[b]	Required	Required[b]
[a]Communication with ATC before operation may still be required				
[b]May be waived for certain types of operations or under certain conditions				

IV.3   Classification Based on Autonomy:

Another way to categorize UAVs that is also of interest for certification purposes is based on their level of autonomy. Already UAVs are exhibiting autonomy in certain functions, and this trend is expected to increase, especially if one pilot is to control more than one aircraft at the same time, a possibility discussed in Protti and Barzan (2007). In 2005 the autonomous control levels (ACL) were proposed to measure autonomy. More specifically, ten (10) such levels were proposed in Clough (2002a) that were based on requirements like situational awareness, analysis, coordination, decision making, and operational capability. A list of the ACL is presented in **Table I.4** [5].

Table I. 3 Autonomous control levels (Source: Clough (2002a)) [5]

ACL	Level descriptor
0	Remotely piloted vehicle
1	Execute preplanned mission
2	Changeable mission
3	Robust response to real-time faults/events
4	Fault/event adaptive vehicle
5	Real-time multi-vehicle coordination
6	Real-time multi-vehicle cooperation
7	Battlespace knowledge
8	Battlespace cognizance
9	Battlespace swarm cognizance
10	Fully autonomous

IV.4   Military Classifications:

There are several military UAV classifications in use. The NATO JCGUAV presented in September of 2009 a classification guide based on MTOW; see **Table I.5** [5]

All UAVs are divided into three classes: **Class I** for those weighing less than 150 kg, **Class II** for those in the range 150–600 kg, and **Class III** for those over 600 kg. More information can be found in The Joint Air Force Competence Centre (2010). Class I is subdivided into small (20–150 kg), mini (2–20 kg), and micro. Class III is also subdivided but based on the operational role of the UAV [5].

The JUAV CoE has defined its own categories that depend on the operational characteristics and other UAV attributes. These categories include tactical, operational, and strategic UAV that have different scope and operate under different commands (U.S. Department of Defense, Office of the Secretary of Defense 2007) [5].

Table I. 5 UAV categorization for differentiation of existing systems [5]

	Mass (kg)	Range (km)	Flight alt. (m)	Endurance (h)
Micro	<5	<10	250	1
Mini	<20/25/30/150[a]	<10	150/250/300	<2
Tactical				
Close range (CR)	25–150	10–30	3,000	2–4
Short range (SR)	50–250	30–70	3,000	3–6
Medium range (MR)	150–500	70–200	5,000	6–10
MR endurance (MRE)	500–1,500	>500	8,000	10–18
Low altitude deep penetration (LADP)	250–2,500	>250	50–9,000	0.5–1
Low altitude long endurance (LALE)	15–25	>500	3,000	>24
Medium altitude long endurance (MALE)	1,000–1,500	>500	3,000	24–48
Strategic				
High altitude long endurance (HALE)	2,500–5,000	>2,000	20,000	24–48
Stratospheric (Strato)	>2,500	>2,000	>20,000	>48
Exo-stratospheric (EXO)	TBD	TBD	>30,500	TBD
Special task				
Unmanned combat AV (UCAV)	>1,000	1,500	12,000	2
Lethal (LET)	TBD	300	4,000	3–4
Decoys (DEC)	150–250	0–500	50–5,000	<4

[a]Varies with national legal restrictions

IV.5   Classification Based on Ownership

Finally UAVs – like other aircrafts – can be categorized based on their ownership as *public* or *state* when they are owned and operated by public entities like federal agencies or local law enforcement and *civil* when they are owned by industry or private parties; see Hempe (2006) [5].

V.   AN INTERESTING CIVILIAN UAVS APPLICATIONS

V.1   Survey of Unmanned Aerial Vehicles (UAVs) for Traffic Monitoring:

UAVs applied on surveying the traffic monitoring and management. Although there is voluminous research on the subject, UAVs are proven to be a viable and less time consuming alternative to real-time traffic monitoring and management as they provide the dynamic "eye-in-the-sky" solution to the problem[5].

V.2   Cooperative Unmanned Aerial Systems for Fire Detection, Monitoring, and Extinguishing:

UAVs have a big interesting employment to forest fires cooperative. It presents a decision and control architecture for multi-UAS teams that are equipped with diverse sensors (e.g., infrared and visual cameras) and details the perception techniques (fire segmentation, geo-localization, and data fusion) that are used toward fire extinguishing [5].

V.3   Measurement and Exploration in Volcanic Environments:

A challenging application for UAVs in volcanic environments, as they may be used to collect typical aerial measurements and data, the main forms of measurements concern the collection of visual/thermal images and gas analysis and sampling. An overview of the major worldwide projects carried out in the last few years by several research organizations is summarized and discussed [5].

V.4   Load Transportation, Deployment, and Aerial Manipulation:

A novel and very challenging applications of using UAVs for aerial manipulation and load transportation, has a specific application of using autonomous helicopters equipped with robotic arms for aerial manipulation is detailed, along with field experiments demonstrating joint load transportation with multiple autonomous helicopters [5].

V.5   Unmanned Aircraft Systems for Maritime Operations:

Technological trends are highlighted focusing on developments relevant to maritime UAS operations, Trends including miniaturization of sensors and computer systems, high energy density of power sources, and increased subsystem standardization and modularity will have important effects in the future, including increased system autonomy via new command and control frameworks [5].

V.6   Autonomous Remote Sensing of Invasive Species from Robotic Aircraft:

A number of environmental research experiments focused on autonomous remote sensing, detection, classification, and management of invasive species, weeds, in Australia. In these experiments, three distinct families of weeds on three different

terrains are investigated. In the first group of experiments, a helicopter UAV equipped with a high-resolution imaging payload is flown over difficult to reach water channels and wetlands for detection of aquatic weeds. The second set of experiments is performed in relatively flat rangelands to map woody infestations. The third set of experiments is focused on the airborne detection of wheel cacti on remote mountainous terrain using fixed-wing aircrafts. Successful results of these experiments suggest that robotic aircrafts in a properly designed UAS can play an important role in environmental robotic science [5].

V.7   Cyber-Physical Systems Enabled by Small Unmanned Aerial Vehicles:

A several examples of unmanned aircraft sensing-enabled cyber-physical system (CPS) scenarios, enabling adaptive management and effective control of complex physical systems such as water distribution based on measurement of soil moisture and crop evapotranspiration, radio tag-based tracking of fish, alternative energy harvesting, mapping of invasive plant species, and airborne plume (pollution) tracking [5].

I.   SCOPE

This chapter contains the design of an air vehicle that can carry a surveillance payload for a specific mission. The design process includes sizing and aerodynamic overall layout configuration. The choice of the aerial vehicle is inspired from the wide range of mini UAV class, where the skywalker is a leading enterprise in this field.

The skywalker technology Co.,Ltd enterprise focuses on development and innovation of aeromodelling aircraft. It has a series of model aircrafts such as Skywalker Titan, Skywalker X8 and Skywalker EVE-2000. The latter model has the main inspiration of our design.

Skywalker EVE-2000		Skywalker Titan		Skywalker E-2000	
Wing span	2240mm	Wing span	2160mm	Wing span	2030mm
Fuselage length	1270mm	Fuselage length	1230mm	Fuselage length	1120mm
Wing area	49dm²	Wing area	52.5dm²	Wing area	48dm²
Flying weight	3000~4500g	Flying weight	4500~6000g	Flying weight	2500~3000g
Material	imported EPO	Material	imported EPO	Material	imported EPO

Figure II. 1 Skywalker professional Aerial Carrier [S4]

II.   DESIRED MAIN SPECIFICATIONS OF THE UAV

The mission requirements supervise the design of a mini unmanned air vehicle (mini UAV) based on the classification illustrated in *chapter I table I.1,* the table below shows a general specifications of the aircraft model after typical UAVs consideration.

Table II. 1 Aircraft specifications

	Specifications
Designated task	Mini unmanned aerial vehicle (mini UAV)
Payload	Total aircraft weight < 5 kg with camera and data logger
Takeoff	Runway takeoff or rubber bands launch
Recovery	Runway landing or Recovery with a flexible wire network
Altitude and cruise speed	300m; 50-70km/h
Range	Range of 5 km radius base
Operation time	Sufficient time to get the range limit and at least 10 min loitering

III.   DATA COLLECTION

The collected data about these UAV systems is divided into the following tables: **Table II.2** UAVs Performance, **Table II.3** UAV Specifications, **TableII.4** UAV Flight requirement [3].

Table II. 2 UAVs performance [3]

sn	UAV Systems	Endurance (hour)	Range (km)	Ceiling (m)	Service alitude (m)	Cruise speed (km/hr)	Loiter Speed (km/hr)	Maximum Speed (km/hr)
1	RAVEN	1.50 ÷ 1.80	10	426	30 ÷ 152	-	20	57
2	DRAGON EYE	1	5	152	30 ÷ 152	35	-	35
3	PUMA	4	10	152	30 ÷ 152	-	25	50
4	SWIFT	1.25	10	150	30 ÷ 150	-	32	82
5	POINTER	1.5	-	-	-	-	35	80
6	JAVELIN	2	-	300	300	-	32	80
7	EVOLUTION	1.5	-	-	-	48	-	65
8	AZIMUT	2	50	1500	300	50	36	120
9	BIODRONE	2.17	50	1500	300	60	36	120
10	ALADIN	1	5	150	150	-	45	90
11	ORBITER	1.5	15	4500	-	120	46	140

Table II. 3 UAV Specifications [3]

sn	UAV Systems	WEIGHT			GEOMETRY		PROPULSION SYSTEM
		Launch (kg)	Payload (kg)	Empty (kg)	Wing Span (m)	UAV Length (m)	
1	RAVEN	1.9	0.18	1.72	1.4	0.9	Electric
2	DRAGON	2.7	-	-	1.1	0.9	Electric
3	PUMA	5.5	-	-	2.6	1.8	Electric
4	SWIFT	2.8	0.18	2.62	1.1	0.9	Electric
5	POINTER	4.54	0.91	3.63	2.75	1.83	Electric
6	JAVELIN	6.8			2.44	1.83	Gasoline
7	EVOLUTION	3.72	0.68	3.04	1.64	0.98	Electric
8	AZIMUT	9	1.2	7.8	2.9	1.82	Electric
9	BIODRONE	12	1.2	10.8	3.4	1.8	Electric
10	ALADIN	3.2	-	-	1.46	1.53	Electric
11	ORBITER	6.5	1.5	5	2.2	1	Electric

Table II. 4 UAV Flight requirements [3]

sn	UAV Systems	Launch	flight Modes		Navigation	
			Manual	Autonomous	Autopilot	GPS
1	RAVEN	Hand	Yes	Yes	-	-
2	DRAGON EYE	Hand, Bungee	Yes	Yes	-	-
3	PUMA	Hand	Yes	-	-	-
4	SWIFT	Hand, Bungee	Yes	Yes	-	-
5	POINTER	Hand	Yes	Yes	Yes	Yes
6	JAVELIN	Hand	Yes	-	-	-
7	EVOLUTION	Hand, Bungee	Yes	Yes	Yes	Yes
8	AZIMUT	Hand, Catapult	Yes	-	Three Axes	-
9	BIODRONE	Hand, Catapult	Yes	Yes	Three Axes	Yes
10	ALADIN	Hand, Bungee	Yes	-	Yes	-
11	ORBITER	Hand, Bungee	Yes	-		

IV.   MISSION ANALYSIS

The mission requirements enable us to define the desired UAV typical mission, which is broken down into a number of different phases as shown in the figure bellow:
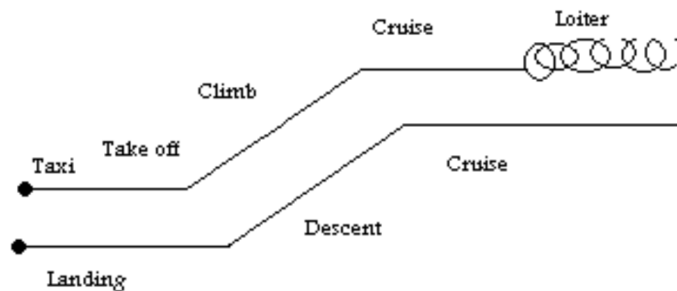
Figure II. 2 Mission Profile

The mission phases are defined as:

Phase 1: Engine start and warm up **(Taxi)**.

Phase 2: Launch by rubber band or to let the UAV run on ground **(takeoff)**.

Phase 3: Climb to the cruise altitude (300 m) **(Climb)**.

Phase 4: Cruise to the desired altitude (300 m) with cruise speed (50 - 70km/h) to the target area or to the area required for reconnaissance **(Cruise)**.

Phase 5: Loiter over the target area or to the area required **(Loiter)**.

Phase 6: Cruise back to the launch area **(Cruise)**.

Phase 7: Descent of the air vehicle from the cruise altitude to the level of the operator **(Descent)**.

Phase 8: Landing and engine shut down at a suitable altitude and place **(Landing)**.

V.   UAV SIZING AND OVERALL LAYOUT

V.1.   Configuration choice:

After reviewing the technological environment; an analysis was prepared at this level and a decision was made about the configuration choice as summarized in the table below based on the skywalker EVE-2000 and similar mini UAVs.

Table II. 5 Mini UAV configuration

N.	Attribute	UAV
1	Materials	Mainly composite
2	Manufacture	Modular
3	Engine type	Electrical engine
4	Landing gear type	tricycle
5	Fixed or retractable	fixed
6	Engine location	Under wing
7	Number of engine	2
8	Wing location	High wing
9	Tail configuration	T-tail configuration
10	Wing configuration	Cranked wing

Recently, the composite materials have become more popular in the aviation industry. Making the whole UAV out of composite materials may not be the best choice for sunny weather, since ultra-violet radiation deteriorates properties of resin matrix. Using a combination of composite materials, wood and epoxy would be the most attractive option, as the composites are needed to lower the overall weight of the aircraft, while composite airframe give to our mini UAV sufficient strength and rigidity and great life cycle.

Double outrunner RC motors are selected as an initial choice similarly to skywalker Aerial Carrier **figure II.1**. This choice provides a large variety on-the-shelf motors and battery adaptation from 3S batteries to 6S batteries. Furthermore, it offers more flexibility to the design.

High mounted wing provides more stability and enough space to install motors under the wing for our mini UAV model [2]. A cranked wing has a similar shape to elliptical wing and a large wing aspect ratio for better performance as well. This will be explained in detail later. The tail adopted is T-tail, because it moves the horizontal tail faraway from wing down wash and motor wind disturbance in comparison with V-tail configuration demands a complex control system, therefore, it is discarded.

V.2.   <u>Weight Estimation:</u>

To define the total weight of the mini UAV a kit of avionics system is chosen with a weight of around 400 grams to do the mission task, the first estimation of battery weight was selected upon of the similar mini UAV and configuration layout choice (motors number).

The empty weight was established based on the previous design on the institute work experience. Finally, it's adjusted in the detail design using CAD software based on the internal structure weight defined.

Mini UAV weight distribution, $W_T = W_{avioncs} + W_{battery} + W_{propulsion} + W_{empty}$, it shows all components and weights for our mini UAV. The table below regroups the different elements of weight [10].

Table II. 6 Mini UAV Weight estimation

Component	N°	Part name	Number	Weight (grams)	Total weight (grams)
Overall layout	01	Fuselage	1	700	2206.8
	02	Wing (right)	1	550	
	03	Wing (left)	1	550	
	04	Wing connector	2	60	
	05	Wing screw	4	6.8	
	06	Vertical tail unit	1	120	
	07	Horizontal tail unit	1	120	
	08	Assembly glue	1	40	
	09	Landing gear	1	60	
Control and propulsion system	01	Motor	2	248	407
	02	Controller (ESC)	2	78	
	03	Propeller	2	46	
	04	Propeller hub	2	35	
	05	Elevator servo	1	19	
	06	Aileron servo (flat)	2	38	
	07	Rudder servo	1	19	
Battery	01	Battery (4S) or (6S)	2 or 1	1386	1386
Avionics	01	Pitot tube	1	10	395.8
	02	Kestrel autopilot	1	55	
	03	Furuno GPS	1	18	
	04	500 line CCD camera	1	61	
	06	380 line CCD camera	1	30.5	
	08	Aerocomm modem	1	20	
	07	Modem antenna	1	9	
	09	6v regulator	1	19	
	10	Autopilot wire bundle	1	8	
	11	Camera switching device	1	9	
	12	1200mA autopilot battery	1	74	
	13	250mW Video transmitter	1	19.3	
	14	Canon recorder	1	30	
	15	Video overlay device	1	33	
				TOTAL	**4471.6 grams**

V.3.   Airfoil Selection:

An initial phase in the design of the aircraft model involved selecting an appropriate airfoil shape which would be adequate enough to act as the main lifting shape of the plane. It's thought very early on that the chosen airfoil must show **acceptable data at low speeds** as well as possessing a **moderate camber** and a **thickness to chord ratio** [07] .The figure II.3 represents four candidates airfoils Clark Y, Eppler E 374, NACA 2411 and Selig S 7075.
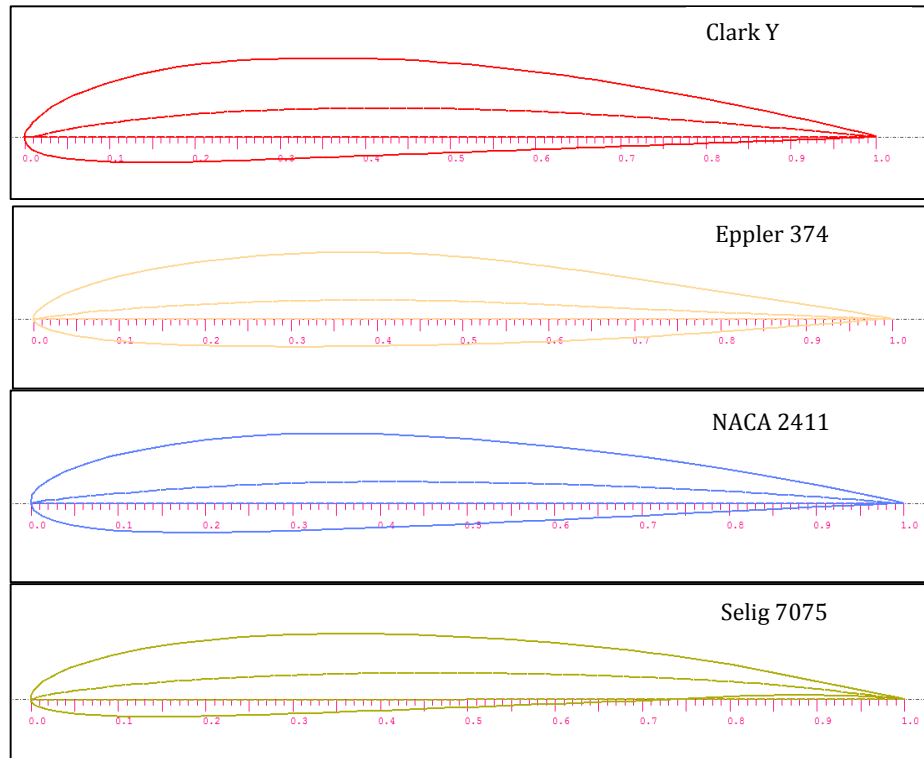
Figure II. 3 Candidates Airfoils sections

The selected airfoil also had to allow the aircraft to meet the required lift coefficients as well as having the lowest penalty on the overall drag as possible [07].

XfLR5 software is used in order to test a range of two dimensional airfoil sections in an attempt to find one which matched all of the design requirements. A group of useful airfoils was shortlisted at the initial phase, a decision making process will be done after analysis.

Such airfoils were not randomly selected out of the XfLR5 analysis but were rather handpicked **based on their geometry**. It is decided that the bottom of the airfoil was to be as **flat as possible and has sufficient thickness** in order to make fabrication of the wing easier. Also the airfoils were chosen based on the high maximum lift to drag ratio coefficient requirements predicted for the aircraft.

The figure below describes a sensitive analysis of the change of Reynolds number with change of the two mains proprieties, the length represents the chord of the UAV model taken from $20cm$ to $30cm$ and the flight velocity from $50km/h = 13.89m/s$ to $60km/h = 16.67m/s$. Reynolds number is changed between 200 000 and 270 000, a Reynolds number around 250000 is selected to analyzed the airfoils.

$$Re = \frac{\rho\, U\, L}{\mu} \tag{II.1}$$

Where

$\rho = 1.1901\,[\text{kg/m}^3]$: Air density at 300m

$\mu = 1.819\,10^{-5}\,\left[\dfrac{\text{kg}}{\text{m s}}\right]$: Viscosity at 300m
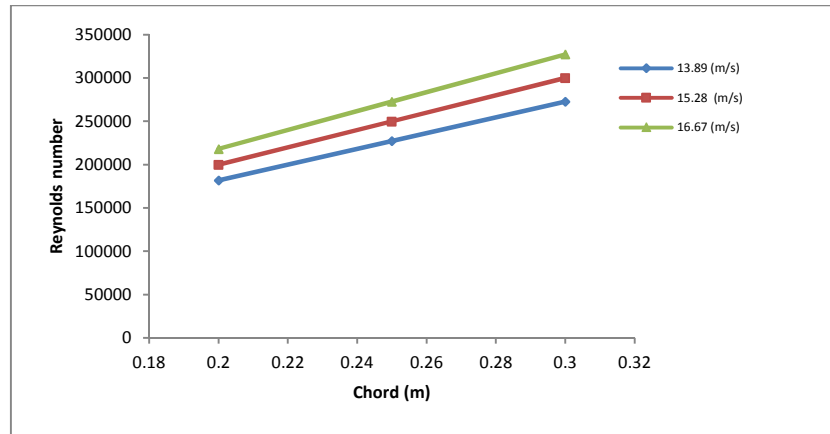
Figure II. 4 Estimation of flight Reynolds number

The Reynolds number which is about 250000 results from the expected flight velocities and wing chords.

Lift and drag coefficient curve versus AOA (Alpha):
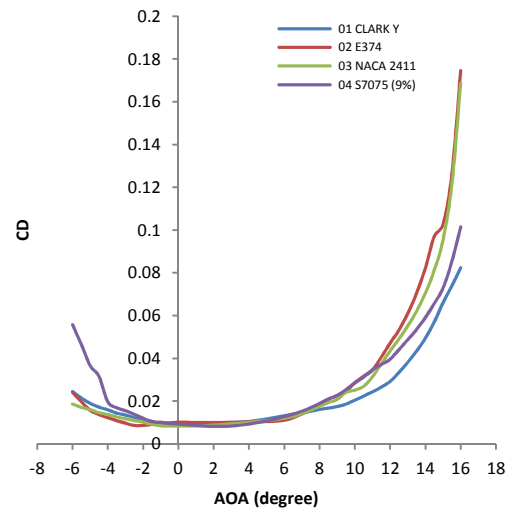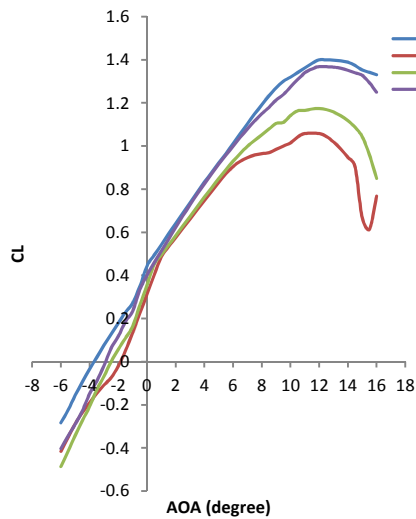
Figure II. 5 Lift coefficient vs AOA (XFLR 5)   **Figure II. 6 Drag coefficient vs AOA (XFLR 5)**

Lift to drag ratio curves represented in the following figures:
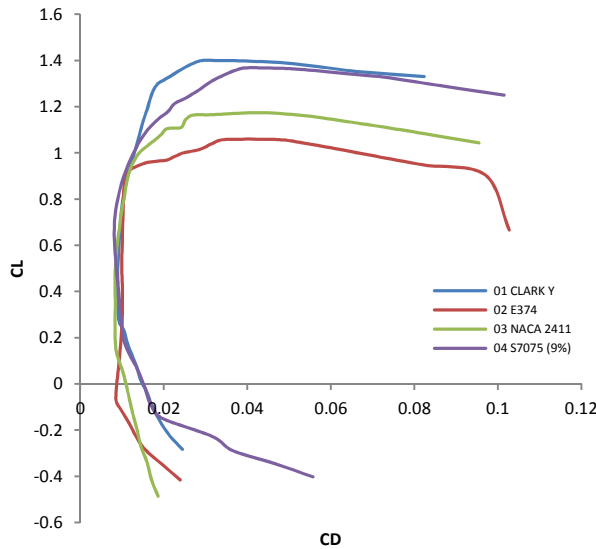
Figure II. 7 Lift to drag ratio curve
(XFLR 5)
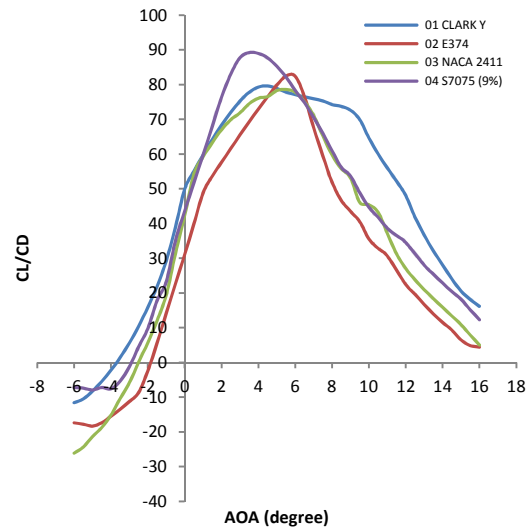
Figure II. 8 Lift to drag ratio vs AOA
(XFLR 5)

The table II.7 below describes each airfoil in terms of its useful properties.

Table II. 7 Candidates airfoils

Airfoil	CL_{max}	$\alpha_{max}(°)$	CL/CD @ α_{max}	CD_{min} @ $\alpha = 5°$	t_{max}
Clark Y	**1.40**	**12**	**78.5**	0.0115	**11.71%@29%c**
EPPELER 374	1.06	12.0	58.72	**0.0104**	11.73%@30.8%c
NACA 2411	1.17	12.0	30	0.0108	12% @30.9%c
S7075	**1.36**	**13.5**	**86**	**0.0107**	**9% @30.1%c**

After considering the original airfoils carefully, the S7075 and Clark Y have important reasonable properties, the Clark Y has more thickness than S7075 which insure a space for structural design.

Clark Y was preferred, because have best aerodynamic performance.

From simulation at XFL5 software of Clark Y airfoil between a Reynolds number about 100 000 to 220000 is tolerable, regarding the small chord and low velocity conditions of mini UAVs.
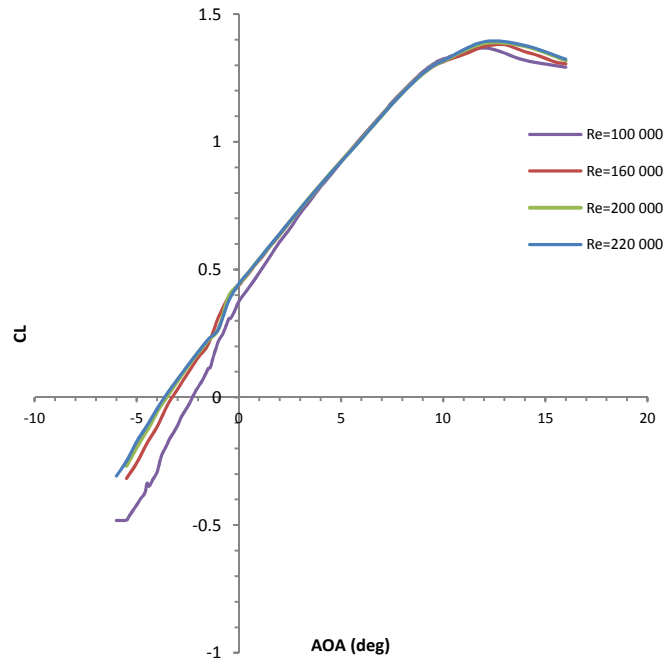
Figure II. 9 Lift coefficient vs AOA curve of Clark Y

(XFLR5 software)

The Clark Y airfoil wind tunnel test data curves realized by J.Robertson confirm the maximum and tendency of the lift coefficient curve, this is a Clark Y (B) lift coefficient at Re=200000 and 300000 additional Reynolds number test in [Ref.12].
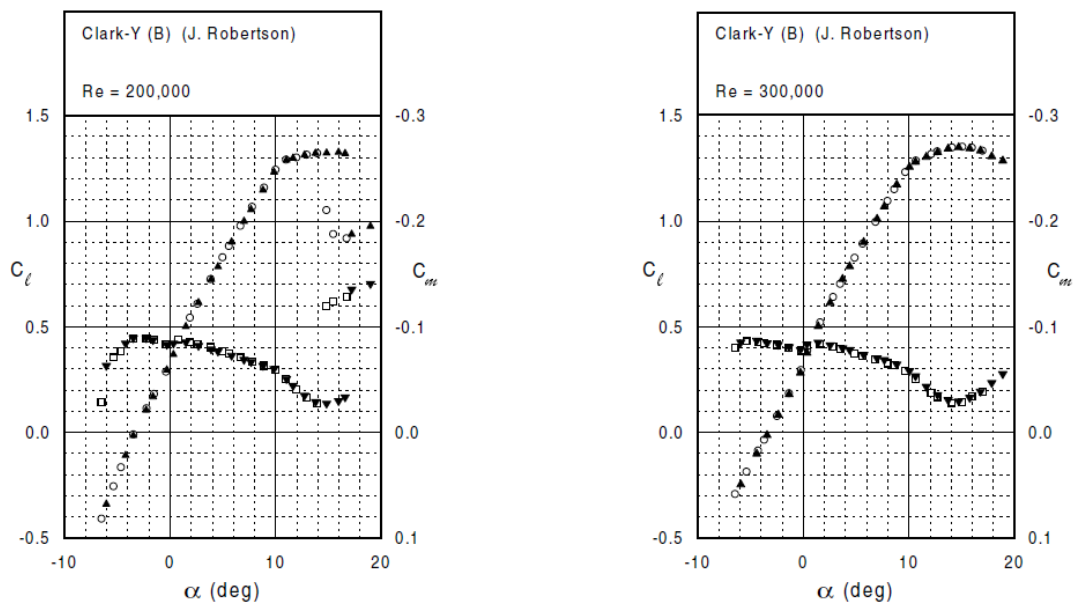
Figure II. 10 Lift coefficient vs AOA curve of Clark Y (B)

(J.Robertson) [Ref.12]

V.4.   Wing planform design:

Let's start with this table of wing planform advantages and disadvantages from [Ref.11]

Table II. 8 Wing profile categories

Profile	Advantages	Disadvantages
Elliptical	1. Lowest induced drag 2. Stalls evenly across spans	1. Difficult to fabricate
Rectangular	1. Constant Re reduces risk of tip stall 2. Easy to fabricate	1. Higher induced drag 2. Higher bending moments
Tapered	1. Lower induced drag than rectangular planform 2. Smaller bending moment	1. Risk of tip stall
Combined Rect. & tapered	1. Approach advantages of elliptical 2. Easier to fabricate	1. Hazards of tip stall remains

From table the wing was selected to be combined (rectangular and tapered) called cranked wing for better performance benefit with no sweep, dihedral or twist. A high wing had already been selected for roll stability therefore dihedral was unnecessary due to manufacturing complexity and the stability benefits from sweep were also not required.

A cranked wing would help us to gain a better value for Oswald's span efficiency factor e, which would reduce the drag due to lift. The positive effect gained of cranked wing was accepted.

It was common knowledge amongst the designer teams that our configuration would generate excess drag in the air due to fixed landing gear. The larger aspect ratio reduced the induced drag and the design team hoped this could offset some of the extra parasite drag created from our configuration.

A value of $C_{l_{max}} = 1.35$ from airfoil curve can be extract as a maximum airfoil lift coefficient designated by small "l" from figure II.10.

So $C_{L_{max}}$ air vehicle (3D mini UAV) designated with "L" is less than $C_{l_{max}}$ airfoil (2D), the maximum aircraft lift coefficient develops from maximum airfoil lift coefficient multiplied 0.9 to get max lift coefficient of wing, multiplied by 0.95 to get maximum complete aircraft lift coefficient $C_{L_{max}}$ shown in the Eq. II. 1

$$C_{L_{max}} = C_{l_{max}} \times 0.9 \times 0.95 \tag{II.2}$$

$$C_{L_{max}} = 1.35 \times 0.9 \times 0.95 = 1.15 \tag{II.3}$$

In the next Simulation chapter this value of $C_{L_{max}} = 1.15$ need to be checked in the curve of (C_L vs AOA)

Let's now find the wing loading $W/_S$ from

$$W = \frac{1}{2}\rho\, S\, V_{Stall}{}^2 C_{L_{max}} \tag{II.4}$$

From (Eq. II.4):

$$W/_S = \frac{1}{2}\rho V_{Stall}{}^2 C_{L_{max}}$$ (II.5)

The weight of aircraft is about 4500 grams now, the table below regroups three UAVs has a weight around our design

Table II. 9 Typical mini UAVs weight consideration

Mini UAV	Weight (grams)	Span b (mm)	Surface (dm²)	wing loading (g/dm²)
C-ASTRAL BARMOR	4500	2300	67	67.16
SKYWALKER EVE-2000	4500	2240	49	91.84
POINTER FQM-151A	4120	2740	72.16	57.10

If this mini UAVs flights with our airfoil Calrk Y with $C_{L_{max}} = 1.15$ result at sea level, what's the flying velocity of this mini UAVs?

$$V = \sqrt{\frac{W}{\frac{1}{2}\rho S\ C_{L_{max}}}}$$ (II.6)

A sensitive analysis will be done and resumed in these three tables:

Table II. 10 C-astral barmor lift coefficient sensitive analysis

	$C_{l_{max}}$	$S(m^2)$	$W\ (grams)$	$\rho\ (kg/m^3)$	$V\ (m/s)$
	1	67	4500	1.225	10.366
	1.1	67	4500	1.225	9.884
C-ASTRAL BARMOR	1.15	67	4500	1.225	9.667
	1.2	67	4500	1.225	9.463
	1.3	67	4500	1.225	9.092
	1.4	67	4500	1.225	8.761

Table II. 11 Skywalker EVE-2000 lift coefficient sensitive analysis

	$C_{l_{max}}$	$S(m^2)$	$W\ (grams)$	$\rho\ (kg/m^3)$	$V\ (m/s)$
	1	49	4500	1.225	12.122
	1.1	49	4500	1.225	11.558
SKYWALKER EVE-2000	1.15	49	4500	1.225	11.304
	1.2	49	4500	1.225	11.067
	1.3	49	4500	1.225	10.636
	1.4	49	4500	1.225	10.249

Table II. 12 Pointer FQM-151A lift coefficient sensitive analysis

	$C_{l_{max}}$	$S(m^2)$	$W\ (grams)$	$\rho\ (kg/m^3)$	$V\ (m/s)$
	1	72.16	4120	1.225	9.558
	1.1	72.16	4120	1.225	9.113
POINTER FQM-151A	1.15	72.16	4120	1.225	8.913
	1.2	72.16	4120	1.225	8.725
	1.3	72.16	4120	1.225	8.383
	1.4	72.16	4120	1.225	8.078

From this sensitive study the small value of the lift coefficient of these mini UAVs $C_{L_{max}} = 1$ gives **12.122 m/s** flying velocity, the largest value of these mini UAVs $C_{L_{max}} = 1.4$ gives **8.078 m/s** flying velocity.

The different $C_{L_{max}}$ bring to mind different airfoils selection, our selection is Clark Y airfoil with $C_{L_{max}} = 1.15$, imagine this airfoil was installed on these mini UAVs the velocities obtained are the stall speed of each aircraft which are resumed in this table:

Table II. 13 Typical mini UAVs velocities at $C_{L_{max}} = 1.15$

	$C_{l_{max}}$	S(m²)	W/S (g/dm²)	V $_{Stall}$(m/s)
SKYWALKER EVE-2000	1.15	49	91.84	11.304
C-ASTRAL BARMOR	1.15	67	67.16	9.667
POINTER FQM-151A	1.15	72.16	57.10	8.913

The Skywalker EVE-2000 and C-astral barmor have 4500 grams takeoff weight and a Stall velocity range [11.304 to 9.667] with our airfoil $C_{l_{max}}$ calculated before, any Stall velocity in this range is acceptable as a first estimation at sea level.

Exanimate these Stall velocities range to see the adequate surface area using these two flowing equations.

$$W/S = \frac{1}{2} \rho \, C_{L_{max}} V_{stall}^2 \tag{II.7}$$

$$S = \frac{\frac{1}{2} \rho \, C_{L_{max}} V_{stall}^2}{W} \tag{II.8}$$

Table II. 14 Stall speeds iterations versus candidate surface area

V $_{Stall}$(m/s)	$C_{l_{max}}$	W/S (g/dm²)	S(m²)	
11.304	1.15	91.84	49.00	Same surface as Sky EVE-2000
11	1.15	86.90	51.80	V $_{Stall}$ ↓; S ↑
10.5	1.15	79.20	56.85	V $_{Stall}$ ↓; S ↑
10.4	1.15	77.70	57.90	V $_{Stall}$ ↓; S ↑
10	1.15	71.80	62.67	V $_{Stall}$ ↓; S ↑
9.667	1.15	67.16	67.06	Same surface as C-astral barmor

A compromise between lower stall velocity limit and surface area should be done, large surface area remind us to a heavy wing structure and more cost, a 57.90 m² surface area value refers to V $_{Stall}$ = 10.40 m/s and W/S = 77.70(g/dm²) is acceptable.

A very light aircraft (VLA) that is certified with EASA3 may not have a stall speed greater than 45 knot = 23.15 m/s and it's the lowest speed certification; our result V_{stall} = 10.40 m/s is acceptable.

$$V_s \leq 61 \; knot \; (FAR \; 23) \tag{II.9}$$

$$V_s \leq 45 \; knot \; (EASA \; CS - VLA) \tag{II.10}$$

Table II. 15 Reference area parameters results

Take-off weight $(grams)$	4500
$C_{L_{max}}$	1.15
Density $(^{kg}/_{m^3})$	Sea level(1.225)
Wing loading $(^{g}/_{dm^2})$	77.7
Wing area (dm^2)	57.90

After the wing area calculation determines the others wing parameters (Span, Chord and Aspect ratio(AR)) bring up a simple calculation of mini UAVs.

An assumption that the wing of these mini UAVs is rectangular, the wings chords can be determined.

$$c = {S}/{b} \tag{II.11}$$

$$AR = {b^2}/{S} \tag{II.12}$$

Table II. 16 Mini UAVs wing parameters estimation

	$Span \; (mm)$	$S(dm^2)$	$Chord(mm)$	$Aspect \; ratio \; (AR)$
SKYWALKER EVE-2000	2240	49	218.75	10.240
POINTER FQM-151A	2740	72.16	263.36	10.404
C-ASTRAL BARMOR	2300	67	291.30	7.896

Using XFLR-5 V39 Software to design the wing planform, starting with 250mm near to Pointer FQM root chord to get an aspect ratio more than 10 with a no swept wing from leading edge, based on the table above and an approximate geometrical study compare to an elliptical wing as shown in figure below.

The wing split place (the section divided the wing to a rectangular part and tapered part) was chosen as follow:

- The arrangement for transportation using a backpack.
- The middle part can carry enough space for fuselage placement and the two motors with propellers.
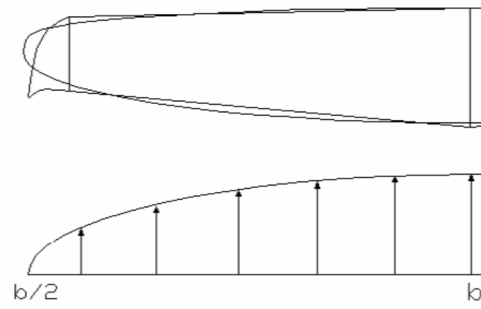
Figure II. 11 Approximate wing geometry to elliptical one [Ref.11]

To identify the others parameters like main aerodynamic chord and split position from rectangular sections to tapered wing sections and wing tip chord, with respect of smooth wing tip was done using XFLR5 software, a first appreciation of aerodynamic results was obtained. Our model will be simulated with ANSYS Fluent this why it will interest to this last software to analyze the aerodynamic results in the next chapter.
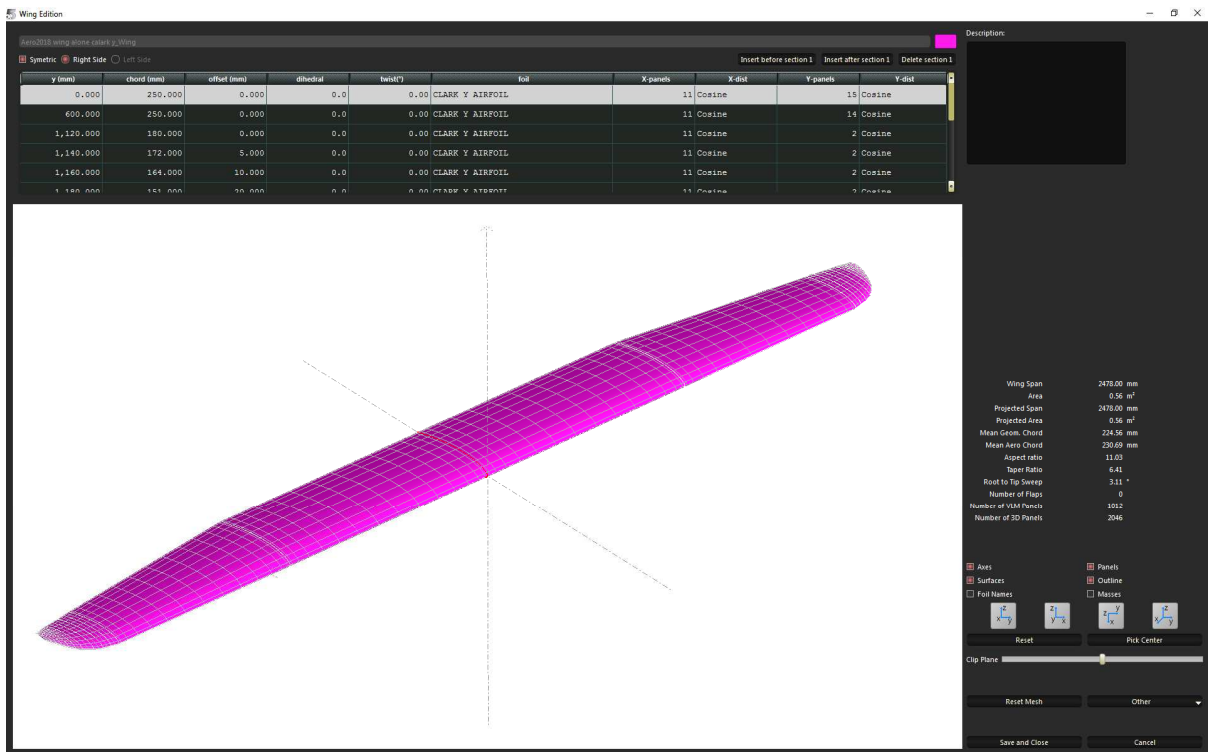
Figure II. 12 Wing plan form drawing (XFLR 5 V39)

These results were resumed in this table:

Table II. 17 Wing parameters

C_{root}	C_r (mm)	250
C_{tip}	C_t (mm)	36
Span	b (mm)	2478
Aspect ratio	$AR = b^2/S$	10.82
Main aerodynamic chord	mac (m)	230

Finally, the wing dimensions presented on this sketch
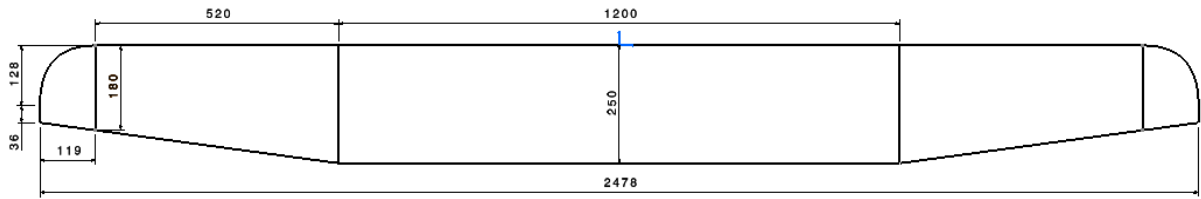
Figure II. 13 Wing dimensions (mm)

V.5.   Fuselage design:

A proposition of two different fuselages can carry the avionics systems and batteries were designed, with respect of the equipment's arrangement; one with a boom separated from the main fuselage and the second with one unit from fuselage nose to the aft fuselage.

V.6.   First fuselage proposition:

This configuration has advantage of easy separation of the boom from main fuselage; the boom can be replaced easily in case of damage.

The main body is large to support avionics systems and two batteries type 3S or 4S can pack to gather horizontally.
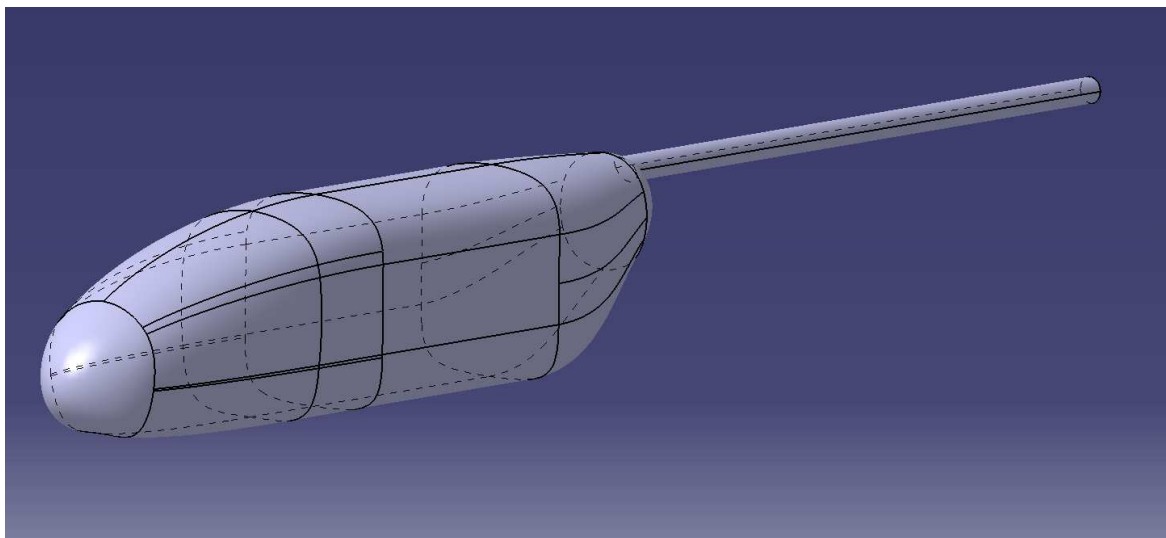
Figure II. 14 Fuselage configuration with an aft boom separated option
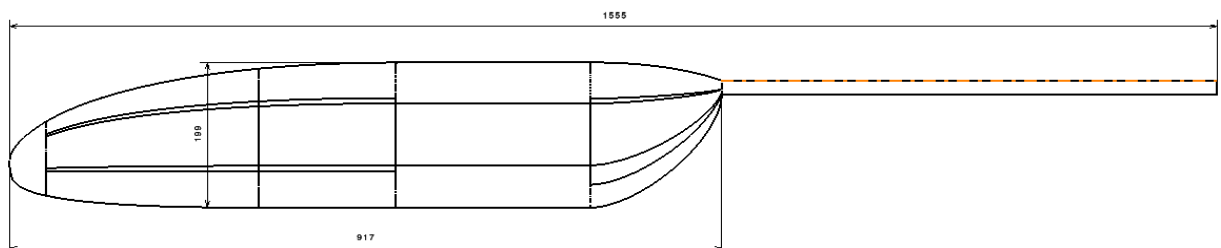
Figure II. 15 Fuselage configuration with an aft boom separated option dimensions

V.7.   Second fuselage proposition:

The second fuselage proposed with one unit body, can carry as the first fuselage the avionics systems and batteries.

The main reason for this layout is to be attached with the vertical tail and cutting to two halves using the symmetrical plan and will be prepared and manufactured to gather.
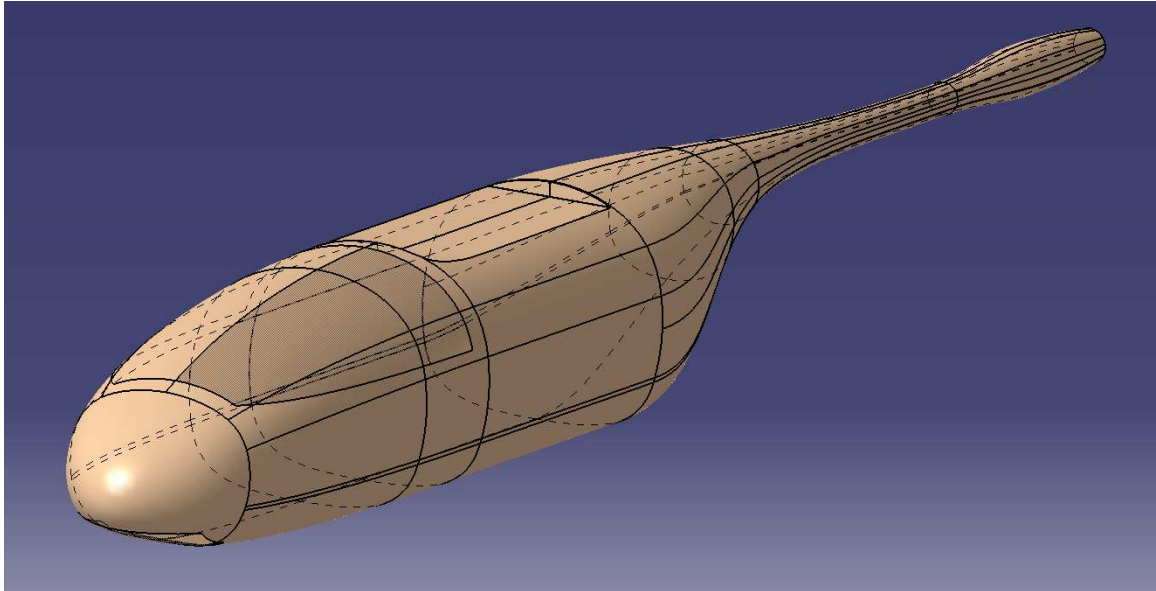
Figure II. 16 fuselage configuration with one complete body unit
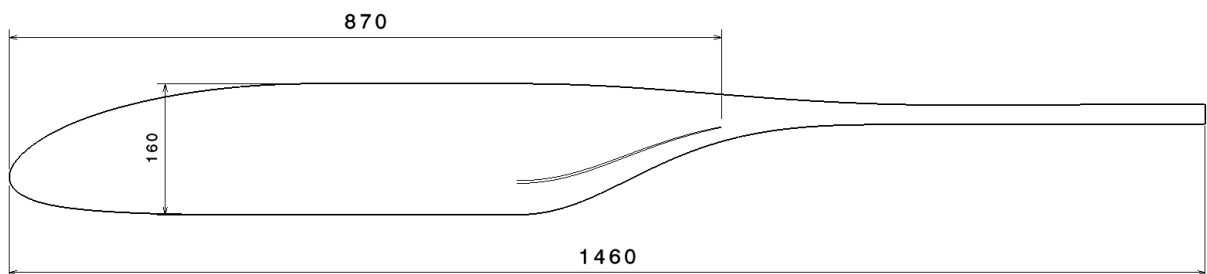
Figure II. 17 fuselage configuration with one complete body unit dimension

The second configuration was accepted as final choice.

Table II. 18 Fuselage dimensions Results

	Our model	Sky EVE-2000
Length (mm)	1460	1270
Width (mm)	177	160
Height (mm)	160	110

V.8.   Tail design:

The tail assembly (appendage) represents the collection of structures at the rear of the airplane. The tail assembly consists of (1) the **vertical stabilizer** (fin) and rudder which provide directional stability in yaw, and (2) the **horizontal stabilizer** and elevator which provide longitudinal stability in pitch [13].

Figures below illustrate the numerous forms that a tail assembly may take.

Conventional	T–tail	Cruciform
(a)	**(b)**	**(c)**
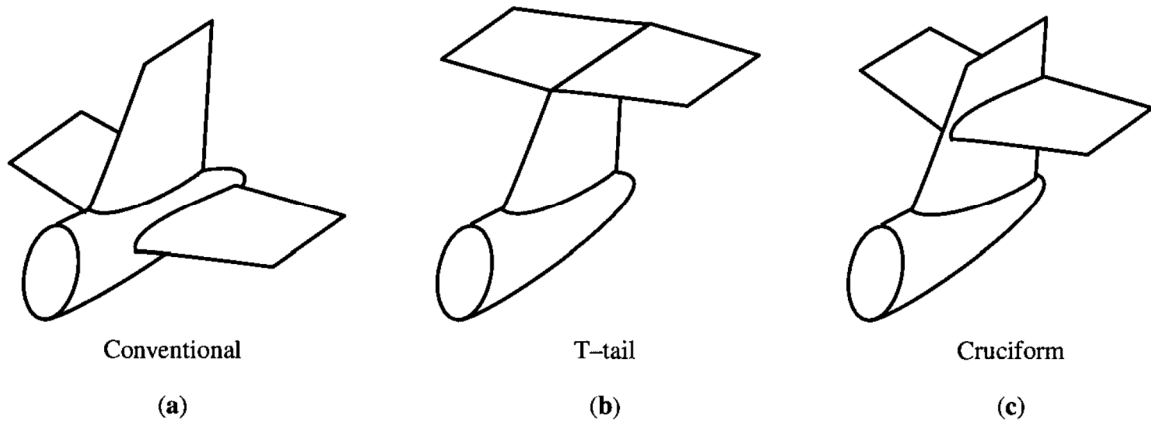
Figure II. 18 Some different Tails form assembly configurations

The T-tail arrangement was preferred to help the horizontal tail acts as an endplate on the vertical tail, allowing the vertical tail to experience a smaller induced drag and a higher lift slope; hence the aspect ratio of the vertical tail can be made smaller when the T tail configuration is used. Another advantage of the T-tail is that the rudder is not blanketed at stall.
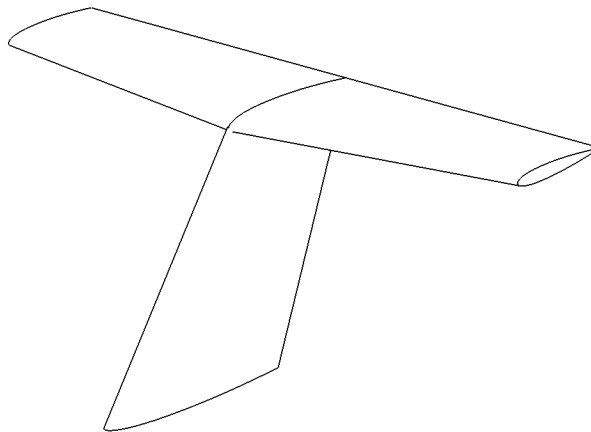
Figure II. 19 T-tail configuration unit

The horizontal tail and vertical tail on almost all airplanes use a symmetric airfoil section. A popular choice is the NACA 0012 airfoil. We will use the same for our design on both the horizontal and vertical tails.

V.9.   Horizontal tail:

First, let's initiate a tapered horizontal tail as mentioned in the **figures II.18,** the tail dimension and parameters was selected to satisfy the longitudinal stability and control.

The horizontal tail volume is an important key, Digital Mockup (DMU 2D Viewer) with CATIA software helps to define an initial horizontal tail volume V_H, this method will be demonstrated on **Appendix A**.

$$V_H = \frac{L_h S_h}{C_w S_w}$$ (II.13)

The taper ratio

$$\lambda = \frac{C_{tv}}{C_{rv}}$$ (II.14)

The table below estimates from Digital Mockup (DMU 2D Viewer)

Table II. 19 Typical UAVs horizontal tail dimensions approximation (DMU 2D Viewer)

	Skywalker EVE-2000	Sky observer (ZETA)	Pointer FQM
Real $S_w(\text{m}^2)$	0.49	0.57	0.72
$C_w \approx C_r(\text{mm})$	218.75	205	255
$b_h(\text{mm})$	545	459	790
$C_{rh}(\text{mm})$	165	120	170
$C_{th}(\text{mm})$	122	95	110
$L_h(\text{mm})$	960	700	1125

From these dimensions above, a **half** horizontal surface area can be calculated, using trapezoidal area equation calculation or by reproduction of the drawing surface using CATIA software.

$$S_h = \frac{(C_{rh}+C_{th})\frac{b_h}{2}}{2}$$ (II.15)

Multiply by 2 to get the **total** horizontal surface area

$$S_h = \left[\frac{(C_{rh}+C_{th})\frac{b_h}{2}}{2}\right] \times 2$$ (II.16)

Table II. 20 Typical UAVs horizontal tail parameters estimation

	Skywalker EVE-2000	Sky observer (ZETA)	Pointer FQM
$S_h = \left[\frac{(C_{rh}+C_{th})\,b_h}{2}\right]$ [m²]	0.062	0.049	0.111
$V_H = \frac{L_h S_h}{C_w S_w}$	1.05	0.53	0.68
AR_h	4.8	4.3	5.62

For our design a choice of horizontal tail volume V_H and distance L_{ht} will be selected, the range is taken from the estimations previously listed [0.53 to1.05], [700 to 1125] respectively.
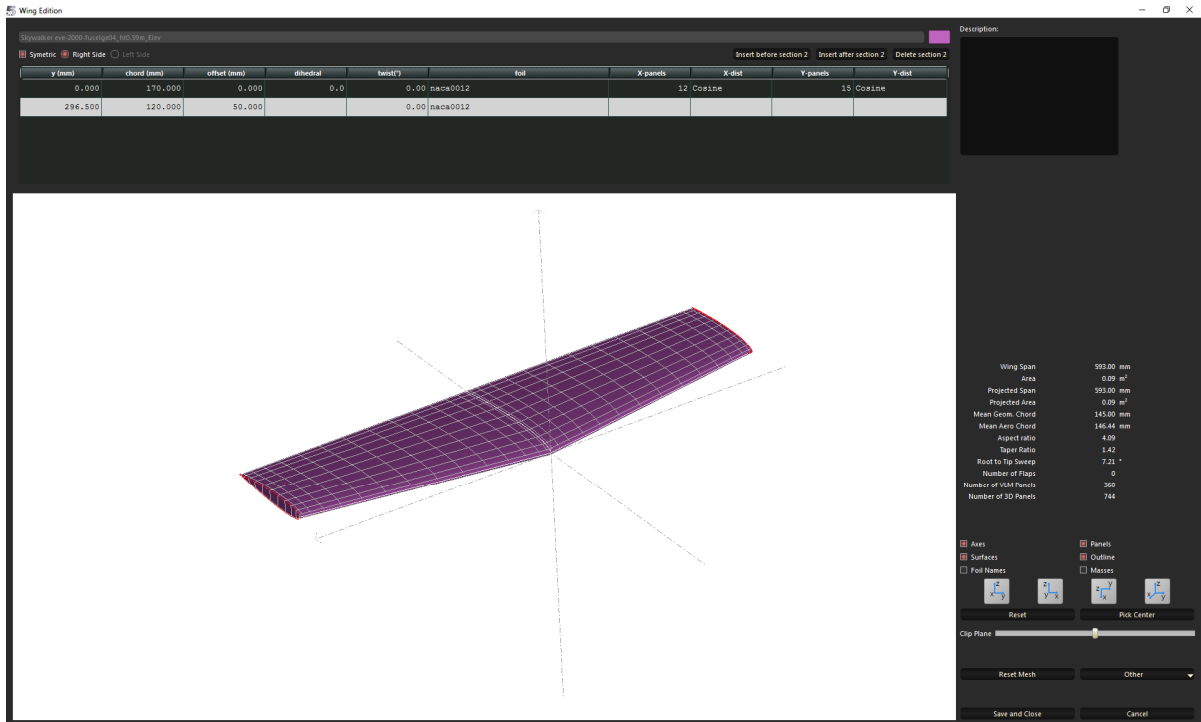
Figure II. 20 Horizontal tail drawing (XFLR5 software)

The defined parameters of the horizontal tail are regrouped on the table below.

Table II. 21 Horizontal tail parameters

Parameters	typical values (table II.22)	Results
λ	-	0.7
V_H	[0.53-1.05]	0.6
$L_h(\text{mm})$	-	1000
$S_h \ (mm^2)$	[0.049-0.111]	0.088
$b_h(\text{mm})$	[545-790]	600
$C_{rh}(\text{mm})$	[120-170]	117
$C_{th}(\text{mm})$	[95-122]	120
$mac_h(\text{mm})$	-	145
AR_h	[4.3-5.62]	4.1

A drawing illustrte the general horizontal tail dimension
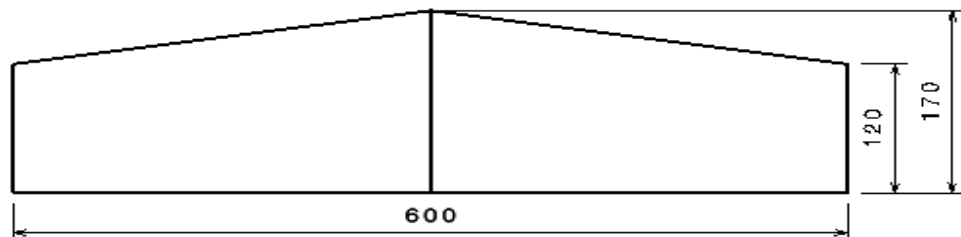
Figure II. 21 Horizontal tail dimensions (mm)

V.10. Vertical tail design:

Also, a tapered vertical tail was selected. The vertical tail volume was obtained with the same steps as horizontal tail.

$$V_v = \frac{L_v \, S_v}{b \, S_w}$$ (II.17)

Where S_v is the vertical tail area, and L_v is the distance between vertical tail aerodynamic center and the wing fuselage aerodynamic center

The taper ratio λ

$$\lambda = \frac{C_{tv}}{C_{rv}}$$ (II.18)

The table below estimated from Digital Mockup (DMU 2D Viewer)

Table II. 22 Typical UAVs horizontal tail dimensions approximation (DMU 2D Viewer)

	Skywalker EVE-2000	Sky observer (ZETA)	Pointer FQM
S_w(mm)	0.49	0.57	72.16
$C_w \approx C_r$(mm)	218.75	205	255
b_v(mm)	230	225	270
C_{rv}(mm)	240	200	275
C_{tv}(mm)	135	103	212
Estimate L_v(mm)	900	600	1080

From the above dimensions a **half** vertical surface area can be calculated, using trapezoidal area equation calculation or by reproducing the drawing surface using CATIA software.

$$S_v = \frac{(C_{rv} + C_{tv})\frac{b_v}{2}}{2}$$ (II.19)

Multiply by 2 to get the **total** vertical surface area

$$S_v = \left[\frac{(C_{rv} + C_{tv})\frac{b_v}{2}}{2} \right] \times 2$$ (II.20)

Table II. 23 typical UAVs vertical tail surfaces area estimation

	Skywalker EVE-2000	Sky observer (ZETA)	Pointer FQM
$S_v = \left[\frac{(C_{rv} + C_{tv})\, b_v}{2}\right]$ [m²]	0.043	0.034	0.066
$V_v = \frac{L_v \, S_v}{b_w S_w}$	0.035	0.018	0.036
AR_v	1.23	1.49	1.11

The horizontal tail volume V_H and distance L_{ht} take a range [0.53 to1.05] and [700 to 1125] from the estimations previously listed respectively.
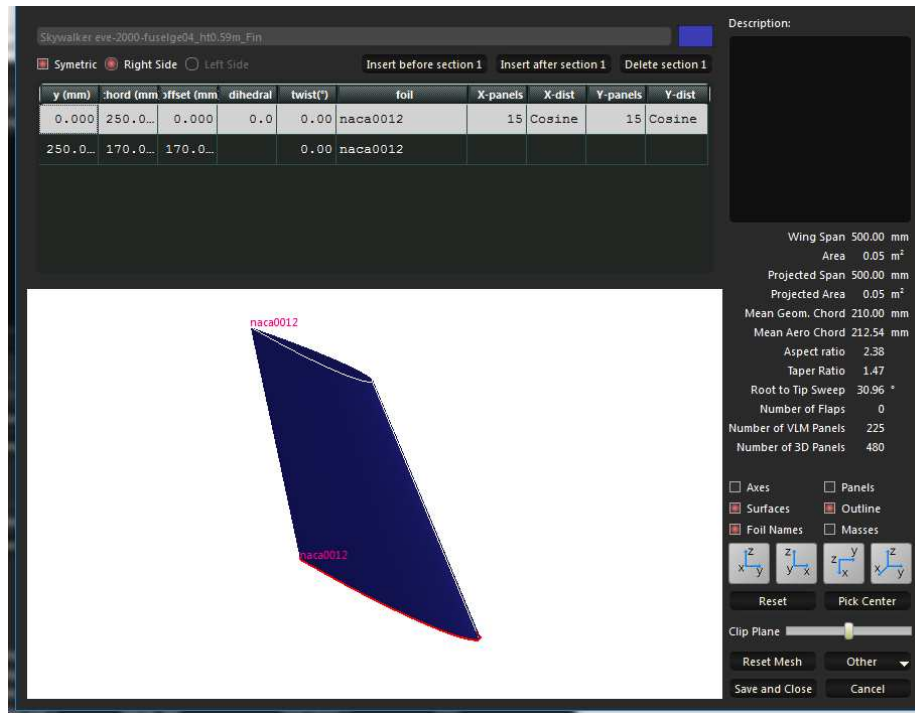
Figure II. 22 Vertical tail drawing (XFLR5 software)

The parameters define and horizontal tail results regroup on the table below.

Table II. 24 Vertical tail parameters

Parameters	Typical values (table II. 22 and II.23)	Results
λ	[0.6-1.0] [Ref 01]	0.68
V_V	[0.018-0.036]	0.032
L_v(mm)	[600-1080]	880
$S_v\ (m^2)$	[0.034-0.066]	0.052
b_v (mm)	[225-270]	250
C_{rv}(mm)	[200-275]	250
C_{tv}(mm)	[103-212]	170
mac_v (mm)	-	210
AR_v	[0.7-1.2] [Ref 01]	1.19

The following drawing illustrtes the general horizontal tail dimension
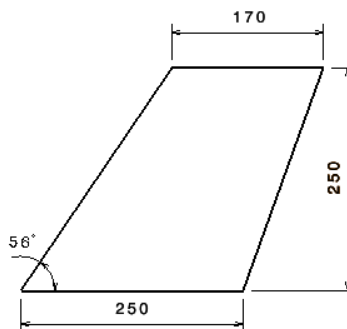
Figure II. 23 Vertical tail dimensions (mm)

V.11. LANDING GEAR DESIGN

The landing gear was downloading from https://grabcad.com/library/nose-gear-rc-plane-1 and https://grabcad.com/library/landing-gear-for-rc-aircraft-1 . This landing gear was selected for its adaptation with RC aircraft models (geometry, wheels), support the weight of the mini UAVs with respect of a good choice of fabrication materials, the landing gear parameters illustrated on the figure below must be verified when the 3D model will assemble, this landing gear generates a less drag and easy to manufacture.
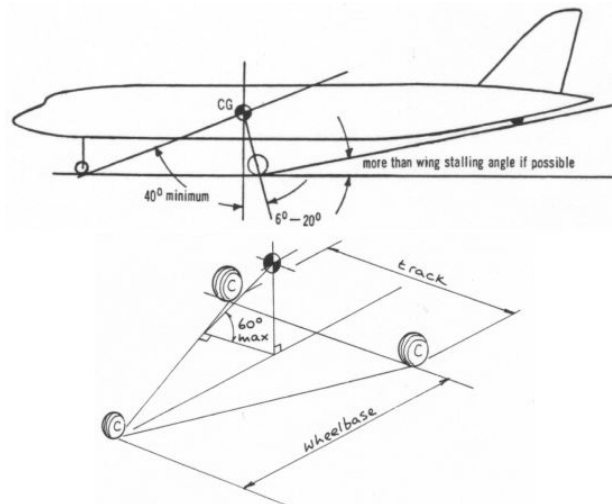
Figure II. 24 Landing gear criteria's
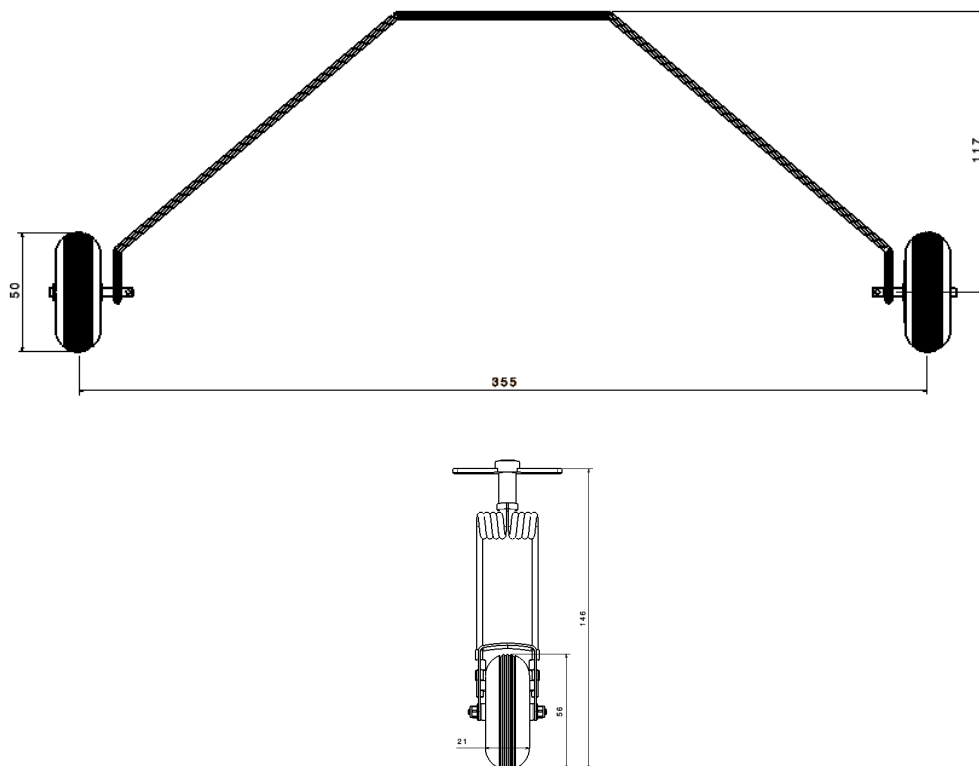
Figure II. 25 Landing gear dimensions (mm)

VI.   CENTER OF GRAVITY AND INERTIAL MOMENT'S ESTIMATION

Using XFLR5 software, creation of the configuration and weights repartition was done
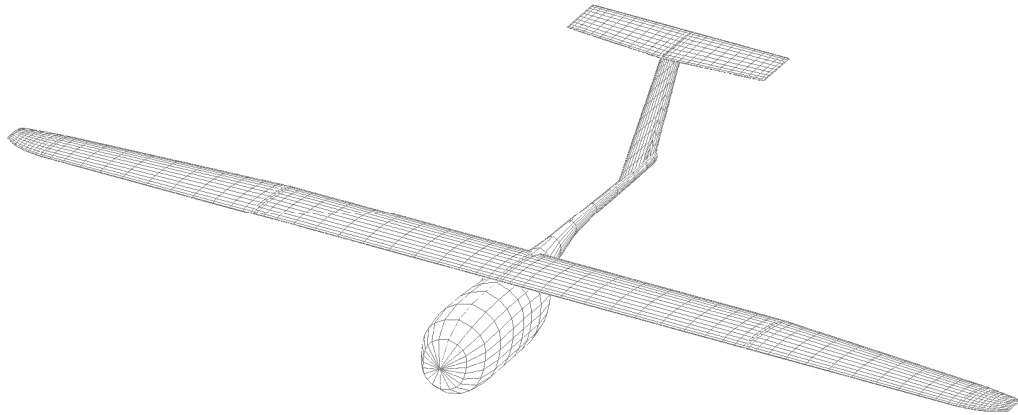
Figure II. 26 Whole configuration assembly (XFLR5 software)

Assembly the model is one of the most important phases in the design, the wing construction angle and horizontal tail angle is well-defined with starting values of 2 degrees and -2.5 degrees respectively. A positive wing construction angle gives advantage to shorter the aircraft takeoff distance; horizontal tail angle permits enough force to rotate the aircraft nose up during takeoff and define the aircraft stability criteria's.
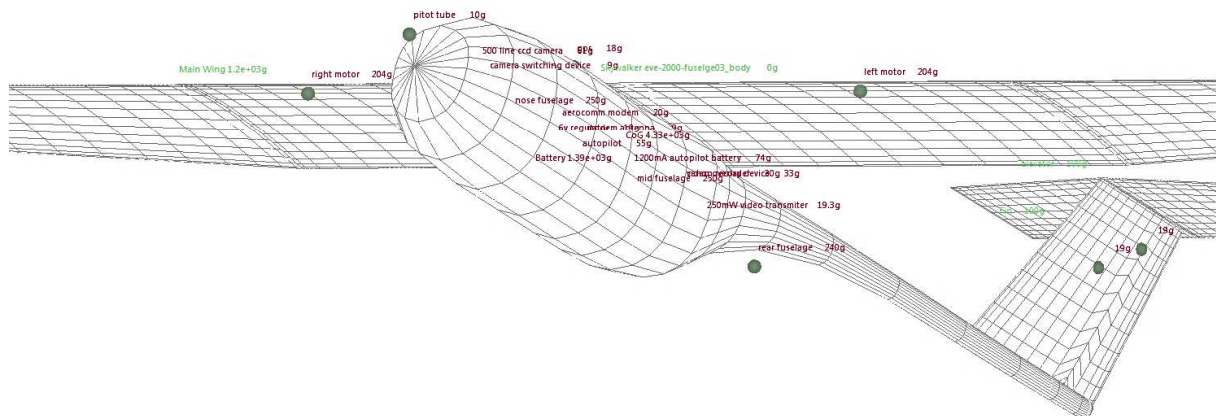
Figure II. 27 Model assembly and weights repartition (XFLR5 software)

For this configuration a forward CG location was chosen and the aerodynamic center will be back. A static margin of 15 percent will be purchase; it's clear that the horizontal tail and his incidence angle bring back the aerodynamic center of wing-fuselage configuration, the horizontal tail volume is 0.6 more than usual aircraft around 0.5 from (Ref.01).

Let's begin with CG of 35 percent and simulate the model in the next chapter, and from CFD analysis of the curve of moment coefficient versus lift coefficient will revolted the aerodynamic center location and the static margin correspond to it.

Figure II. 28 Model inertial moment's estimation (XFLR5 software)

A weight repartition was done and the CG position was fixed at 35% of main aerodynamic chord, this CG position gives a distance of 80.012 mm from wing leading edge. In the next chapter this value will be discussed depending of the moment curve slope (aerodynamic center position) to maintain a static margin around 15%.

The inertial moments are:

$$I_{XX} = 0.568 kg/m^2 \quad I_{YY} = 0.389 kg/m^2 \quad I_{ZZ} = 0.884 kg/m^2 \quad I_{XZ} = 0 \, kg/m^2$$

VII.   CONTROL SURFACES

There are two main aspects to design the control surfaces, i.e. their position and size. Varying them will give different degrees of control effectiveness in terms of roll, pitch and yaw.

VI.1.   Aileron control surface:

The aileron requirements were obtained from Ref.01, the choice of values will be achieved from the following requirements.

Table II. 25 Aileron requirements

	Typical parameters [Ref.01]	Selected values
S_a/S_w	0.05 to 0.07	0.05
b_a/b	0.2 to 0.4	0.325
b_{ai}/b	0.6 to 0.8	0.55
C_a/C	0.2 to 0.25	0.296

The aileron dimensions values are:

Table II. 26 Aileron result values

$b_a/2$	410 mm
$b_{ai}/2$	690 mm
C_a	69 mm
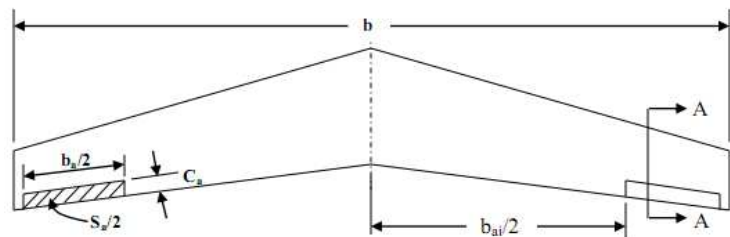
Figure II. 29 Aileron dimensions

VI.2.   Elevator control design:

Same as ailerons selection, the elevator selection values are:

Table II. 27 Elevator requirements

	Typical parameters [01]	Selected values
S_e/S_h	0.2 to 0.4	0.36
b_e/b_h	0.8 to 1	1
C_e/C_{ht}	0.2 to 0.4	0.35

The elevator dimensions values results are:

b_e	600 mm
C_e	60 mm

Table II. 28 Elevator result values
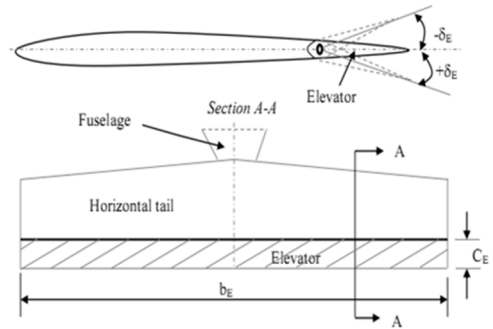
Figure II. 30 Elevator parameters

VI.3.   Rudder control design:

Continue with same Reference requirements [01], the rudder typical values and selection revealed also in these following tables:

Table II. 29 Rudder requirements

	Typical values [01]	Selected values
S_r/S_v	0.2 to 0.4	0.36
b_r/b_v	0.8 to 1	1
C_r/C_{rv}	0.2 to 0.4	0.35

The rudder dimensions values results are:

b_r	250 mm
C_r	70 mm

Table II. 30 Rudder result values
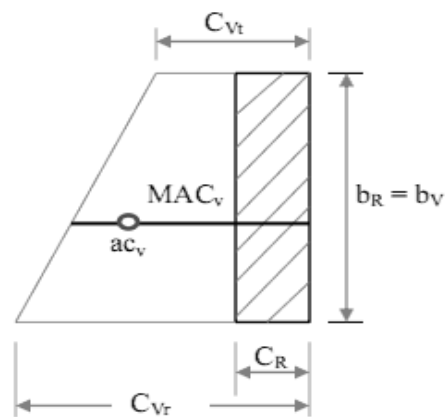
Figure II. 31 Rudder parameters

VIII.   3D MODEL CONCEPTION (using CATIA software):

CATIA V5-R20 software has a great help to design our 3D model based on the results dig up in the previous sections, the CATIA software has many workshops. The shape workshop [Shape] has the main role to develop our model.

Generative shape design is an attractive space for the external shape design; aerodynamics designers progress their ideas on this space.
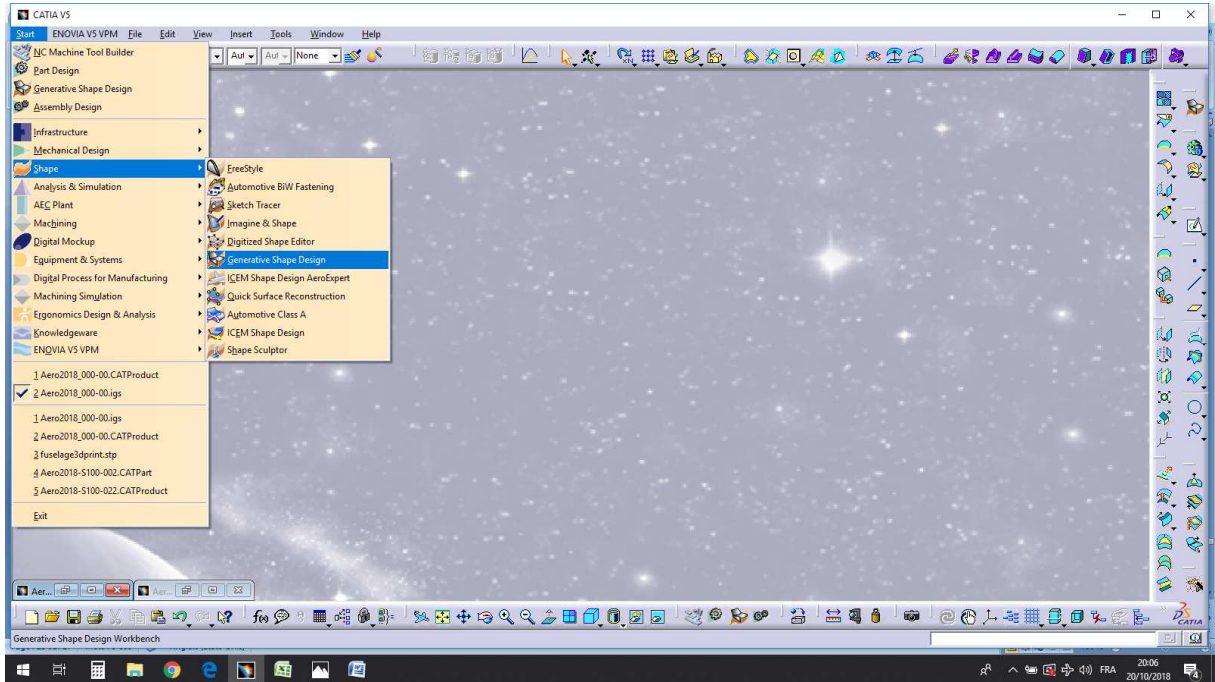
Figure II. 32 CATIA software interface

This model will be divided in to three main components wing, fuselage and tail, let's start with fuselage steps design.

VII.1. <u>Fuselage conception:</u>

The fuselage component initiated with a 2D sketch in the symmetrical aircraft plan, this sketch defines the limits and the size of our fuselage. A 2D frames sketch added to define the thirds dimensions, these figures point up these steps
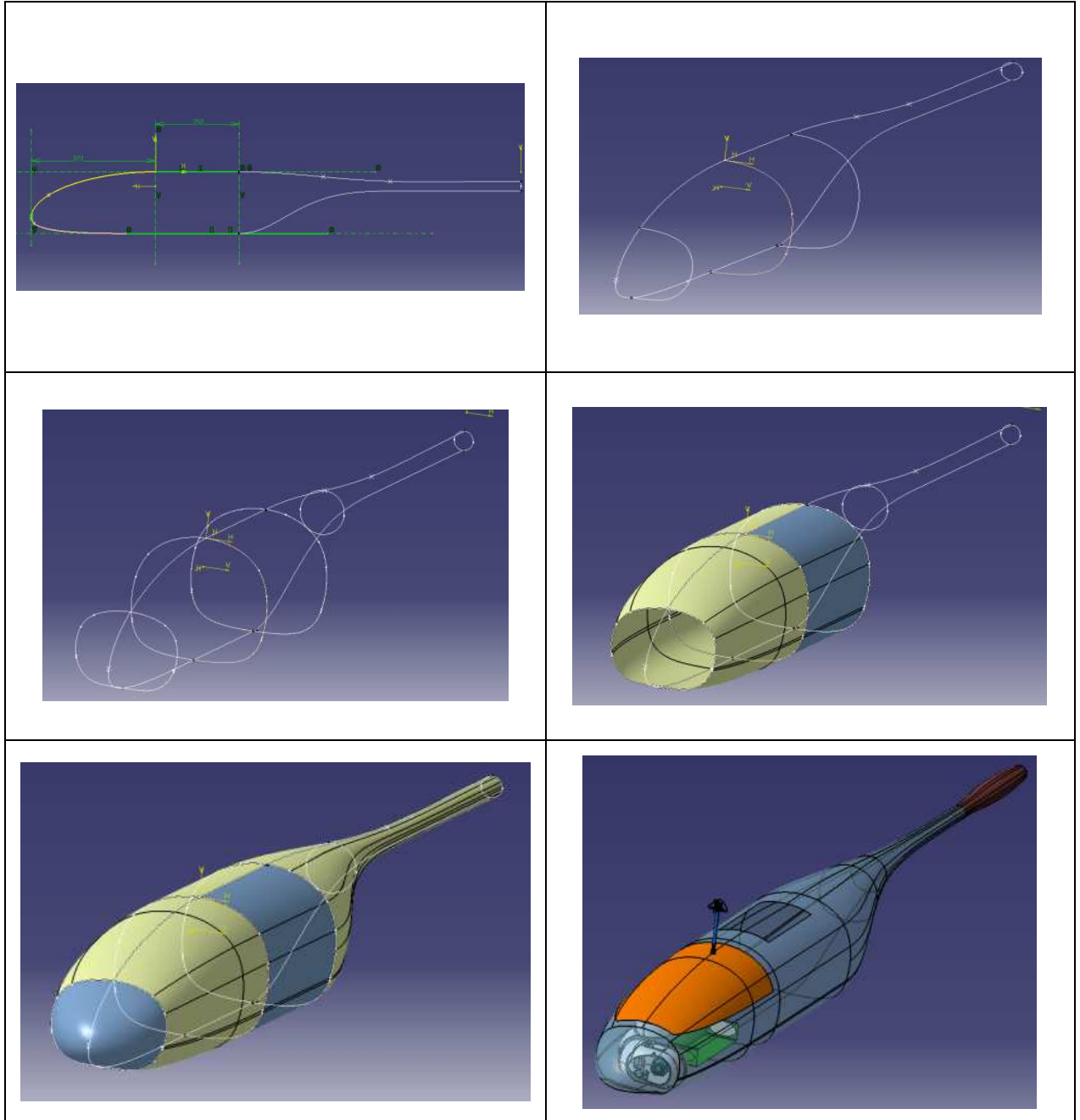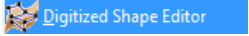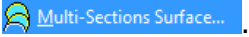
Figure II. 33 Fuselage 3D model design

VII.2. Wing conception:

The wing three dimension CATIA software conception starts with import of Airfoil coordinates data (Cark Y.data) in **APPENDIX B** using the digitized shape editor . Different plans locations were defined according to the sections of the wing. A guide lines helps to conduct the outer wing skin using multi-section surface .

These six images resumed a general steps to draw a wing
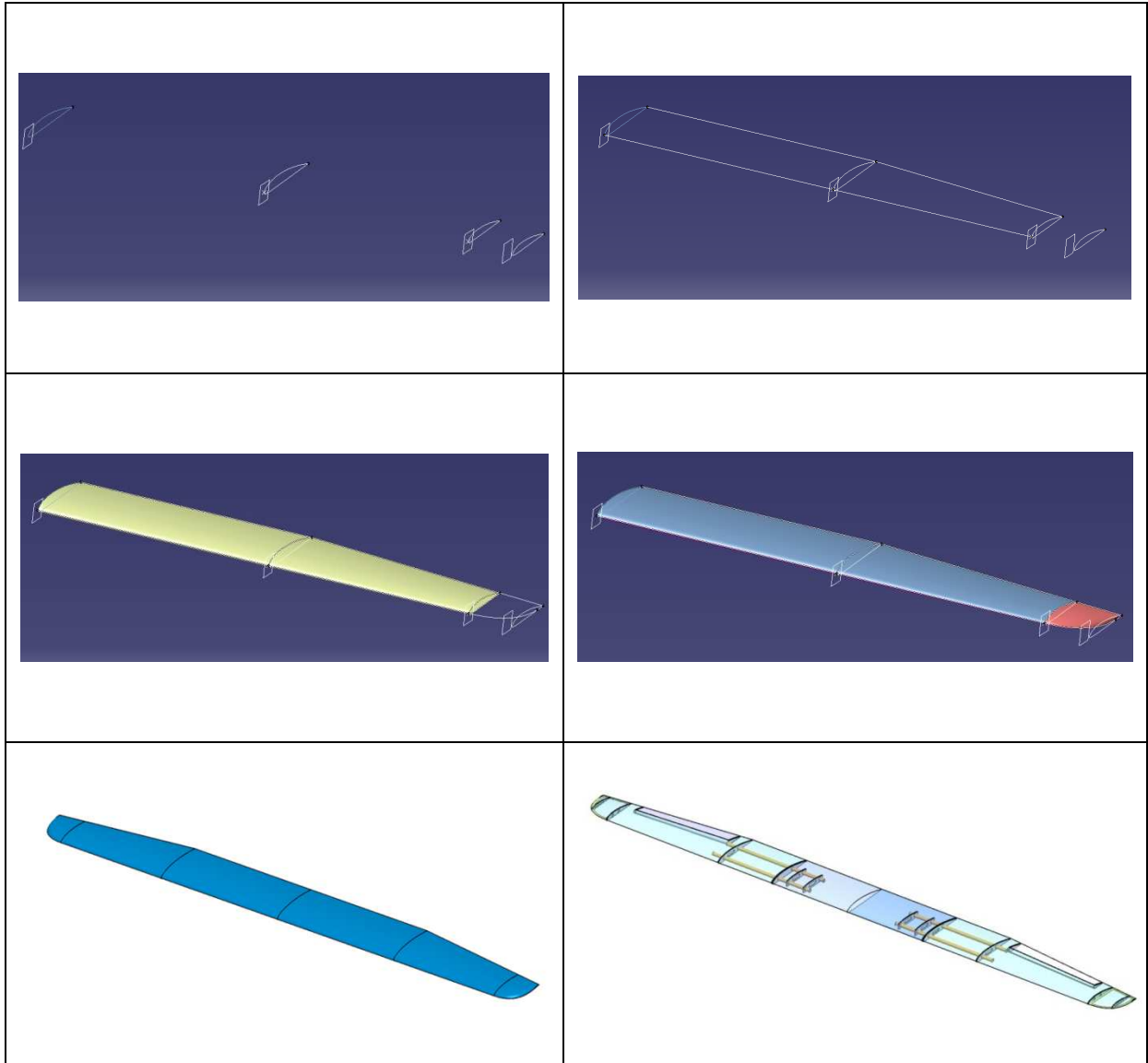
Figure II. 34 Wing 3D model design

VII.3. Tail conception:

From the previous tail design section, the profile NACA0012 will use the coordinates NACA0012 presented in **APPENDIX B**.

There is no difference between tail and wing conception steps, these five images helps to understand the way to draw the 3D tail concept.
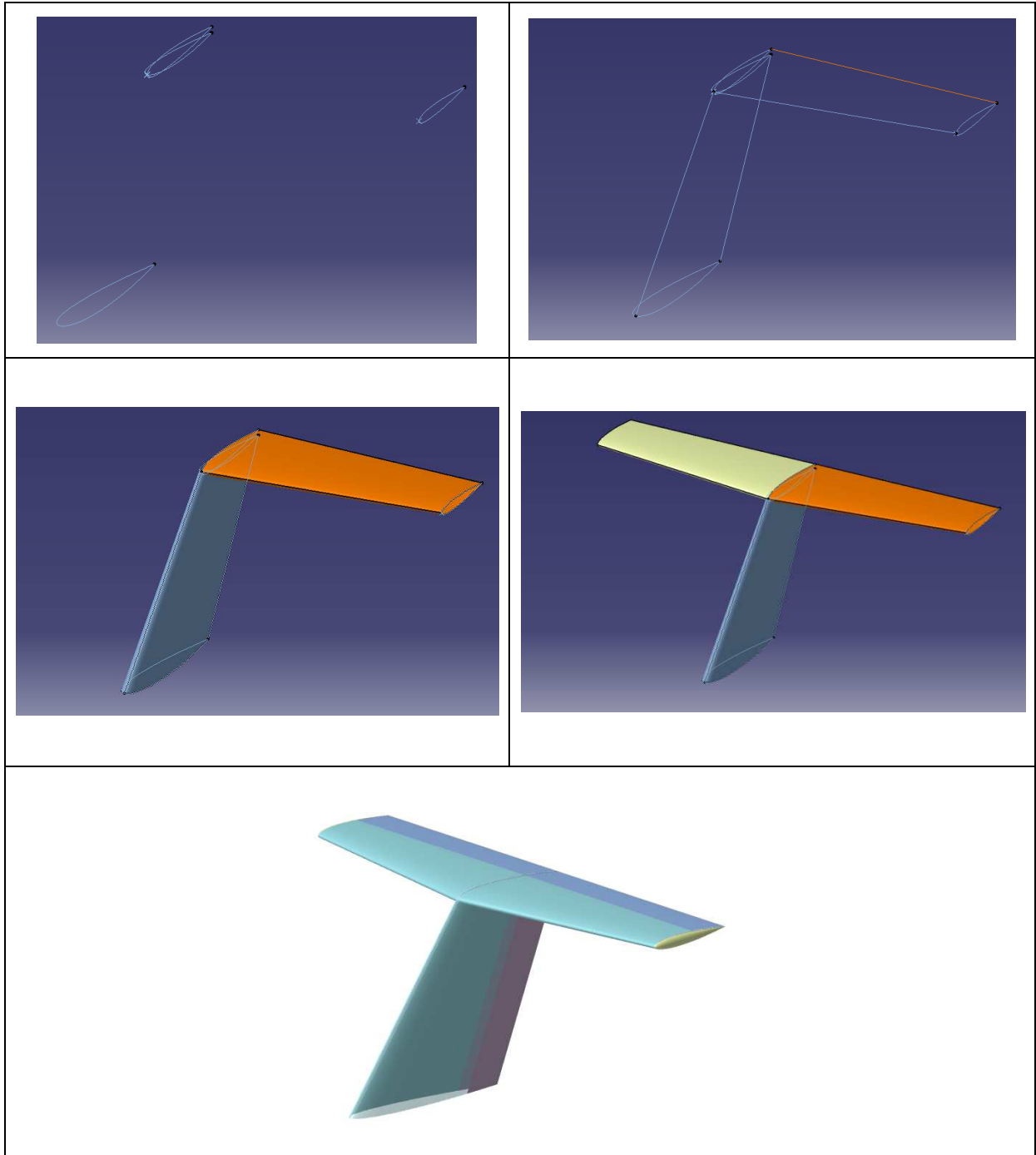
Figure II. 35 Tail 3D model design

VII.4. Whole Model assembly:

As a result, the whole model assembly will be achieved using the wing-fuselage and at the same time a downloading motors with 3 blades propellers. In addition, mounting the avionics systems and the tail within the control surfaces, at last, the landing gear will take place in the whole model assembly to get the following minUAV named IAES2018-XXXX.
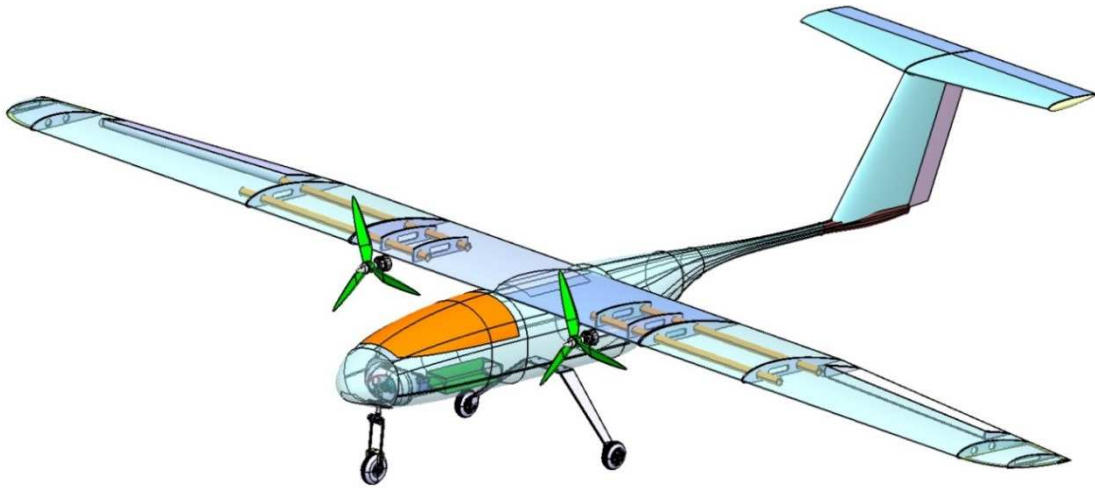
Figure II. 36 Whole Model assembly IAES2018-XXXX
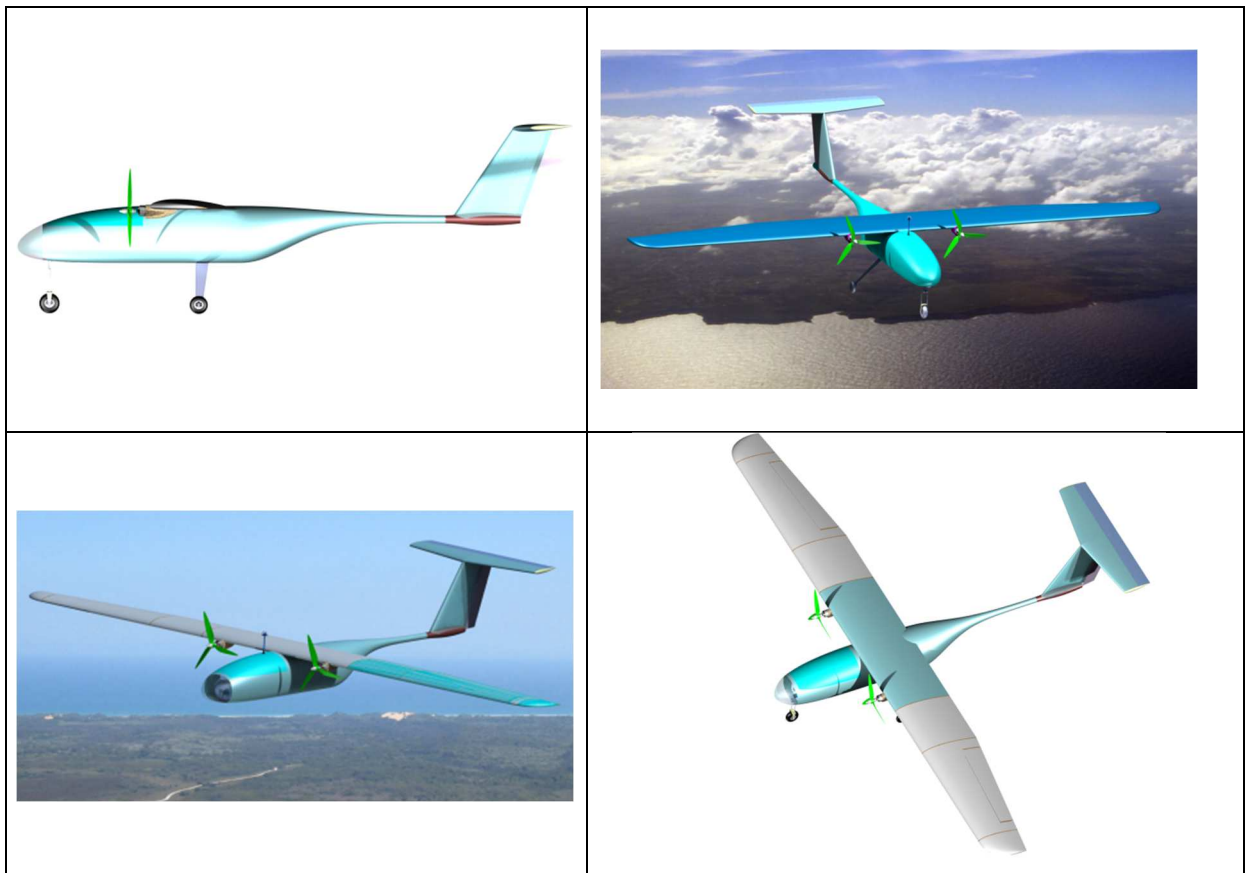
Figure II. 37 IAES2018-XXXX views

IX.   CONCLUSION

After get hold of the conception and the aerodynamic design, a 3D concept was established with respect of the different criteria's to minimize as possible the potentials of waste time in sizing and aerodynamics parameters choice review, the next chapters will be a benefit tools to understand the previous choices and confirm the suitable selections and validating the concept.

In the fourth chapter the propulsion system will be reviewed, the propellers will have changes in term of number of blades from three to two, due to in short supply data in this level at this time.

The landing gear needs an additional review to satisfy requirement for takeoff (20 degrees) at least, the configuration has around 15 degrees.

To not forget the important role of our teachers who spent their lives to build our nation, this model will take the name of our teacher **Dr. TAHI Ali**, is not with as in this existence but his work is still exist.

mini UAV **IAES2018-TAHI.A** overall sizing is:

Table II. 31 mini UAV IAES2018-TAHI.A overall sizing

Parameter	Result
Type	Mini UAV (fixed wing)
Weight	4500 $grams$
Wing span	2477 mm
Length	1550 mm
High	526 mm
V_c	50 km/h
V_{Stall}	37.45 km/h
CG position	80.05 mm
I_{XX}	0.588 kg/m^2
I_{YY}	0.388 kg/m^2
I_{ZZ}	0.884 kg/m^2

I.   COMPUTATIONAL TECHNIQUES USING CAD AND CFD ANALYSIS

I.1   Scope:

In this chapter of the thesis, CFD analysis of designed aircraft, as well as outer body geometry improvements in order to obtain better aerodynamic characteristics will be explained in details.

I.2   Geometric model preparation:

In the recent years, the computational approach has been widely used in order to design, analyze and optimize the desired products. The computer aided tools contribute in waste time reduction, product optimization, facilitation in modeling and reduction in cost.

However, people having strong background in both computational tools and technical knowledge are required so as to gather proper and accurate results. In **the first step**, the geometric model has been designed in CAD CATIA V5 software in details, the outer shape saved in (**.stp)** format so as to import it into **ANSYS geometry design modeler** (ANSYS geometry DM). However, one should pay attention not to create unrequired sharp corners, overlapping of lines in order not to have error message during meshing process. Sometimes, precautions even such as virtual topology or pinch control may not be enough.

Figure III. 1 Full model preparation for CFD analysis
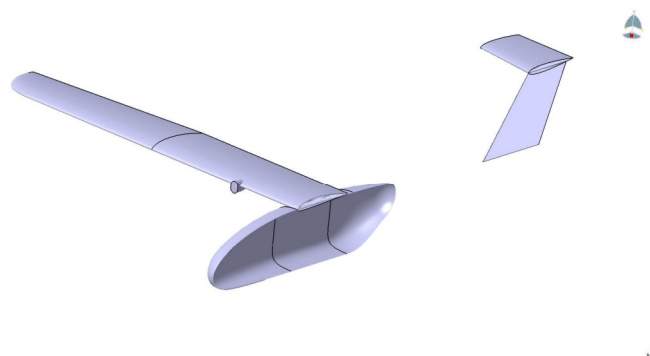
Figure III. 2 A half model configuration

In **the second step**, slight geometrical modifications to the main fuselage geometry has been employed to get easy meshing, the sharp angles, slivers, spikes, faces have been repaired and merged for accurate meshing and computational results.
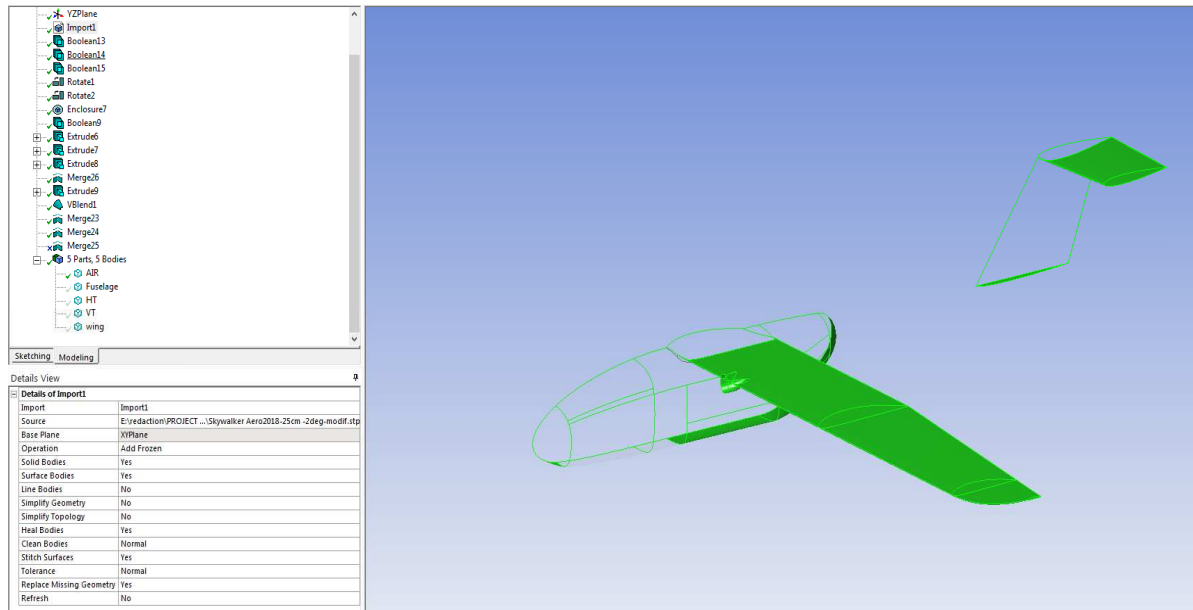
Figure III. 3 Geometrical modifications (ANSYS geometry DM)

Then, the control volume should be sized by considering the flow not to reach the enclosure boundaries. In short, assuming that the aircraft is located in the center by considering vertical direction, control volume size should be at least 6~10 times greater than the aircraft length in all directions.
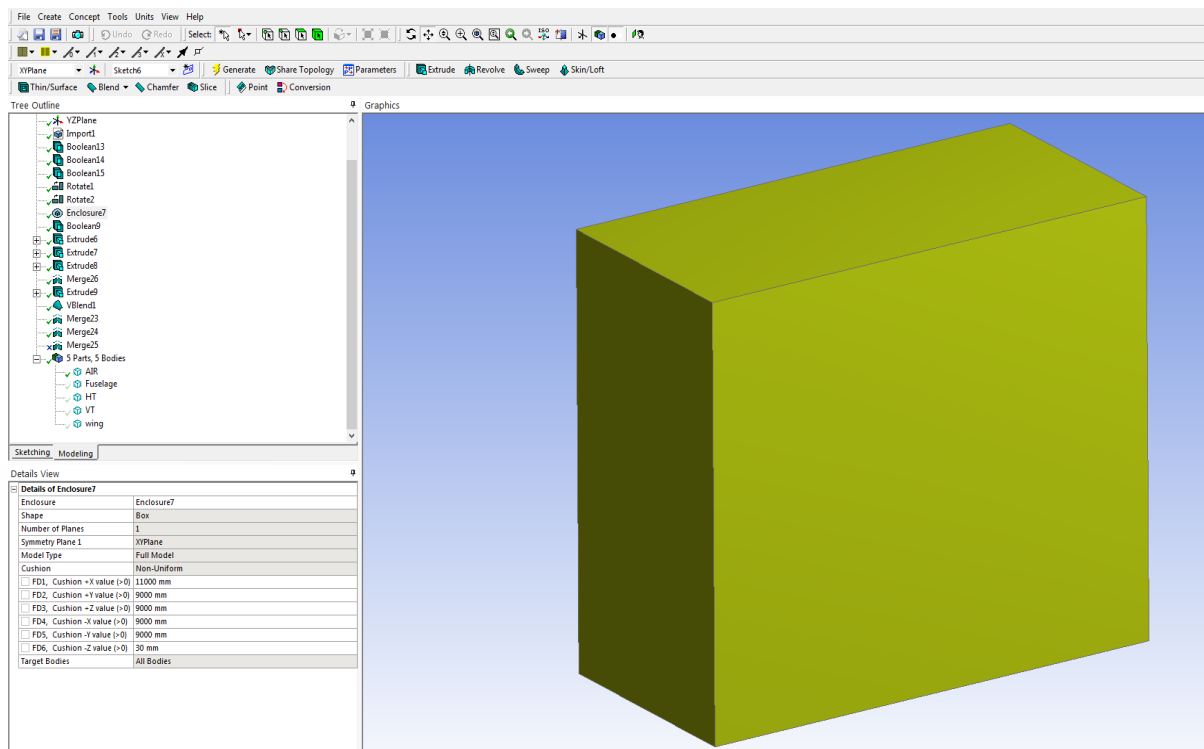
Figure III. 4 The control volume domain (ANSYS geometry DM)

Explicitly, the greater is the control volume size, the more confidential is the result. Even though there is not strict rule in computation domain sizing; flow velocity, body geometry, viscosity, turbulence model and mesh type plays a significant role. However, an optimum point should be attained during computation with inferior computers. Also the control domain size in vertical plane has been halfed to reduce computation time.

In the third step, creates influence bodies around geometries separately to refine mesh and permits the generation of the inflation layers coherence.
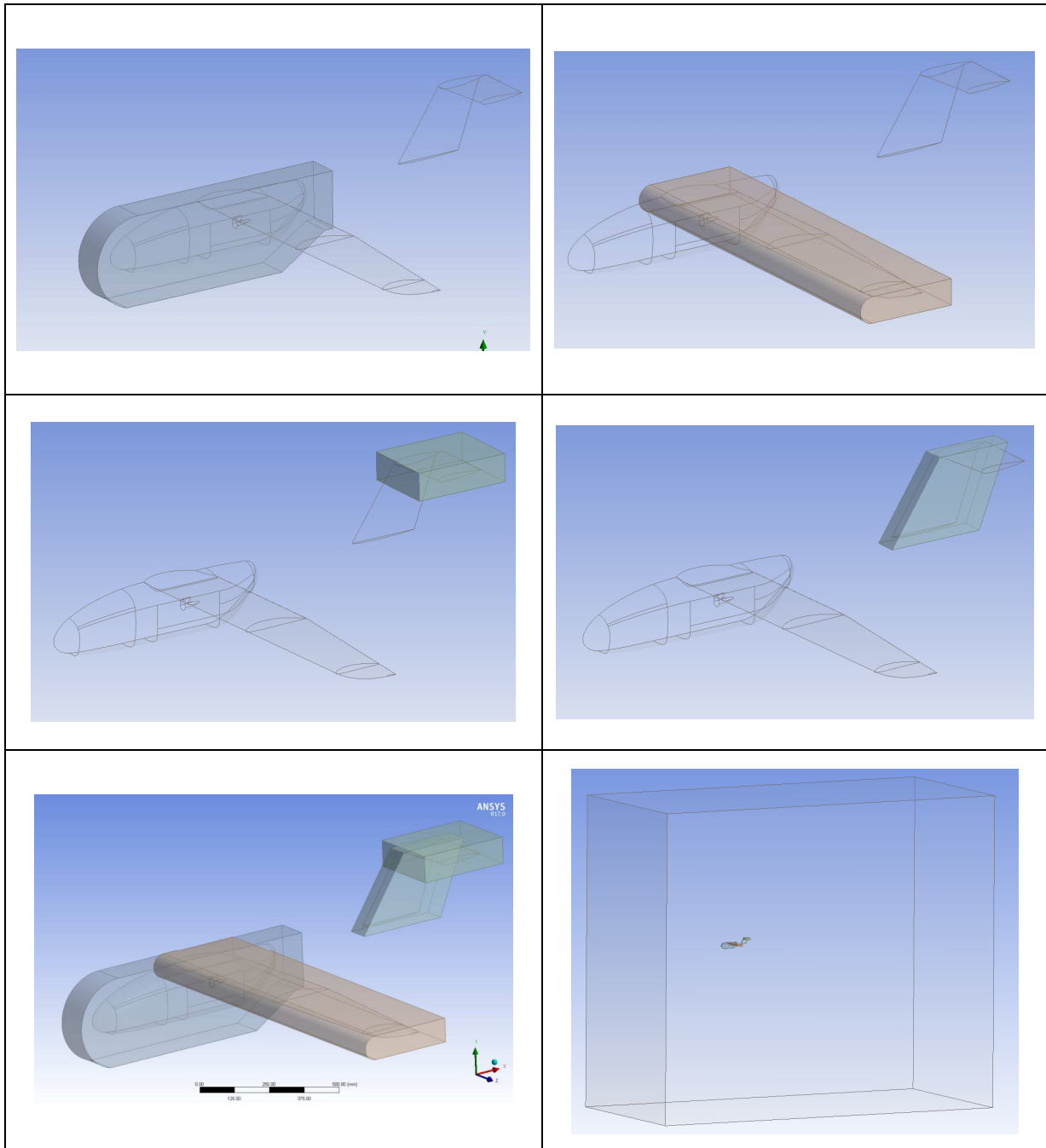
Figure III. 5 Working control volume (ANSYS geometry DM)

I.3   Mesh parameters test:

In the given study, fine and coarse meshing relevance and medium smoothing combined with inflation layers have been employed so as to obtain values at an acceptable interval and capture the near wall flow. In addition, orthogonal quality and skewness were seriously observed in each meshing process and re-meshing were performed for meshing process having poor quality meshes. Samples generated meshes for the study are given in **figures III.6**.
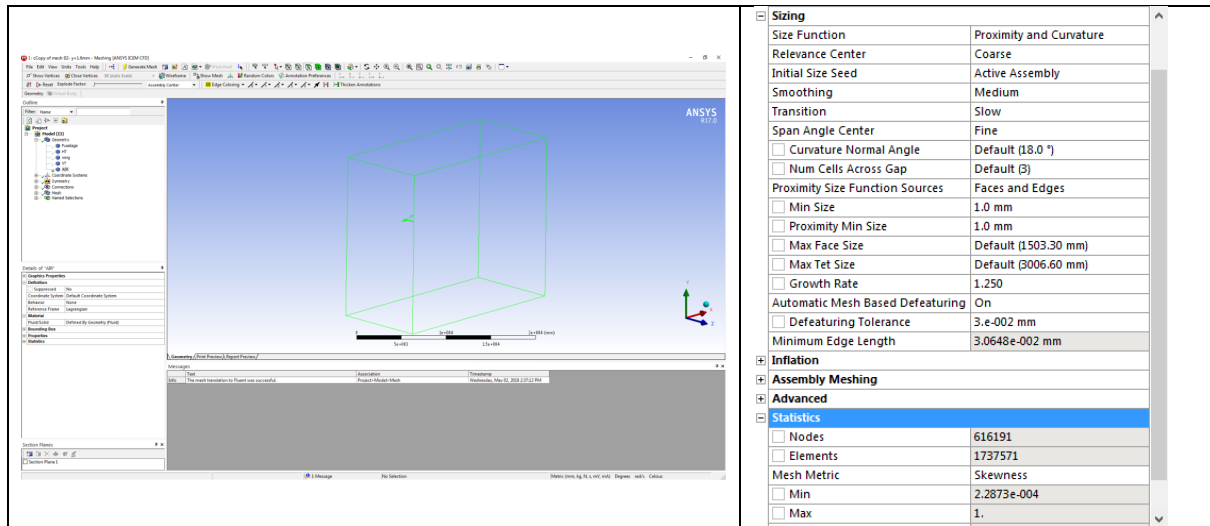
Figure III. 6 Mesh parameters (ANSYS Mesh Modeler)

Mesh quality is described by various parameters, such as orthogonal quality, skewness, aspect ratio, jacobian ratio, warping factor, parallel deviation and maximum corner angle. However, orthogonal quality and skewness are the most essential parameters in quality assesment. Orthogonal quality is computed for cells using the vector from the cell centroid to each of its faces, the corresponding face area vector and the vector from the cell centroid to the centroids of each of the adjacent cells. The value should be as maximum as possible close to unity to get desired results. Aspect ratio is a measure of the stretching of the cell. It should be avoided from sudden changes in aspect ratio in the flow field. Skewness is defined as the difference between the shape of the cell and the shape of an equilateral cell of equivalent volume. Highly skewed cells can reduce accuracy and convergence tendency. The value should be as maximum as possible close to zero to get desired results. In short, a CFD user should avoid using meshes having orthogonal quality and skewness values below 0.01 and 0.1 respectively, and such poor quality cells can be improved before the analysis. [09]
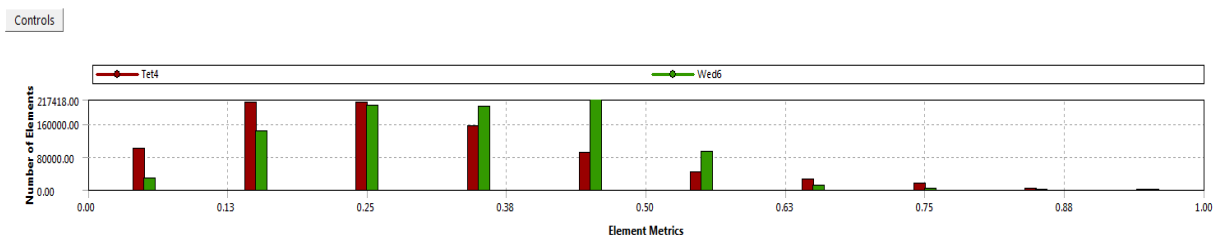
Figure III. 7 Mesh control (ANSYS Mesh Modeler)
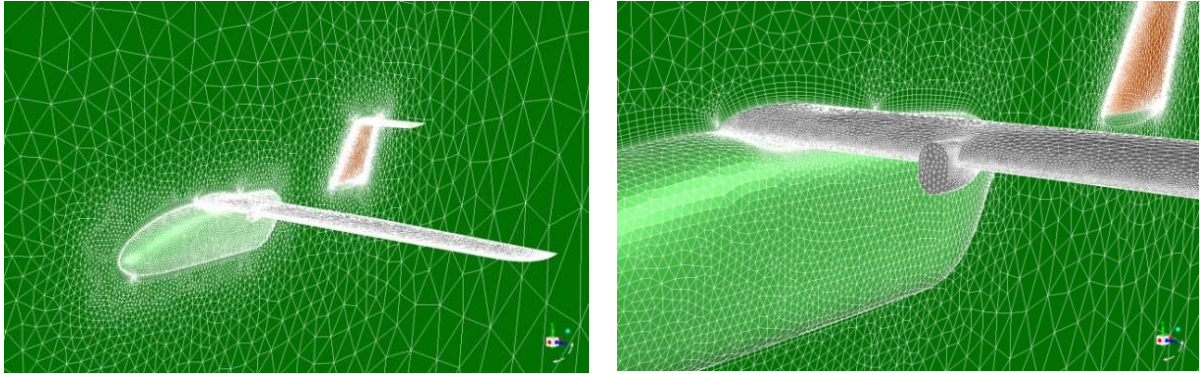
Figure III. 8 The mesh generating around the model

A mesh number about 2 000 000 is used to resolve the problem. In addition, y^+ values were the greatest concern of mesh quality assessment process. The parameter value of great than 30 is desired; however, one should consider that proper y^+range is highly depended on the Re number. In the study, variation of y^+ is in acceptable range according to ref. In addition, one of the deductions is that optimum mesh number provides better convergence rate and stability. Depicted mesh numbers guide us how to mesh accurately for the remaining aircraft configurations and angle of attacks. [09]

ANSYS Fluent software has been implemented in order to get results for different configurations and angle of attack values after exporting from ANSYS mesh design modeler (.msh). 3-D Navier Stokes coupled with turbulence model has been employed during the processes. **Inlet boundary** condition has been defined as velocity inlet in which the inlet velocity is defined. **Outlet boundary** condition has been defined as pressure outlet in which the outlet pressure is defined as zero gage pressure. Iterations have been continued until desired residuals have been reached. Sides of the control volume have been defined as **symmetry boundary** condition. Afterward post processing the results.
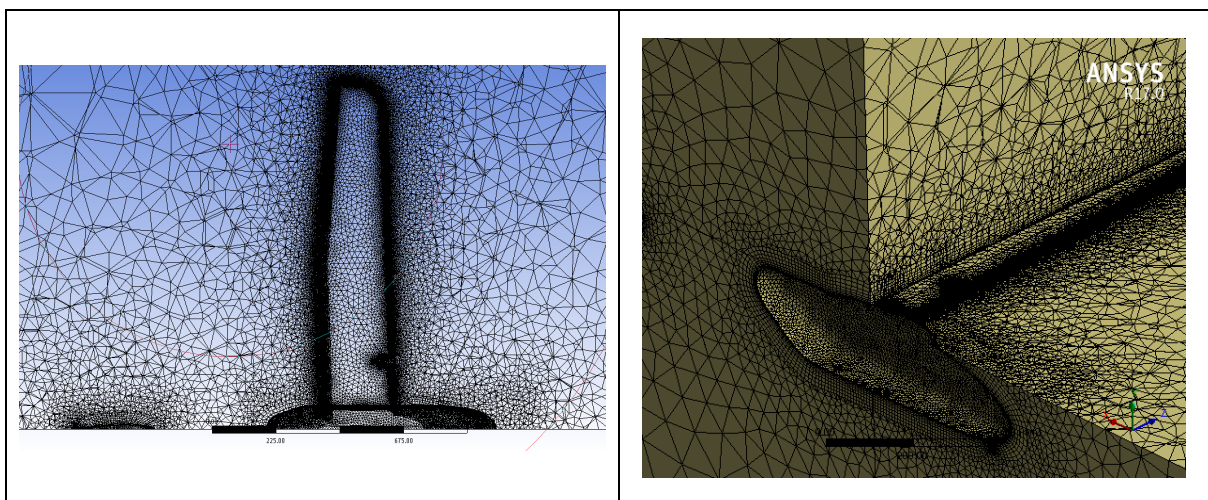
Figure III. 9 Mesh density and inflations results

II.   NUMERICAL METHODS FOR EXTERNAL AERODYNAMIC ANALYSIS

CFD analysis is a well-established technique for a wide range of applications, such as external flow, flow combined with heat transfer, fluid structural interaction, internal flow problems and etc. Especially CFD analysis plays a significant role in demonstrating the performance and improvement of a new aircraft design. The major advantage of a CFD process is the ability to inexpensively generate a desired amount of simulations inducing to understand the performance of the designed geometry. However, deep knowledge about the CFD tool, methods and post processing is required to gather correct results. Actual flows encountered in daily life are usually turbulent, such as exit flow from an air conditioning device or flow around an automobile. Turbulent flow is a flow type characterized by chaotic characteristic changes including high momentum convection, low momentum diffusion and fast altering in both pressure and velocity. As a result, unsteady vortices are generated and they might interact with each other; hence, rise in drag is inevitable. Intermediate stage between laminar and turbulent flow is called as laminar to turbulent transition. In laminar flow, kinetic energy of the fluid is such low that chaotic changes encountered in turbulent flow are not available. The way to differ flow types of laminar and turbulent is performed by the Reynolds number where U is the flow velocity, is the mean chord length and is kinematic viscosity. *Re* number is usually referred as the ratio of inertial to viscous forces. The expression is given in equation III.1 [09].

$$Re = \frac{U \, c}{v} \qquad\qquad\qquad\qquad\qquad\qquad (III.1)$$

Turbulence model is a computational way to approximate the mean flow equations. Most of the engineering applications do not need to deal with the details of turbulent fluctuations. Turbulent model theories are based on Boussinesq theorems stating that Reynolds stresses are directly related with the mean deformation rate [09].

CFD simulation is a useful tool in order to simulate the desired model or case without need of costly experimentations. However, a compromise between solution accuracy and computation time should be established. Solution accuracy increases with models having higher number of equations; however, the benefit comes with deterioration in CPU time. Hence, the essential point must be to select appropriate equation type by considering the application, accuracy and computation effort. The accuracy of CFD predictions for turbulent flow, in particular 3D simulations, is highly dependent on the quality of the turbulence modeling whose flow characteristics include 3D boundary layers with strong streamline curvature, separation and strong vortices. The model recommended for aerodynamic simulations is Spalart Almars. However, by considering computation effort and satisfactory solution accuracy, Spalart Almars model has been employed during the CFD analyses [09].
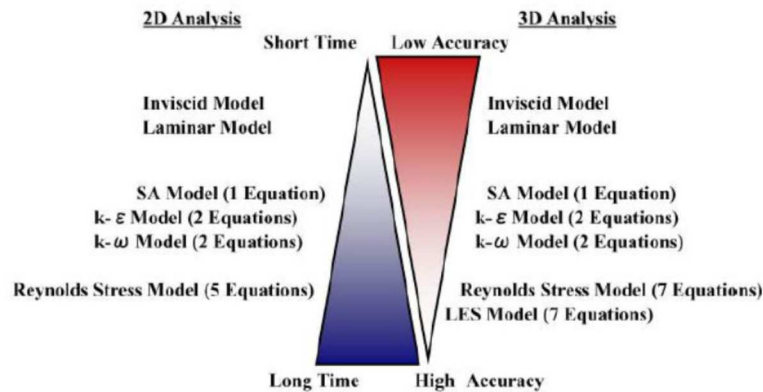
Figure III. 10 Relationship between CPU time and accuracy

Solver is chosen as pressure based, instead of density based due to the fact that cruise speed of ($50 \, km/h = 15.89 \, m/s$) is in the interval of incompressible region. At the inlet, **velocity inlet boundary** condition has been chosen. As for the walls of control volume, **symmetry condition** is the most suitable selection. At the outlet, **pressure outlet boundary condition** has been chosen. **Turbulent intensity**, which is the ratio of fluctuating velocity to main velocity, is difficult to calculate, a value of 5 was assumed.

Convergence is another important issue to assess results of an analysis to be satisfactory or not. Computation tools run successive iterations until the residuals of the variables fall below a desired value. However, this does not signify that the results of the analysis has converged, more iteration might be needed. In the study, the convergence criteria are assumed as for the continuity and for the momentum equations. Authorities state that convergence criteria of for velocity components are enough. These depicted criterions require at least 600 iterations in this study. On the other hand, one can deduce that higher is the mesh number and quality, better is the convergence rate. In addition, second order discretization sheme selection is a must for such a study due to the fact that flow is not straight in some regions.
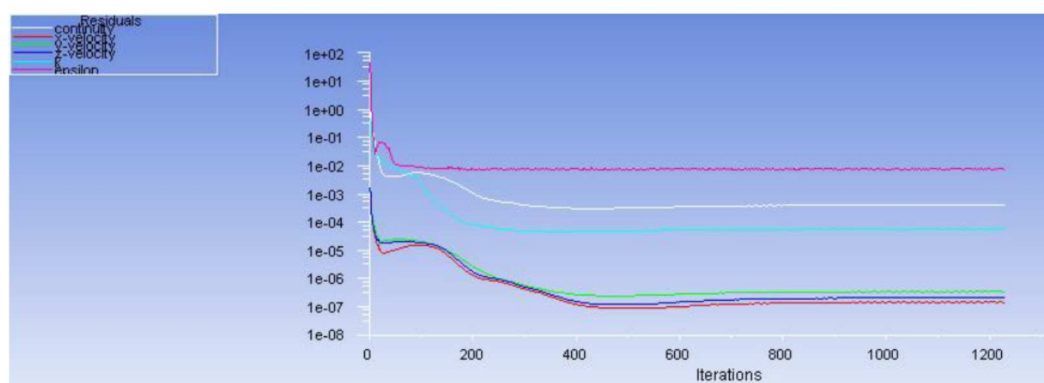
Figure III. 11 Residuals vs number of iterations AOA=16 degree

For boundary conditions, at the inlet a velocity inlet boundary is used, the flow **velocity is 13.8 m/s** and **flow angle** distribution were specified. A pressure outlet boundary was prescribed at the **outlet (1101325 Pascal)**.

The total pressure distribution results
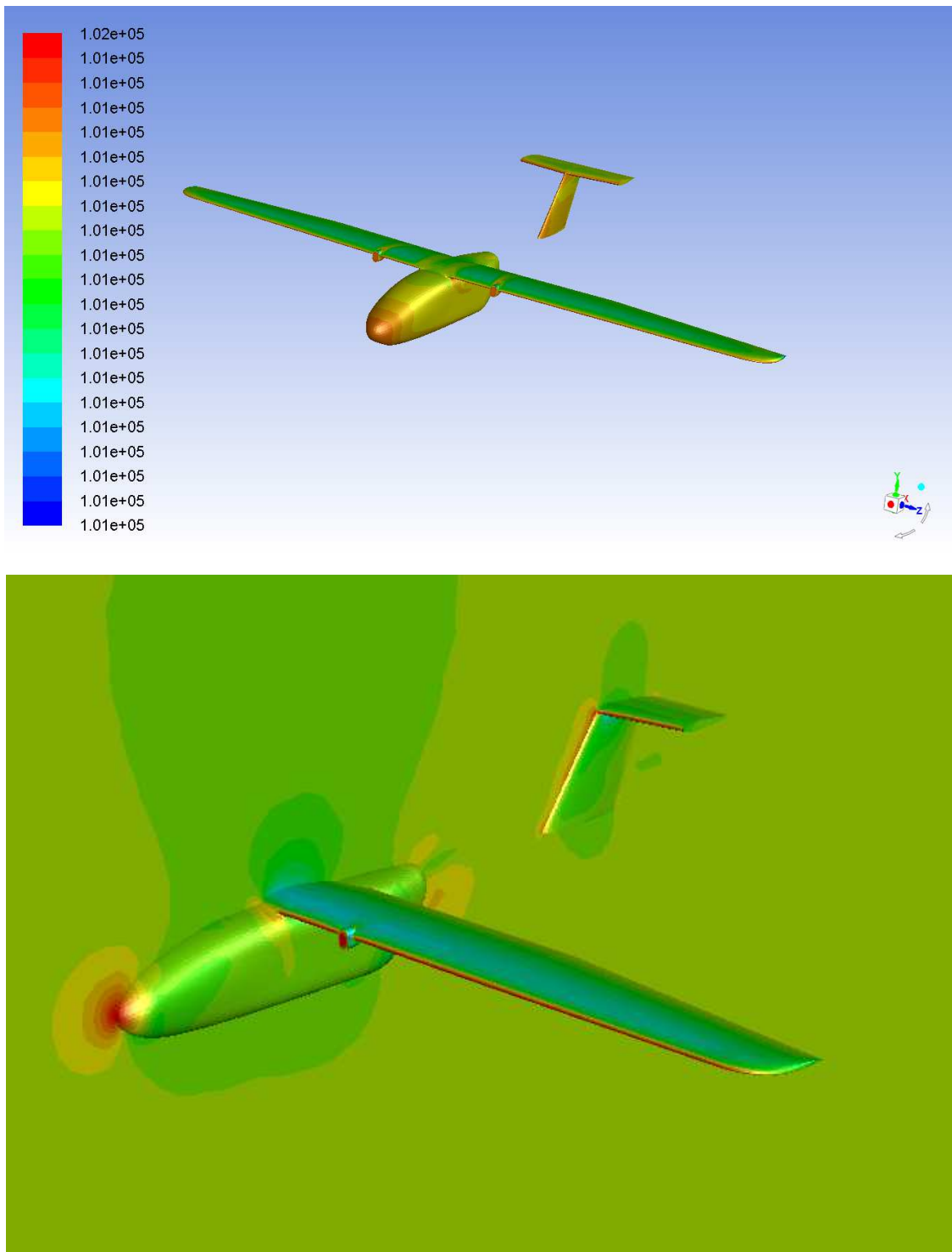
Figure III. 12 Total pressure distribution

III.   SIMULATION RESULTS

The simulation results using this CFD model with different angles of attack are plotted in different curves.

Table III. 1 CFD results

$Alpha$	cm	C_L	C_D	C_L/C_D	$C_L^{3/2}/C_D$	C_L^2
-6	0.1202	-0.1666	0.0462	-3.6072	-	0.0277
-4	0.0746	0.0130	0.0404	0.3209	0.0366	0.0002
-2	0.0322	0.1896	**0.0388**	4.8914	2.1300	0.0360
0	0.0100	**0.3681**	**0.0406**	9.0750	5.5063	0.1355
2	-0.0432	0.5416	0.0471	11.5066	8.4680	0.2933
4	-0.0813	0.7114	0.0555	12.8257	10.8175	0.5060
6	-0.1120	0.8701	0.0674	**12.9001**	12.0328	0.7570
8	-0.1483	1.0042	0.0815	12.3211	**12.3467**	1.0084
10	-0.1820	1.0915	0.0996	10.9539	11.4441	1.1914
12	-0.2289	1.1098	0.1387	8.0032	8.4311	1.2317
14	-0.2960	1.0921	0.2088	5.2294	5.4649	1.1927
16	-0.2665	1.0491	0.2478	4.2331	4.3358	1.1006
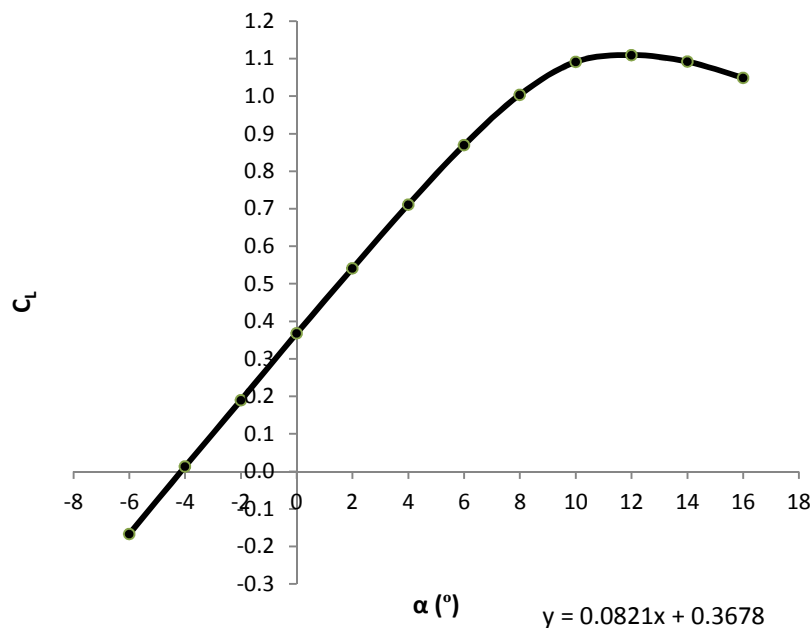
Figure III. 13 Lift coefficient curve vs AOA

The lift curve simulation result has the same tendency of the Clark Y 2D profile **Figure II.10 (J.Robertson)** and a maximum lift coefficient $C_{L_{max}}$ of 1.11 at 12 degree; in other hand this result is less than $C_{L_{max}} = 1.15$ which was assumed in the beginning (Eq. II.3) with 0.03, but steel an acceptable result taken in consideration a little increase of stall velocity in this level (without wind tunnel results).

$$V_{stall} = \sqrt{\frac{W}{\frac{1}{2}\rho\, S\, C_{Lmax}}} = \sqrt{\frac{0.45\ 9.81}{\frac{1}{2}\ 1.225\ 0.579\ 1.11}} = 10.59 \text{ m/s} \tag{III.2}$$

The lift curve slope (C_{L_α}) is another important performance feature of an aircraft, from the linear $C_{L_\alpha} = 0.0821\ \frac{1}{deg} = 4.70\ \frac{1}{rad}$, this lift curve slope can be compared with equation:

$$C_{l_\alpha} = \frac{dC_l}{d\alpha} = 1.8\ \pi\ \left(1 + 0.8\ \frac{t_{max}}{C}\right) \tag{III.3}$$

$\frac{t_{max}}{C} = 11.73\%$ represent the Clark Y airfoil thickness max

$$C_{l_\alpha} = 1.8\ \pi\ (1 + 0.8\ 0.1173) = 6.18\ \frac{1}{rad} = 0.108\ \frac{1}{deg}$$

To get the aircraft lift curve slope C_{L_α} with indices "L" the following empirical equation can be used:

$$C_{L_\alpha} = \frac{dC_L}{d\alpha} = \frac{C_{l_\alpha}}{1 + \frac{C_{l_\alpha}}{\pi\ AR}} \tag{III.4}$$

$$C_{L_\alpha} = \frac{6.18}{1 + \frac{6.18}{\pi\ 10.82}} = 5.23\ \frac{1}{rad}$$

Compare to CFD result $C_{L_\alpha} = 4.70\ \frac{1}{rad} < 5.23\ \frac{1}{rad}$ this CFD result will be adopted to get aircraft performance.

The takeoff analysis will be performed at zero angle of attack correspond to $C_L = 0.37$
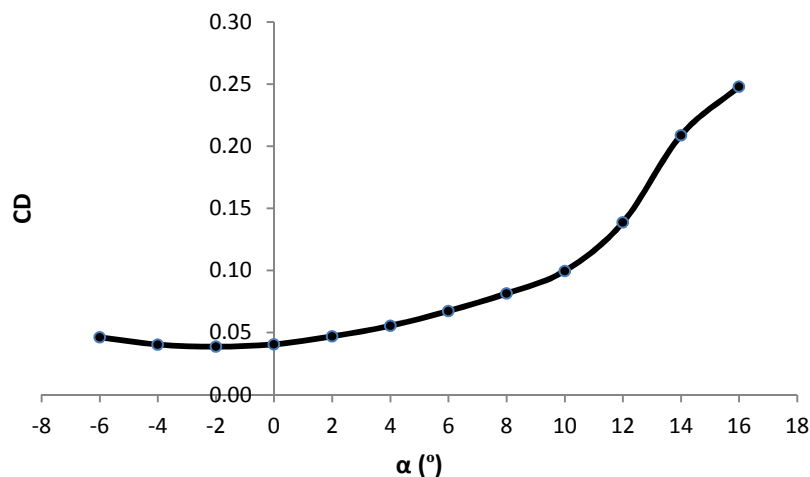
Figure III. 14 Drag coefficient curve versus AOA

Figure III.14 shows the variation of drag coefficient as function of angle of attack. The lowest point of this graph $C_D = 0.0388$ at -2 degree is called minimum drag coefficient $C_{D\,min}$. As the drag is directly related to the cost of flight, $C_{D\,min}$ is of great importance in airfoil selection.
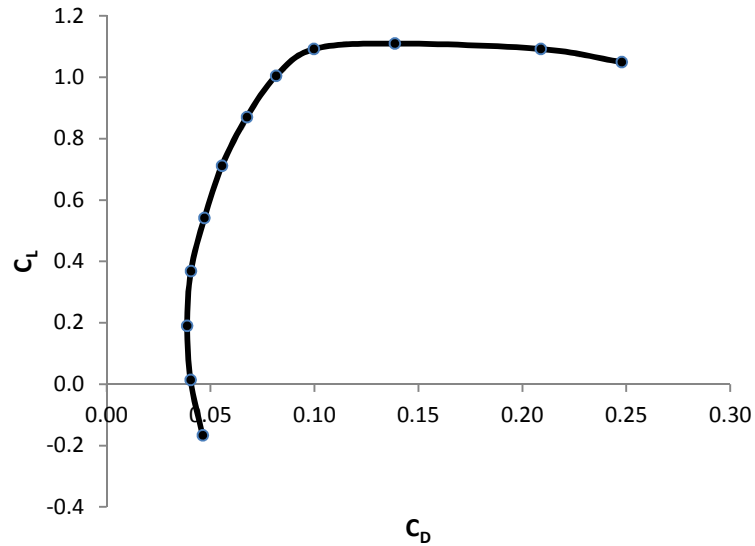
Figure III. 15 Polar curve

From the Polar graph a maximum lift to drag ratio is about $C_L/C_D = 12.90$ at 6 degree angle of attack, to get the maximum range is perfect to fly near to this angle of attack [02].
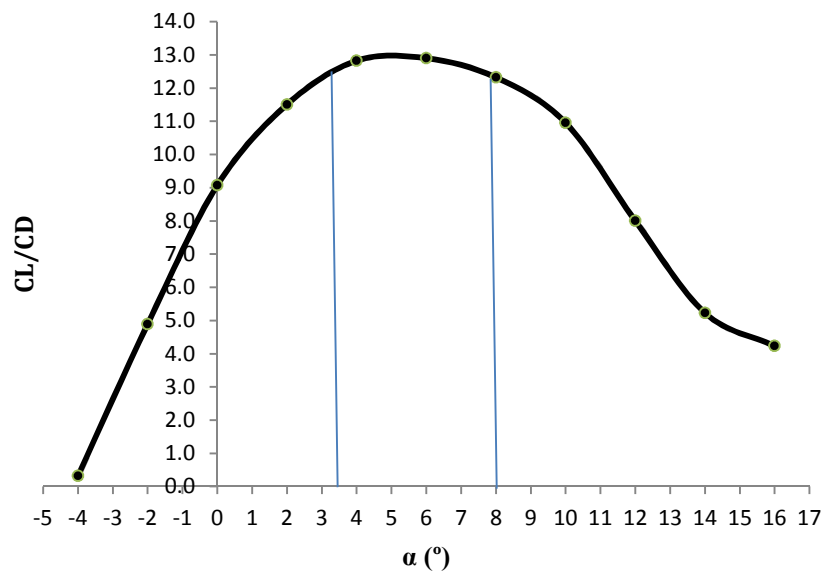
Figure III. 16 Lift to drag ratio versus AOA

Calculate cruise lift coefficient: From chapter II the mini UAV cruise velocity is 50 km/h and $C_{L\,max} = 1.15$ at 300 m

$$C_{L\,cruise} = \frac{W}{\frac{1}{2}\rho\,S\,V_C^2} \tag{III.5}$$

$$C_{L\,cruise} = \frac{0.45 \; 9.81}{\frac{1}{2} \; 1.19 \; 0.579 \; 13.89^2} = 6.66 \; @ \; 3.61 \; \text{degrees}$$

From lift to drag ratio curve versus angle of attack has a better range between **[3.5 to 8]** of flying angles, the angle of attack of 3.61 degrees is in the range.
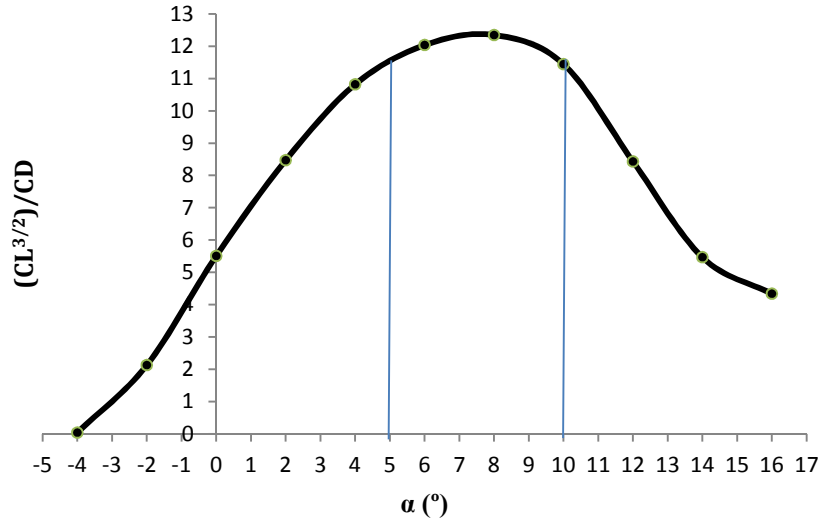
Figure III. 17 (CL³/²)/CD versus AOA

The **figure III.12** characterize $\left(C_L^{3/2}/C_D\right)$ versus AOA, with $\left(\frac{C_L^{3/2}}{C_D}\right)_{max} = 12.35 \; @ \; 8°$, the range [5 to 10] of angles of attack has the highest $\left(C_L^{3/2}/C_D\right)$, this range is useful to get the maximum endurance [02].
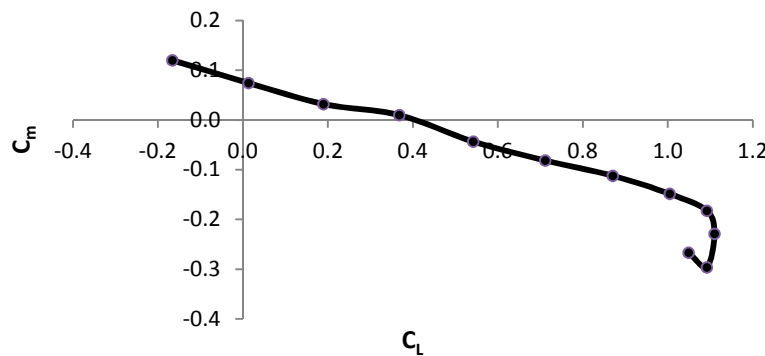
Figure III. 18 Moment coefficient versus Lift coefficient

The moment coefficient versus angle of attack **Figure III.18** simulates at CG of 35% from wing chord, the linear part of this curve gives the moment lift coefficient slope equal to $\frac{dC_m}{dC_L} = -23.21\%$.

This 23.21% is the distance between **CG** and the aerodynamic center **ac** called static margin, ac is at $35 + 23.21 = 58.21\%$ mac.

The moment coefficient has a negative slope and a positive $C_{m0} > 0$ that means the UAV is statically stable.

IV. CONCLUSION

This UAV model has an acceptable result in view of aerodynamics characteristics designed during the preliminary conception and aerodynamic design **chapter II**.

Different parameters result can be resumed in this table:

Table III. 2 CFD Analysis results

Parameter	Result
$C_{L_{max}}$	1.15
C_{L_α}	0.0821
α_{max}	12 degree
$C_{L_{\alpha=0}}$	0.36
$\alpha_{C_L=0}$	4.2 degree
$C_{D_{min}}$	0.0388
$\alpha_{C_{D_{min}}}$	-2
C_{D_0}	0.035
$(C_L/C_D)_{max}$	12.90
$\alpha_{(C_L/C_D)_{max}}$	6 degree
$\left(C_L^{3/2}/C_D\right)_{max}$	13.25
$\alpha_{\left(C_L^{3/2}/C_D\right)_{max}}$	8 degree
$\dfrac{dC_m}{dC_L}$	0.2321
C_{m_0}	0.08
$C_{L_{C_m=0}}$	0.41

I.   SCOPE:

This chapter describes the definitions and principles of flight performance and the steps to calculate Power Available and Power required, and provides the performance analysis of envelope curve, Climb and Ceiling, Descent in detail, as well as typical Profiles Performance Calculation. The chapter also answers the question whether the flight performance of the design of aircraft can meet the requirements of mini UAV specification.

II.   POWER PLANT AND BATTERY DEFINE

The UAV is powered by two electrical engines driving a fixed-pitch puller propeller with Two-blades.

II.1   Electric motor selection:

There are two different types of electric motors that can be used. The first type is **the brush motor** which has an internal contact between the brush and the armature. During high frequency switching this contact may cause arcing and heating especially at high currents. This problem contributes to a major hindrance in its cooling. Motor cooling is directly related to establishing maximum efficiency.

The second type is **the brushless motor**, which generates higher torque with less heat because the effective resistance of the brushes is much higher. Foremost, brushless motors can fit much thicker wires than a brush motor of equivalent size, thus lowering resistance, increasing efficiency, and increasing torque. Because of these facts, brushless motors have the inherent capability to spin faster, operate at higher currents, and produce more power without the performance deteriorating at high currents and temperatures. Hence, most recent SUAVs have been using the lighter-weight, smaller brushless type motor in order to get higher power with less radio noise generated to interfere with the avionics. This benefit will increase the reliability of the communication between airplane and ground station. A recently developed rotating-case brushless motor has been designed to produce higher torque and therefore allow the use of large size propellers without gearboxes.

A **Sunny Sky 2216** brushless outrunner motor is selected to estimate our mini UAV performance based on similar typical UAVs and the steps cited in *APPENDIX C* .

Table IV. 1 Typical UAVs Motor

UAV	Motor type	Motor kv (kv)
Skywalker EVE-2000	Skywalker2816	650
Skywalker TITAN	Skywalker2820	650
Sky Observer	Out-runner brushless 4250	950

II.2   Propeller:

Since a mini UAV flies at low speed with Sunny Sky brushless motor of a small Kv around $800kv$ with a gross weight layout about 4500 grams, these refer to a large size propeller diameter 10 inch or more and attend to select a two blades fixed-pitch propeller **APC 11×4.7**. (**APPENDIX C**)

This propeller has a successful adaptation with the select motor. Furthermore a

series of tests were done to this propeller illustrated on. (**APPENDIX C**)

II.3   Battery selection:

Flight duration is mainly dependent upon battery's performance. It's better to have a lightweight battery with a high capacity under high loaded conditions, as well as having a high energy density (Wh/kg). Recently, battery technology has risen to a new level. Representative of these new higher energy density batteries are: disposable LiSO2 (Lithium Sulpher Oxide), rechargeable LiON (Lithium Ion), and rechargeable Lithium-Polymer [11].

Two Lithium-Polymer batteries are chosen for the mini UAV because of its high energy density and cost effective, reusable characteristics.

Table IV. 2 Specifications of selected battery [11]

Specification	Thunder power 2050 4S4P
Nominal Capacity	7600mA (**112.5 Wh**)
Output	14.8 V
Dimension	50mm x 245 mm x 28 mm (616 g)
Applications	RC aircraft and helicopters
Max. Current Rating	5C max Avg. Discharge
Impedance (ohm)	0.0125
Energy Density (Wh/kg)	182.6

III.   DRAG ESTIMATION

The aircraft drag can be expressed:

$$C_D = \frac{1}{2} \rho V^2 S C_D \tag{IV.1}$$

The drag coefficient breakdown is:

$$C_D = C_{Dp} + C_{Di} \tag{IV.2}$$

$$C_D = C_{D0} + C_{Di} \tag{IV.3}$$

$$C_D = C_{D0} + k C_L^2 \tag{IV.4}$$

$$k = \frac{1}{\pi\, AR\, e} C_L^2 \tag{IV.5}$$

      To find the drag coefficient C_D, C_{D0} (parasite drag) should be determined. For this a **buildup method** [01] will be used.

      The Oswald efficiency factor **e** is a parameter, which expresses the total variation of drag with lift [02]. It would be 1.0 for an elliptically loaded wing with no lift-dependent viscous drag. We can obtain an Oswald efficiency factor, 0.735, from the following equation**:**

      $$e = 1.78\,(1 - 0.045\, AR^{0.68}) - 0.64 \tag{IV. 6}$$

      Where AR=10.82, and leading edge sweep angle (Λ_{LE}) smaller than 30°

After calculation of C_{D0} and k from Oswald efficiency, C_D can be exploited.

III.1   Determine the parasite drag components by buildup method :

      The component buildup method estimates the subsonic parasite drag of each component "form factor" (**FF**) that estimates the pressure drag due to viscous separation. Then the interference effects on the component drag are estimated as a factor "Q" and the total component drag is determined as the product of the wetted area. **Cf**, **FF**, and **Q**. [01]

(Note that the interference factor **Q** should not be closed with dynamic pressure **q**.)

      Miscellaneous drags (CD_{misc}) for special features of an aircraft such as flaps, unretracted landing gear, an upswept aft fuselage, and base area are then estimated and added to the total, along with estimated contributions for leakages and protuberances ($C_{D_{L\&P}}$). Subsonic parasite-drag buildup is shown in the following equation, where the subscript "**c**" indicates that those values are different for each component. [01]

$$(C_{D0})_{subsonic} = \frac{\sum(C_{fc} FF_c Q_c S_{wet_C})}{S_{ref}} + C_{D_{misc}} + C_{D_{L\&P}} \tag{IV.7}$$

III.1.1 <u>Flat-plate friction coefficient</u>

For turbulent flow, which in most cases covers the whole aircraft, the flat-plate skin friction coefficient is determined by the C_f equation . Note that the second term in the denominator, the Mach number correction, goes to 1.0 for low-subsonic flight.

$$C_f = \frac{0.455}{(log_{10}R)^{2.58}(1+0.144M^2)^{0.65}} \tag{IV.8}$$

III.1.2 <u>Component form factors:</u>

Form factors for subsonic-drag estimation are presented for different components. These are considered valid up to the drag-divergent Mach number. In equation IV.9, the term "$(x/c)_m$" is the chordwise location of the airfoil maximum thickness point. From most low-speed airfoils, this is at about 0.3 of the chord [01].

Wing, tail, strut, and pylon:

$$FF = \left[1 + \frac{0.6}{(^x/_c)_m}\left(\frac{t}{c}\right) + 100\left(\frac{t}{c}\right)^4\right]\left[1.34M^{0.18}(\cos\Delta_m)^{0.28}\right] \tag{IV.9}$$

Fuselage and smooth canopy:

$$FF = \left(1 + \left(\frac{60}{f^3}\right) + \left(\frac{f}{400}\right)\right) \tag{IV.10}$$

Nacelle and smooth external store:

$$FF = 1 + \left(\frac{0.35}{f}\right) \tag{IV.11}$$

Where

$$f = \frac{l}{d} = \frac{l}{\sqrt{(^4/_\pi)A_{max}}} \tag{IV.12}$$

III.1.3 <u>Component interference factors:</u>

Parasite drag is increased due to the mutual interference between components. For a nacelle or external store mounted directly on the fuselage or wing, the interference factor Q is about 1.5. For more accuracy the fuselage is split to two parts a body and a boom because of the dramatically changing of size [01].

For a high-wing, a midwing, or a well-filletted low wing, the interference will be negligible so the Q factor will be about 1.0 [01].

The fuselage has a negligible interference factor (Q=1.0) in most cases. For tail surfaces, interference ranges from about 3% (Q=1.03) for a clean V-tail to about 8% for H-tail. For a conventional tail, 4-5% may be assumed. [01]

Component parasite drags can now be determined using Eq. IV.7 and the skin friction coefficients, from factors, and interference factors [01].

III.1.4 Miscellaneous drags:

The gear drag can be estimated as the summation of the drags of the wheels, struts, and other gear components using the data of the table 12.5 (from Ref [01]).

These values time the frontal area of the indicated component yield **D/q** values. The drag presented as drag divided by dynamic pressure (**D-over-q or D/q**). **D/q** has unit of square feet (or meters) and so is sometimes called the "drag area".

D/q divided by the wing reference area yields the miscellaneous parasite drag coefficient.

Our landing gear is considered as regular wheel and tire, than these values can be chosen.

FOR NOSE GEAR:

For tire: $\left(\frac{D_{noise\,tire}}{q}\right) \Big/ FA = 0.25$ FA: Frontal area   (IV.13)

$$FA = 0.0011 \; m^2$$

So

$$\left(\frac{D_{noise\,tire}}{q}\right) = 0.0002625$$

From this

$$C_{D\,noise\,tire} = \left(\frac{D_{noise\,tire}}{q\,S_{ref}}\right) = 0.0002625$$

For structure: $\left(\frac{D_{noise\,str}}{q}\right) \Big/ FA = 1.2$ FA: Frontal area   (IV.14)

$$FA = 0.002 \; m^2$$

So

$$\left(\frac{D_{noise\,str}}{q}\right) = 0.0024$$

From this

$$C_{D\,noise\,str} = \left(\frac{D_{noise\,str}}{q\,S_{ref}}\right) = 0.0042$$

$$C_{D\,noise\,gear} = C_{D\,noise\,tire} + C_{D\,noise\,str} = 0.0047$$

FOR MAIN GEAR:

For tire: $\left(\frac{D_{main\,tire}}{q}\right) \Big/ FA = 0.25$ (IV.15)

$$FA = 0.0021 \; m^2$$

So

$$\left(\frac{D_{main\,tire}}{q}\right) = 0.0002625$$

From this

$$C_{D\,main\,tire} = \left(\frac{D_{noise\,tire}}{q\,S_{ref}}\right) = 0.000525$$

For structure: $\left(\frac{D_{noise\,tire}}{q}\right)\Big/_{FA} = 1.2$ (IV.16)

$$FA = 0.0025\,m^2$$

So

$$\left(\frac{D_{noise\,tire}}{q}\right) = 0.003$$

From this

$$C_{D\,main\,str} = \left(\frac{D_{noise\,str}}{q\,S_{ref}}\right) = 0.0053$$

$$C_{D\,main\,gear} = C_{D\,main\,tire} + C_{D\,main\,str} = 0.0062$$

Total

$$C_{D0\,gear} = C_{D\,noise\,gear} + C_{D\,main\,gear} = \mathbf{0.0109}$$

III.1.5 Leakage and proturbance drag

Proturbances include antennas, lights, and such manufacturing defects. Typically these dag increments are estimated as a percent of the total parasite drag, from 5-10% for propeller aircraft [01].

Table IV. 3 Subsonic C$_{D0}$ estimation

Parameters		Wing	V-tail	H-tail	Boom	Fuselage
Velocity V (m/s)		13.88	13.88	13.88	13.88	13.88
	Viscosity μ × 10^{-5} ($kg\,s/m^2$)	1.8187	1.8187	1.8187	1.8187	1.8187

	Densityρ (kg/m^3)	1.1901	1.1901	1.1901	1.1901	1.1901
	Speed of sound a (m/s)	339.27	339.27	339.27	339.27	339.27
	l (m)	0.23	0.21	0.146	0.63	0.7
	$Mach$ M	0.0409	0.0409	0.0409	0.0409	0.0409
	Re	208927	207876	143224	620075	684640
	C_{fc}	0.0061	0.0061	0.0066	0.0049	0.0048
	Q	1.0	1.03	1.08	1.3	1.0
	S_{wet} (m^2)	1.114	0.107	0.177	0.059	0.404
	$(x/c)_m$	0.302	0.3	0.3	/	/
	(t/c)	0.117	0.12	0.12	/	/
$C_{D0} = \dfrac{\sum (C_{fc} FF_c Q_c S_{wet_C})}{S_{ref}}$		0.0111	0.0012	0.0023	0.0014	0.0097
		0.0257				
$C_{D L\&P} = 10\%$ of C_{D0}		+10%				
$(C_{D0})_{subsonic}(UAV\ clean\ configuration)$		0.0283				
$C_{D0} = C_{D\,Miscellaneous}\ (LG: landing\ gear)$		0.0109				
$(C_{D0})_{subsonic}(UAV\ configuration\ with\ LG)$		0.0403				

After C_{D0} estimation the total C_D can be determined:

$$C_D = C_{D0} + K C_L^2$$

$$k = \frac{1}{\pi\ AR\ e} = \boldsymbol{0.040} \qquad for\ AR = 10.82\ \ e = 1.78\ (1 - 0.015\ AR^{0.68}) - 0.64 = 0.735$$

$$\boldsymbol{C_D = 0,0403 + 0,04\ C_L{}^2}$$

IV.   PERFORMANCE FOR STEADY LEVEL FLIGHT

IV.1   Assumption:

- Unaccelerated level flight ;
- Incidence angle neglected ;
- Horizontal flight ;
- Uniform movement ;
- Symmetrical flight ;
- T the thrust with flight direction path ;
- P=m g on the SUAV symmetrical plan.

IV.2   Equilibrium forces:
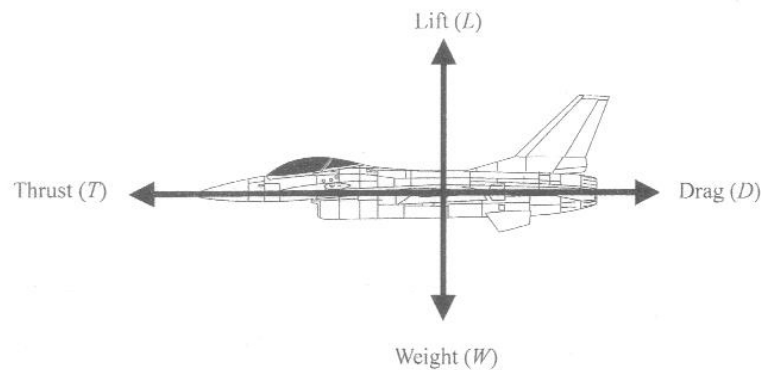
Figure IV. 1 Simplified illustration of four forces acting on an aircraft

Forces decomposition:

$$T - D = 0 \tag{IV.17}$$

And:

$$L - mg = 0 \tag{IV.18}$$

IV.3   Stall speed:

Stall is defined as reduction in lift coefficient due to flow detachment as a result of high angle of attack. Theoretical has been calculated using the following equation;

$$V_{stall} = \sqrt{\frac{2\,m\,g}{\rho\,S\,C_{L_{max}}}} \tag{IV.19}$$

$$C_{L_{max}} = 1.11$$

$$V_{stall} = \sqrt{\frac{W}{\frac{1}{2}\,\rho\,S\,C_{L_{max}}}} = \sqrt{\frac{0.45\ 9.81}{\frac{1}{2}\ 1.225\ 0.579\ 1.11}} = 10.59 \text{ m/s}$$

IV.1   Lift to drag ratio:

The lift to drag ratio is calculated as fallow:

$$\left(\frac{L}{D}\right)_{max} = \sqrt{\left(\frac{1}{(4\,K\,C_{D0})}\right)} \tag{IV.20}$$

The lift the drag ratio of a clean configuration (wing, fuselage and tail) is:

$$\left(\frac{L}{D}\right)_{max} = \sqrt{\frac{1}{(4\,0.040\,0.0283)}} = 14.86$$

From CFD C_{D0} =0.035

$$\left(\frac{L}{D}\right)_{max} = \sqrt{\frac{1}{(4\,0.040\,0.035)}} = 13.36$$

The lift to drag ratio of a min UAV with landing gear is:

$$\left(\frac{L}{D}\right)_{max} = \sqrt{\frac{1}{(4\,0.040\,0.0403)}} = 12.0$$

For the next phases of this chapter C_{D0} =0.0403 and $\left(\frac{L}{D}\right)_{max} = 12.0$ with landing gear is defined to calculate the rest of performance.

IV.2   Velocity for minimal drag:

They state simply that, in level flight, thrust equals drag and lift equals weight. These are expressed using aerodynamic coefficients for the analysis that follows.

$$T = D = q\,S(CD_0 + k\,C_L^2) \tag{IV.21}$$

$$L = W = q\,S\,C_L \tag{IV.22}$$

$$V = \sqrt{\frac{2}{\rho\,C_L}\left(\frac{W}{S}\right)} \tag{IV.23}$$

These equations imply that the actual T/W in level flight must be the inverse of the L/D at that flight condition. The T/W and L/D in level flight can be expressed in terms of the wing loading and dynamic pressure by substituting in Eq. IV.21 into Eq. IV.20, as follows[01]:

$$\frac{T}{W} = \frac{1}{L/_D} = \frac{q\,C_{D_0}}{W/S} + \left(\frac{W}{S}\right)\frac{k}{q} \tag{IV.24}$$

Table IV. 4 velocity effect on typical performance parameters

$H = 0m$							
$V(km/h)$	30	40	50	60	70	80	90
$V(m/s)$	8.33	11.11	13.89	16.67	19.44	22.22	25.00
ρ	1.225	1.225	1.225	1.225	1.225	1.225	1.225
$q = \frac{1}{2}\rho V^2 (N/m^2)$	42.53	75.62	118.15	170.14	231.58	302.47	382.81
$W(kg)$	4.5	4.5	4.5	4.5	4.5	4.5	4.5
$S\ (m^2)$	0.578	0.578	0.578	0.578	0.578	0.578	0.578
$C_L = \dfrac{W}{q\,S}$	1,79	1,01	0,64	0,45	0,33	0,25	0,20
$Lift\ (N) = \frac{1}{2}\rho V^2 S\, C_L$	44,10	44,10	44,10	44,10	44,10	44,10	44,10
C_{D0}	0,04	0,04	0,04	0,04	0,04	0,04	0,04
$D_0(N) = \frac{1}{2}\rho V^2 S\, C_{D0}$	0,99	1,76	2,76	3,97	5,40	7,06	8,93
k	0,04	0,04	0,04	0,04	0,04	0,04	0,04
$D_i(N) = \frac{1}{2}\rho V^2 S\, k\, C_L{}^2$	3,16	1,78	1,14	0,79	0,58	0,44	0,35
$Drag(N) = D_0 + D_i = P_R(N)$	4,15	3,54	3,89	4,76	5,98	7,50	9,28
CL/CD	10,62	12,45	11,32	9,27	7,37	5,88	4,75
T/W	0,09	0,08	0,09	0,11	0,13	0,17	0,21

From table IV.3 the following figure represent the different Drags sources versus UAV velocity (D_0 :zero-lift drag, D_i :drag due to lift and D_T : Total drag)
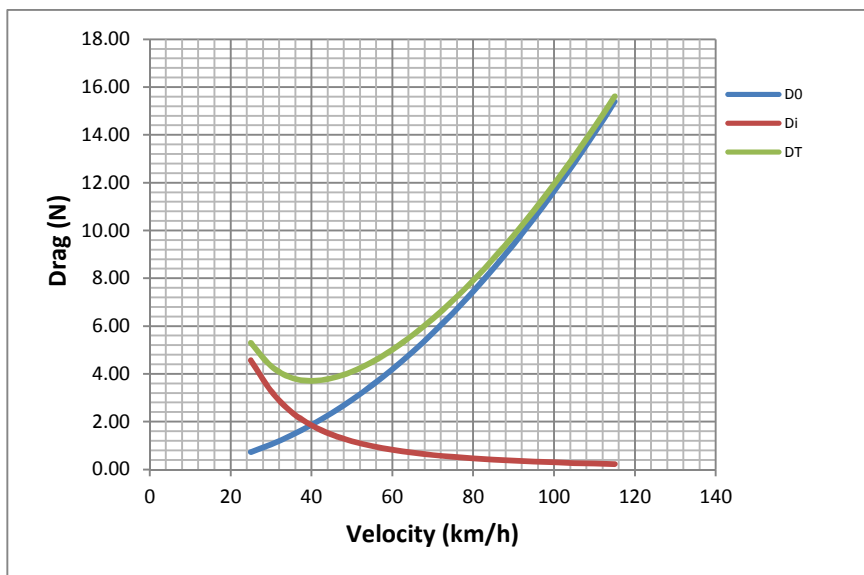
Figure IV. 2 Drag components vs aircraft velocity

The velocity of the minimum drag from the above curve is $11.11\frac{m}{s} = 40\ \frac{km}{h}$

IV.3   Minimum thrust required for level flight:

From Eq. IV.24 it follows that the condition for minimum thrust at a given weight is also the condition for minimum L/D. To find the velocity at which thrust is minimum and L/D is maximum use the following equations [01].

$$\frac{\partial (^T/_W)}{\partial V} = \frac{\rho\, V\, C_{D_0}}{W/_S} - \frac{W}{S}\frac{2\,k}{\frac{1}{2}\rho\, V^3} = 0 \qquad\qquad (IV.25)$$

$$V_{(min\,thrust\,or\,drag)} = \sqrt{\frac{2W}{\rho S}\sqrt{\frac{K}{C_{D0}}}} \qquad\qquad (IV.26)$$

$$V_{(min\,thrust\,or\,drag)} = \sqrt{\frac{2\;4.5\;9{,}81}{1.1901\;0{,}579}\sqrt{\frac{0{,}04}{0{,}0403}}}$$

$$V_{(Dmin)} = 11.29\,\frac{m}{s} = 40.64\,\frac{km}{h}$$

$$C_{L(min\,thrust\,or\,drag)} = \sqrt{\frac{C_{D0}}{K}} \qquad\qquad (IV.27)$$

$$C_{L(min\,thrust\,or\,drag)} = \sqrt{\frac{0.0403}{0.04}} = 1.003$$

The total drag at the lift coefficient for minimum drag is a twice the zero-lift drag [01]

$$D_{min\,thrust\,or\,drag} = q\,S\left[CD_0 + k\left(\sqrt{\frac{CD_0}{k}}\right)^2\right] = q\,S(CD_0 + CD_0) \qquad\qquad (IV.28)$$

$$D_{min\,thrust\,or\,drag} = \left(\frac{1}{2}\;1.1901\;11.29^2\right)0{,}579\,(0.0403 + 0.0403) = 3.54\,N$$

IV.4   Power Required for Level Flight:

The conditions for minimum thrust and minimum power required are not the same. Power is force times velocity, which in steady level flight equals the drag times the velocity [01].

$$P = D\,V = qS(C_{D_0} + KC_L^2)\,V = \frac{1}{2}\rho V^3 S(C_{D_0} + KC_L^2) \qquad\qquad (IV.29)$$

$$P = \frac{1}{2}\rho V^3\,SC_{D_0} \qquad\qquad (IV.30)$$

The velocity for flight on minimum power is:

$$V_{(Pmin)} = \sqrt{\frac{2mg}{\rho SC_{L(Pmin)}}} = \sqrt{\frac{2mg}{\rho S}\sqrt{\frac{K}{3C_{D0}}}} \qquad\qquad (IV.31)$$

$$V_{(Pmin)} = \sqrt{\frac{2\ 4.5\ 9{,}81}{1{,}225\ 0.579}\sqrt{\frac{0{,}040}{3 \times 0{,}0403}}}$$

$$V_{(Pmin)} = 8.32\ m/s$$

$$C_{L(Pmin)} = \sqrt{\left(\frac{3C_{D0}}{K}\right)} \tag{IV.32}$$

$$C_{L(Pmin)} = \sqrt{\left(\frac{3\ 0.0403}{0.040}\right)} = 1.73 \text{ rejected (behind stall speed)}$$

$$V_{(Pmin)} \text{ correspond to } C_{L(Pmin)} \text{ also rejected.}$$

IV.5 Maximum speed:

The maximum velocity analysis procedure of the airplane is determined by the high speed intersection of the **thrust required** and **thrust available curves**.

1- Thrust available curve determination:

Given the wing loading (weight and area), the aircraft drag polar (C_{DO}, K), and the density of **each altitude**:

1- Choose a value for V_i ;

2- For the chosen V_i, calculate the propeller advanced ratio with a high $rpm\left(\frac{r}{min}\right)$ from the relation

$$J = \frac{V}{n\,D} \tag{IV.33}$$

- n propeller rotation $\left(\frac{r}{min}\right)$
- D propeller diameter (m)

3- Determine C_T et C_P from advanced ratio **APPENDIX C;**

4- Calculate thrust of motor from

$$T(N) = C_T\,\rho\,n^2\,D^4 \tag{IV.34}$$

5- Multiply by 2 to get thrust of two motors

6- Repeat steps 1 to 5 for different values of velocity ;

7- Repeat steps 1 to 6 for different altitude.

These steps are resumed in the following table

Table IV. 5 The thrust available

h=0m $\rho = 1.225\ kg/m^3$						
V(Km/s)	30	40	50	60	70	80
V(m/s)	8,33	11,11	13,89	16,67	19,44	22.2
n propeller rotation $\left(\frac{r}{min}\right)$	6000	6000	6000	6000	6000	6000
D propeller diameter (m)	0.2794	0.2794	0.2794	0.2794	0.2794	0.2794
J Advanced ratio	0.11	0.10	0.08	0.03	0.03	0.01
$T(N) = C_T\,\rho\,n^2\,D^4 \times 2$ (tow motors)	16,86	14,42	11,62	8,47	4,97	1, 12

So, the curve will be presented with the thrust required curve

1- Thrust required curve determination:

The thrust required is the sufficient thrust to eliminate the aircraft drag, it was calculated in the **Table IV. 4** $Drag(N) = P_R(N)$
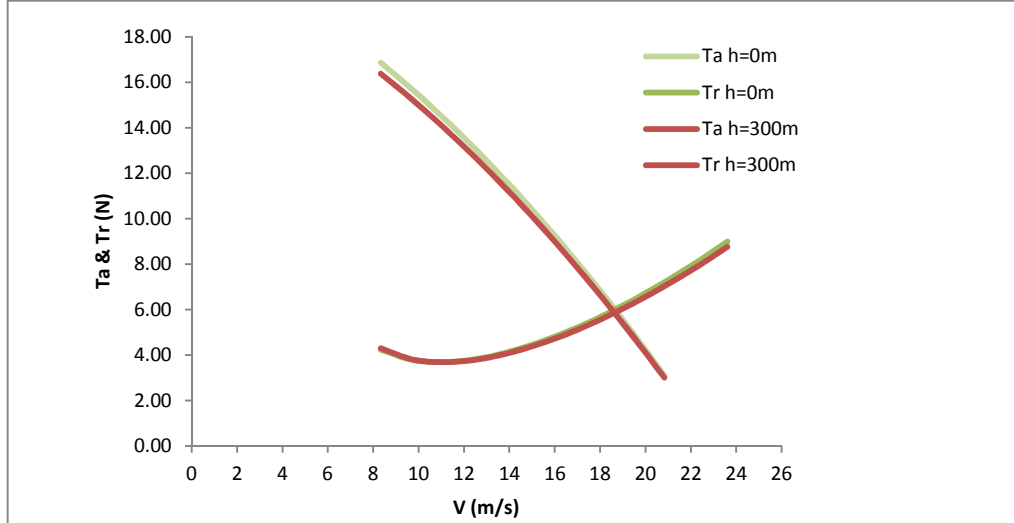
Figure IV. 3 the maximum velocity of the (propeller) mini UAV

From the figure the maximum speed has a small variation with altitude with an average velue of $18.7 \frac{m}{s} = 67.32 \frac{km}{h}$

IV.6   Minimum speed:

In general, Minimum speed can be determined by the stall speed of the airplane in the steady level flight. By definition, V_{min} is much dependent on $C_{L_{max}}$ and wing loading.

$$W = \frac{1}{2} \rho V^2 S C_{L_{max}} \tag{IV.35}$$

$$V_{min} = (\frac{2W}{\rho SCL_{max}})^{0.5} \tag{IV.36}$$

By means of the formulas, we get these results in table:

Table IV. 6 Minimum speed for different altitudes

$C_{L_{max}} = 1.15$

H(m)	0	50	100	150	200	250	300	350
$\rho\ (kg/m^3)$	1.225	1.2191	1.2133	1.2075	1.2017	1.1959	1.1901	1.1844
$V_{min}\ (m/s)$	10.385	10.410	10.435	10.460	10.485	10.511	10.536	10.561

The mini UAV flight envelope at sea level is between $V_{min} = 10.385\ (m/s)\ to\ V_{max} = 18.6\ (m/s)$ with

V.   CLIMB PERFORMANCEAND CEILING ANALYSIS

Rate of climb depends on raw power in combination with the weight of the airplane. The higher the thrust corresponds to lower the drag and the lower the weight, the better the climb performance.

The rate of climb is defined as the vertical component of the airplane's velocity, it depends on the UAV weight and excess power.

$$R/_C = \frac{(\text{Excess power})}{W} = \frac{(T-D)V}{W} \tag{IV.37}$$

$$\sin y = \frac{T-D}{W} = \frac{R/C}{V} \tag{IV.38}$$

The climb angle is defined as

$$y_c = arc(\sin y) \text{ (Degrees)} \tag{IV.39}$$

We follow these steps:

- Calculation for different altitudes.
- Calculate rate of climb max for each altitude.
- Calculation up to cruise altitude.
- Draw curve altitude function rate of climb max.

The analysis procedure:

Given the wing loading (weight and area), the aircraft drag polar (C_{DO}, K), and the density of **each altitude**:

1- Choose a value for V_i ;

2- For the chosen V_i, calculate the propeller advanced ratio with a high $rpm \left(\frac{r}{min}\right)$ from the relation

$$J = \frac{V}{n\,D} \tag{IV.40}$$

- n propeller rotation $\left(\frac{r}{min}\right)$
- D propeller diameter (m)

3- Determine C_T et C_P from advanced ratio **APPENDIX C;**

4- Calculate thrust of motor from

$$T(N) = C_T\,\rho\,n^2\,D^4 \tag{IV.41}$$

Multiply by 2 to get thrust of two motors

5- From **Table IV. 4** the thrust required **:**

$$D(N) = T_R(N) \tag{IV.42}$$

6- Calculate the access power $(T-D)$;

7- Rate of climb $R/_C = \frac{(\text{Excess power})\,V}{W} = \frac{(T-D)V}{W}$;

8- Calculate angle of climb $y_c = arc(\sin y)$;

9- Repeat steps 1 to 8 for different values of velocity ;

10-Repeat steps 1 to 9 for different altitude.

After calculation:

Table IV. 7 Rate and angle of climb for different altitudes

$H\ (m)$	$R/C_{max}\ (m/s)$	$y_C(\text{º})$
0	2.710	14.117
100	2.675	13.93
200	2.641	13.75
300	2.606	13.569
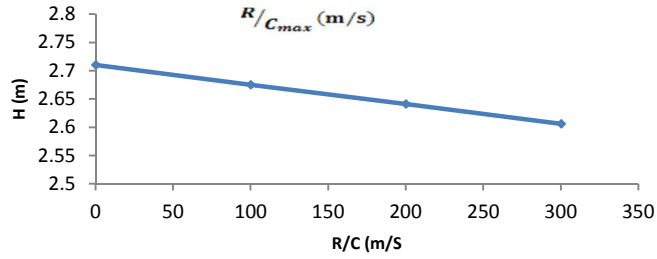
Figure IV. 4 Rate of climb for different altitudes

Maximum speed

VI.   DESCENTE PERFORMANCES
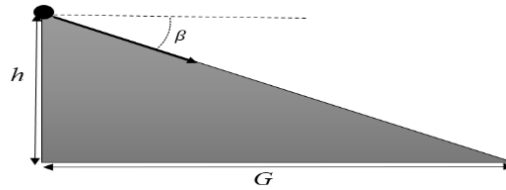
Figure IV. 5 Descent Parameters

The aircraft descent to **h**, with a distance **G**, and an angle β :

$$G = \frac{h}{tan\beta} = h\ \frac{C_L}{C_D} \qquad \text{with } \frac{C_L}{C_D} = 12 \qquad\qquad\qquad (IV.43)$$

$$G_{max} = h\ \left(\frac{C_L}{C_D}\right)_{max} \qquad\qquad\qquad (IV.44)$$

300 meters, the mini UAV distance is:

$$G_{max} = 300 \times 12 = 3600\ m$$

For a minimum glide angle:

$$tan\beta_{min} = \frac{1}{\left(\frac{C_L}{C_D}\right)_{max}} = \frac{1}{12} = 0.083 \qquad \beta_{min} = 4.76°$$

VII.   ENDURANCE AND RANGE

The main source of our design is a battery type 4S with 7600mA (**112.5 Wh**) and discharge C=5.

$two\ batteries\ power = 112.5 \times 2 = 225\ Wh$

The electronics system consume about $643.5\ Wh$ **APPENDIX D**

Endurance **E**:

$$E = \frac{battery\ Energie}{power\ required} = Wh/W \tag{IV.45}$$

$$E = \frac{225\ Wh}{643.7\ Wh} = 0.35\ h = 21\ min$$

The value of is 0.35 hr when the propulsion system consumes maximum power. At cruise, 60% power is required due to partial throttle management. The endurance is 33.6 minutes

The model range calculates from:

$$R = E.V_\infty \tag{IV.46}$$

$R = 33.6 \times 13{,}9 \times 60 = 28022.4\ m = 28.0224\ km$

This UAV flights to 5 km and came back, rest about 18022.4 km for loitering. If the UAV continue loitering with the same speed:

$$E_{loitre} = \frac{18022.4}{13.9 \times 60} = 21.6\ min$$

21.6 min is more than double time of 10 min required from **chapter II**.

VIII. GROUND RUN DISTANCE CALCULATION

Aircraft takeoff is mainly to see the distance of the aircraft during takeoff, the shorter distance means a better performance. Take off phases can be broken into:

- Accelerating ground-run.
- Rotation.
- Lift-off.
- Climb-out.

In general, the ground run distance calculations can illustrate the take-off characteristics of an aircraft. These following equations can be used to calculate acceleration and ground run distance. The calculation parameters include

- $C_L = 0.3681$
- $C_D = 0.406$
- $m = 4.5\ kg$
- Wing area: $S = 0.579\ m^2$
- Rolling friction coefficient: μ=0.04 (ref.01)
- The angle of attack of aircraft is zero.

It is assumed that acceleration is to vary linearly with V^2 up to V_{LOF}, the average acceleration may be calculated using the following equations.

$$S_G = \frac{1}{a} \int_0^{V_{LOF}} V dV = \frac{1}{a}\left[\frac{1}{2}V^2\right]_0^{V_{LOF}} = \frac{1}{2a}V_{LOF}^2 \tag{IV.47}$$

$$S_G = \frac{W}{2g}\frac{V_{LOF}^2}{\left[(T-\mu W)-(C_D-\mu C_L)\overline{q}S\right]} \quad at \quad V = \frac{V_{LOF}}{\sqrt{2}} \tag{IV.48}$$

After calculation:
✓ The take-off velocity:

$V_{LOF} = 1.1\ to\ 1.2\ V_{Stall}$ $\hspace{4cm}$ (IV.49)

$V_{LOF} = 11.64\ to\ 12.07\ m/s$

$$a = 2.40 m/s^2$$

$$So: \quad S_{LOF} = \frac{V_{LOF}^2}{2\times a} = \frac{(12.07)^2}{2\times 2.4} = 114.45 m$$

Conclusion:

Takeoff speed is: 12.07 m/s

Ground run distance is: 114m

IX. CONCLUSION

The mini UAV IAES-TAHI.A meets the requirements proposed in **chapter II**, the following table regroup the performance that can reach.

Table IV. 8 UAV IAES-TAHI.A performance results

Parameter	Result
Engine type	Sunny Sky 2216
Propeller type	APC 11×4.7
Battery type	Thunder power 2050 4S4P
V_{Stall}	10.59 m/s
V_{max}	18.7 m/s
$V_{\min drag}$	11.11 m/s
Rate of Climb R/C_{max}	2.710 m/S
Angle of rate of Climb max	14.117
Distance of descent	3600 m
Angle of descent	4.76°
Ground run distance	114 m
Endurance	33.6 min
Range	28022.4 m

Design a mini UAV IAES2018-TAHI.A open payload carrier is attained. Main specifications are established and set as following; cruising altitude above 300m, endurance of approximately half hour, range of 28 km, carrier payload of 400 grams, wing span of 2,477m. Takeoff gross weight estimation of 4.5 kg has also been performed during the initial steps of the design. In addition, sizing values created with a very interesting 2D mock up by CATIA software using specifics typical UAVs, various parameters are selected so as to obtain a convenient aerodynamic performance.

For instance, the choice of proper airfoil geometry and motors with in propeller, better weight estimation, center of gravity location and outer body sizing, aerodynamic performance parameters and coefficients have been executed delicately. After that, numerical simulation process based on ANSYS Fluent has been also applied.

CFD methods are based on employment of both Navier Stokes and turbulence equations in order to obtain rather realistic results. Various turbulence models are compared with results gathered in previous studies and Spalart Almars model fits best in computation time and accuracy consideration. Mesh independency test has guided the author to select an optimum mesh number and quality. In addition, effect of mesh number in convergence and stability has also been depicted. Meshing process is based on a compromise between computational time and accuracy. Converge criteria are also strictly followed in each calculation.

The study has revealed the employment of the aerodynamic sizing method, and might be enough and adequate to reach desired performance in such mini UAV design.

As perspective in a future work, study of stability and control will give much more detailed analysis, including application of flight quality of various parameters can be applied and discussed. Besides, manufacturing the model and achieve wind tunnel test or flight test will be a great success of this work.

Using CATIA software with Digital Mockup (DMU 2D Viewer) with respect of:

- Source picture confirmation
- Recognized one dimension from the 2D picture
- The dimensions must be on the same plane
- The measured dimensions must be in the same direction (case of picture stretching)
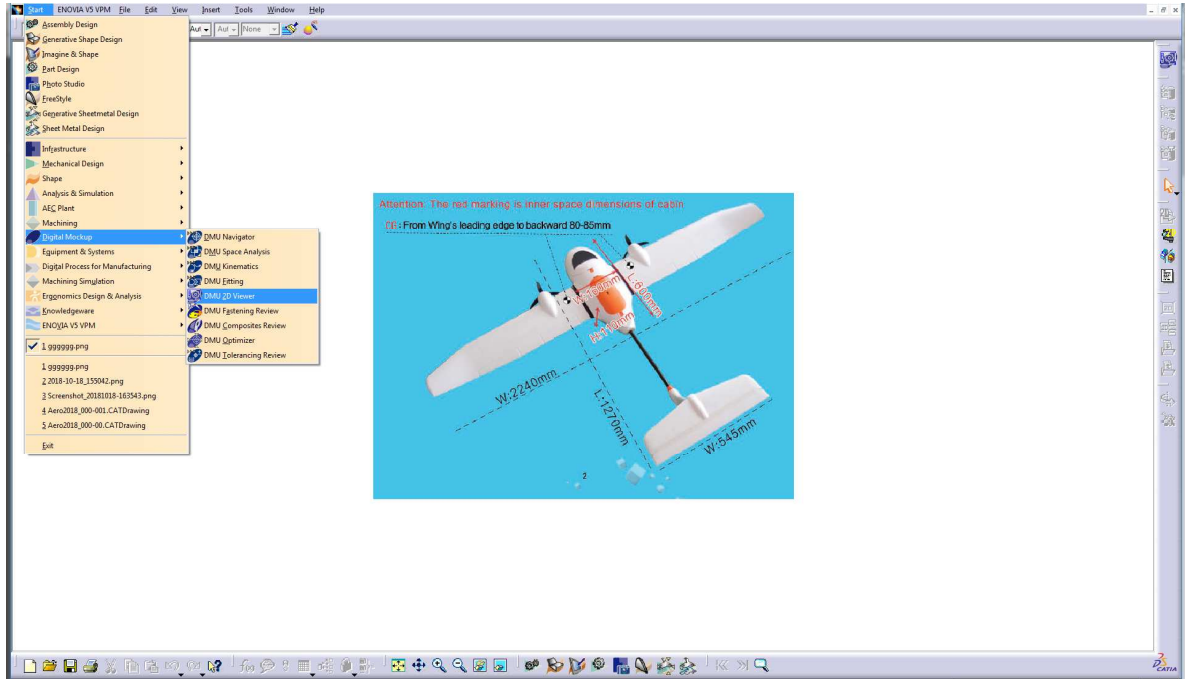
Calibration: Click to dialogue Calibration box
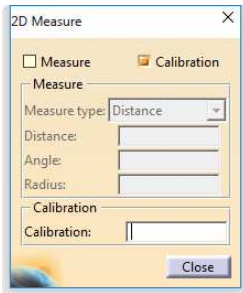
Measure: Click to dialogue measure box
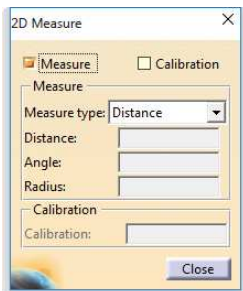
Example 01: Skywalker EVE-2000

1- **source**: EVE-2000 Installation Instruction
    (www.skywalkermodel.com key: skywalker_eve_2000_manual)
2- **recognized one dimension**: Horizontal tail span 454mm
3- **same plane**: Workshop table

Select the 2D calibration icon to calibrate the picture, after that select measure to recognize the others dimensions.
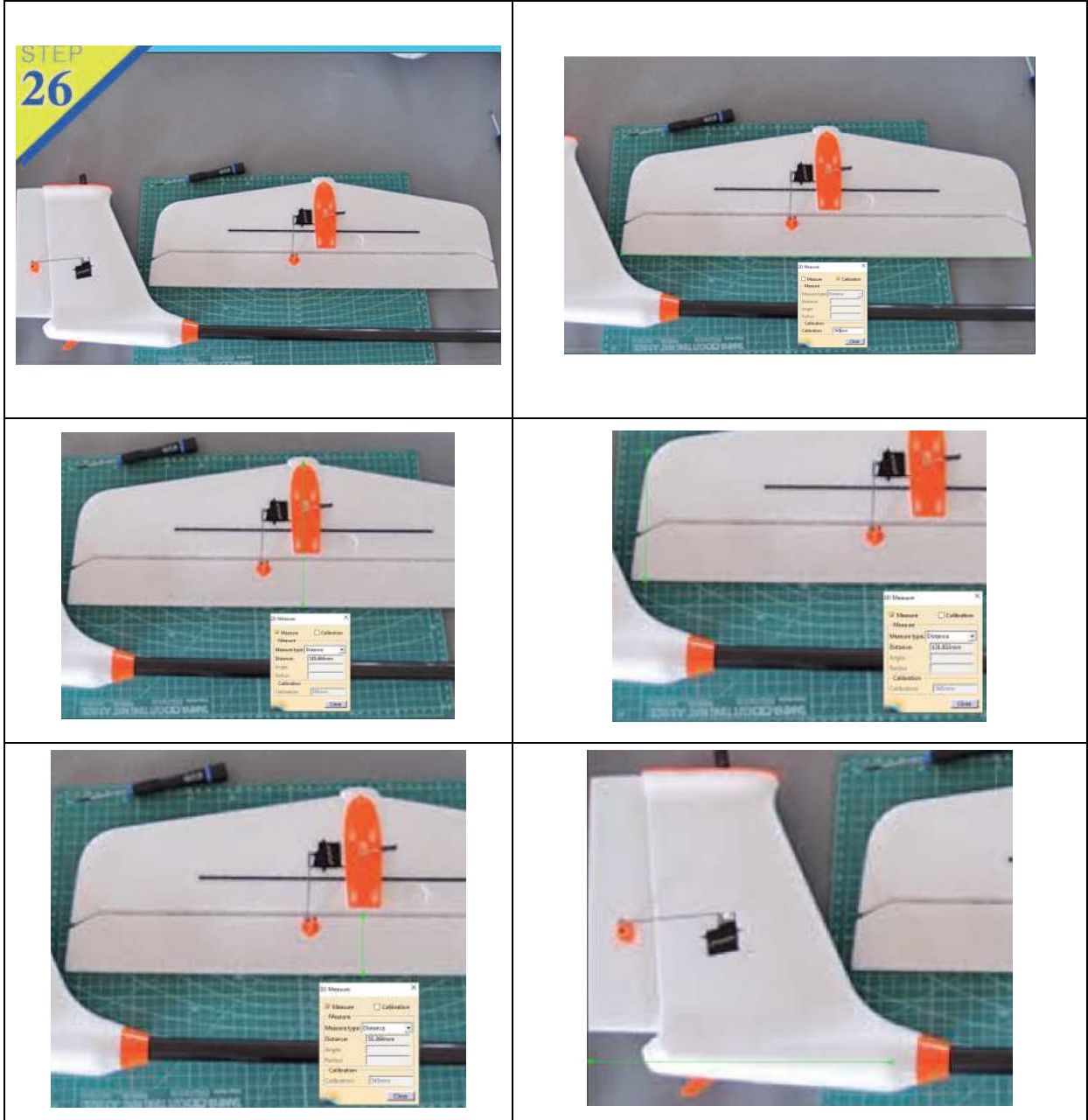
Example 02: Skyobserver (Zeta)

1- **source**: SKY OBSERVER ZETA SCIENCE
   ([777308800X1351914X4.pdf] key: SKY OBSERVER ZETA _manual)
2- **recognized one dimension**: wing span 2000 mm
3- **same plane**: 2D Drwing
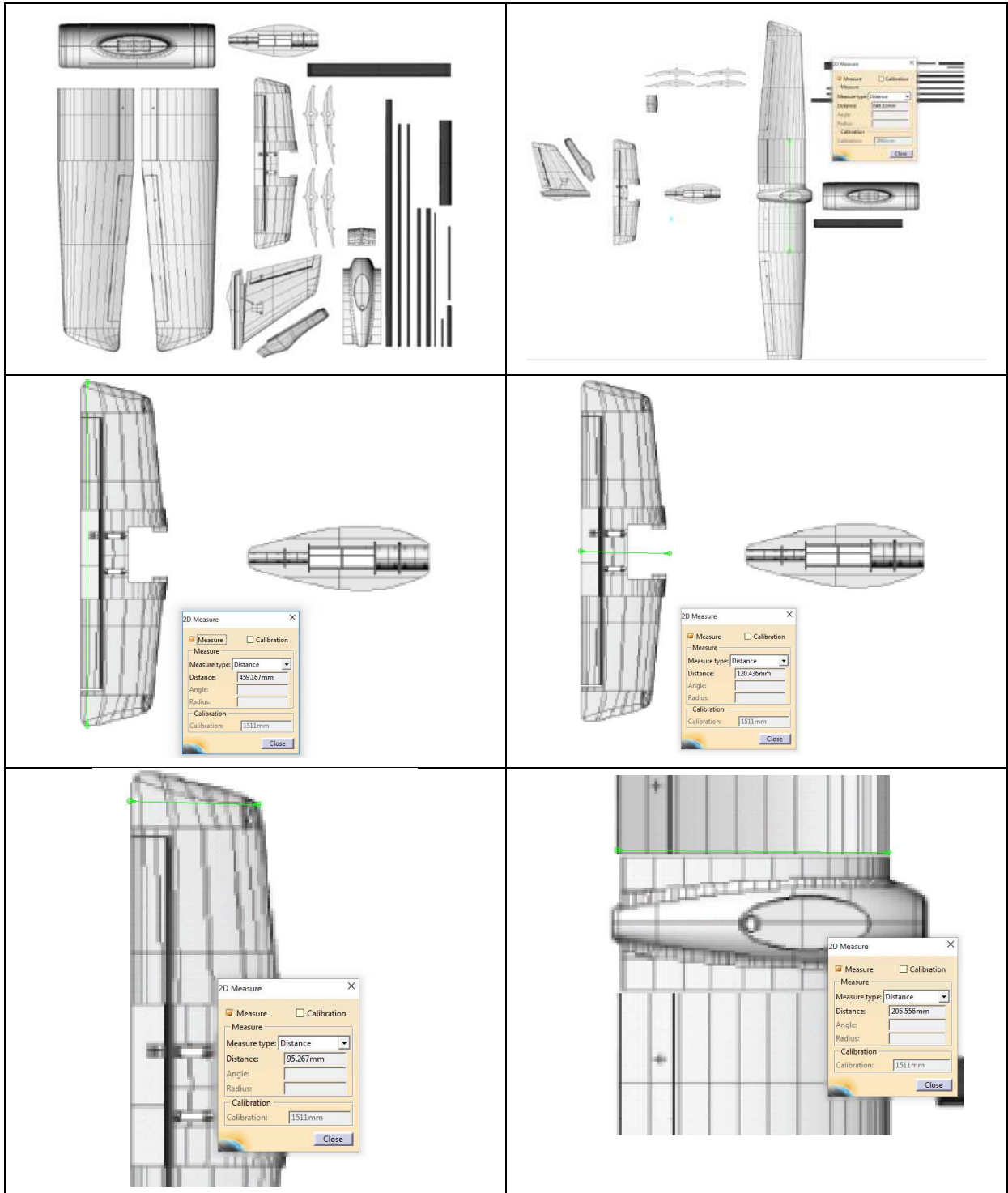
Select the 2D calibration icon to calibrate the picture, after that select measure to recognize the others dimensions.

Clark Y airfoil	
1.0000000 0.0005993	0.0005000 -.0046700
0.9900000 0.0029690	0.0010000 -.0059418
0.9800000 0.0053335	0.0020000 -.0078113
0.9700000 0.0076868	0.0040000 -.0105126
0.9600000 0.0100232	0.0080000 -.0142862
0.9400000 0.0146239	0.0120000 -.0169733
0.9200000 0.0191156	0.0200000 -.0202723
0.9000000 0.0235025	0.0300000 -.0226056
0.8800000 0.0277891	0.0400000 -.0245211
0.8600000 0.0319740	0.0500000 -.0260452
0.8400000 0.0360536	0.0600000 -.0271277
0.8200000 0.0400245	0.0800000 -.0284595
0.8000000 0.0438836	0.1000000 -.0293786
0.7800000 0.0476281	0.1200000 -.0299633
0.7600000 0.0512565	0.1400000 -.0302404
0.7400000 0.0547675	0.1600000 -.0302546
0.7200000 0.0581599	0.1800000 -.0300490
0.7000000 0.0614329	0.2000000 -.0296656
0.6800000 0.0645843	0.2200000 -.0291445
0.6600000 0.0676046	0.2400000 -.0285181
0.6400000 0.0704822	0.2600000 -.0278164
0.6200000 0.0732055	0.2800000 -.0270696
0.6000000 0.0757633	0.3000000 -.0263079
0.5800000 0.0781451	0.3200000 -.0255565
0.5600000 0.0803480	0.3400000 -.0248176
0.5400000 0.0823712	0.3600000 -.0240870
0.5200000 0.0842145	0.3800000 -.0233606
0.5000000 0.0858772	0.4000000 -.0226341
0.4800000 0.0873572	0.4200000 -.0219042
0.4600000 0.0886427	0.4400000 -.0211708
0.4400000 0.0897175	0.4600000 -.0204353
0.4200000 0.0905657	0.4800000 -.0196986
0.4000000 0.0911712	0.5000000 -.0189619
0.3800000 0.0915212	0.5200000 -.0182262
0.3600000 0.0916266	0.5400000 -.0174914
0.3400000 0.0915079	0.5600000 -.0167572
0.3200000 0.0911857	0.5800000 -.0160232
0.3000000 0.0906804	0.6000000 -.0152893
0.2800000 0.0900016	0.6200000 -.0145551
0.2600000 0.0890840	0.6400000 -.0138207
0.2400000 0.0878308	0.6600000 -.0130862
0.2200000 0.0861433	0.6800000 -.0123515
0.2000000 0.0839202	0.7000000 -.0116169
0.1800000 0.0810687	0.7200000 -.0108823
0.1600000 0.0775707	0.7400000 -.0101478
0.1400000 0.0734360	0.7600000 -.0094133
0.1200000 0.0686204	0.7800000 -.0086788
0.1000000 0.0629981	0.8000000 -.0079443
0.0800000 0.0564308	0.8200000 -.0072098
0.0600000 0.0487571	0.8400000 -.0064753
0.0500000 0.0442753	0.8600000 -.0057408

0.0400000 0.0391283	0.8800000 -.0050063
0.0300000 0.0330215	0.9000000 -.0042718
0.0200000 0.0253735	0.9200000 -.0035373
0.0120000 0.0178581	0.9400000 -.0028028
0.0080000 0.0137350	0.9600000 -.0020683
0.0040000 0.0089238	0.9700000 -.0017011
0.0020000 0.0058025	0.9800000 -.0013339
0.0010000 0.0037271	0.9900000 -.0009666
0.0005000 0.0023390	1.0000000 -.0005993
0.0000000 0.0000000	

APPENDIX B: Airfoils Coordinates

NACA 0012 Airfoil			
1.000000	0.001200	0.002013	-0.007875
0.997987	0.001482	0.008035	-0.015484
0.991965	0.002324	0.018019	-0.022768
0.981982	0.003712	0.031883	-0.029647
0.968117	0.005626	0.049516	-0.036024
0.950485	0.008035	0.070776	-0.041794
0.929224	0.010899	0.095492	-0.046859
0.904509	0.014167	0.123464	-0.051135
0.876536	0.017783	0.154469	-0.054564
0.845531	0.021678	0.188255	-0.057123
0.811745	0.025775	0.224552	-0.058831
0.775449	0.029992	0.263066	-0.059753
0.736934	0.034240	0.303488	-0.059998
0.696513	0.038425	0.345492	-0.059675
0.654509	0.042454	0.388740	-0.058782
0.611261	0.046236	0.432883	-0.057313
0.567117	0.049685	0.477568	-0.055281
0.522432	0.052722	0.522432	-0.052722
0.477568	0.055281	0.567117	-0.049685
0.432883	0.057313	0.611261	-0.046236
0.388740	0.058782	0.654509	-0.042454
0.345492	0.059675	0.696513	-0.038425
0.303488	0.059998	0.736934	-0.034240
0.263066	0.059753	0.775449	-0.029992
0.224552	0.058831	0.811745	-0.025775
0.188255	0.057123	0.845531	-0.021678
0.154469	0.054564	0.876536	-0.017783
0.123464	0.051135	0.904509	-0.014167
0.095492	0.046859	0.929224	-0.010899
0.070776	0.041794	0.950485	-0.008035
0.049516	0.036024	0.968117	-0.005626
0.031883	0.029647	0.981982	-0.003712
0.018019	0.022768	0.991965	-0.002324
0.008035	0.015484	0.997987	-0.001482
0.002013	0.007875	1.000000	-0.001200
0.000000	0.000000		

1- **STEP 1:** Depending what type of airplane you have, choose the thrust/weight ratio **g/W**:

Example 1: Scale flight , thrust/weight ratio = 0.70
Example 2: jet, Thrust/weight ratio = 1.5

Type of airplane	thrust-to-weight ratio	
Glider /trainer	0.35 to 0.55	
Scale Flight	0.60 to 0.70	
Sport and slow acrobatic	0.70 to 0.80	
Acrobatic fast	0.80 to 1.00	
Jets and 3D	1.00 to 2.50	

Table 1

Result: thrust/weight ratio

2- **STEP 2**: Calculate how much thrust airplane needs

The calculation is: with the weight of the plane and the thrust/weight ratio, find the necessary thrust:
Thrust = weight x thrust/weight ratio

Example 1: plane weight =1200 g
Thrust/weight ratio = 0.70
Thrust = 1200 x 0.70 = **840 g**

Example 2: plane weight = 1200 g
Thrust/weight ratio = 1.5
Thrust=1200 x 1.5 = **1800 g**

Result: UAV thrust (g)

3- **STEP 3:** Decide if the UAV is Fast or slow aircraft

Step 3- Decide if you want a fast or slow plane

The following table gives the values of air speed, according to the motor Kv (these values are for a fixed propeller pitch and a given battery voltage)
If you want a fast plane, choose high Kv
If you want a slow plane, choose low Kv

Kv	Air speed (Km/h)	Air speed (mph)	
1000	70	43	Table 2
2000	140	87	
3000	210	131	
4000	280	175	

Result: UAV *kv* **(kv)**

Choosing the Kv

Example 1: choose a low Kv because I need more Thrust than speed. A Kv around 1000 will do the job.

Example 2: I want speed on a jet, but I don't want ducted fan, so I choose a Kv around 2500.

4- **STEP 4:** Find the *power/thrust* ratio using *kv*

Table 3: Find the ratio Watts/grams or Watts/ounce

$$\frac{W}{g} = 0{,}17 * \frac{Kv}{1000} + 0{,}09$$

Kv	W/g	W/oz	Kv	W/g	W/oz	Kv	W/g	W/oz
			1700	0,379	10,73	3400	0,668	18,90
			1800	0,396	11,21	3500	0,685	19,39
			1900	0,413	11,69	3600	0,702	19,87
500	0,175	4,95	2000	0,430	12,17	3700	0,719	20,35
600	0,192	5,43	2100	0,447	12,65	3800	0,736	20,83
700	0,209	5,91	2200	0,464	13,13	3900	0,753	21,31
800	0,226	6,40	2300	0,481	13,61	4000	0,770	21,79
900	0,243	6,88	2400	0,498	14,09	4100	0,787	22,27
1000	0,260	7,36	2500	0,515	14,57	4200	0,804	22,75
1100	0,277	7,84	2600	0,532	15,06	4300	0,821	23,23
1200	0,294	8,32	2700	0,549	15,54	4400	0,838	23,72
1300	0,311	8,80	2800	0,566	16,02	4500	0,855	24,20
1500	0,345	9,76	2900	0,583	16,50	4600	0,872	24,68
1600	0,362	10,24	3000	0,600	16,98	4700	0,889	25,16
			3100	0,617	17,46	4800	0,906	25,64
			3200	0,634	17,94	4900	0,923	26,12
			3300	0,651	18,42	5000	0,940	26,60

Result: *power/thrust*

5- **STEP 5:** Calculate the needed power

Step 5: find the power/thrust ratio

With the Kv value, go to figure 1 or table 3 and find the **Power / thrust ratio**

Example 1: from table 3, with 1000 Kv, I find a power/thrust ratio = 0.26 W/g

Example 2: from table 3, with 2500 Kv, I find a power/thrust ratio = 0.515

Example 1: from step 2, I need 840 g of thrust, and using the power/thrust ratio= 0.26 calculate the needed power:

Power (W) = thrust x power/thrust ratio

Power (W) = 840 g x 0.26 W/g = **218 W**

Example 2: from step 2, I need 1800 g of thrust and using the power/thrust ratio = 0.515

Power (W) = 1800 g x 0.515 W/g = **927 W**

Result: Power (W)

6- **STEP 6:** Choose a motor

Example 1: we have 1000 Kv and 218 W (327 W)

Example 2: we have 2500 Kv and 927 W (1800 W)

Now, with this values we can go to manufacturer catalog and choose the motors.

I always recommend to choose higher values of the motor power (40 or 50 % more) to fly easily at 50 to 60 % throttle. The power value in parenthesis reflex this consideration.

The following motor is selected using the steps listed above.

Specifications of the electric motor

Synny Sky brushless outrunner motor

Motor:V2216-12		KV:800		
Technical Datas		**Recommended Prop(inch)**		
KV	800	Standard	3s-1045/1150 / 4S-8040/8050	Max thrust	3S-1150 / 4S-9047/90
Configu-ration	12N14P				
Stator Diameter	22mm				
STator Length	16m				
Shaft Diameter	3mm				
Motor Dimension(Dia. * Len)	Φ27.8×34mm				
Weight(g)	75				
Idle Current(10)@10v(A)	0.3				
No. of Cells(Lipo)	2-4S				
Max Continuous current(A)180S	17A				
Max Continuous Power(W)180S	180W				
Max. efficiency current	(5-15A)>80%				
internal resistance	175mΩ				

Tested with SunnySky motor 20A ESC

Prop	Volts (V)	Amps (A)	Watts (W)	Thrust (g)	Thrust (oz)	Efficiency (g/W)	Efficiency (oz/W
1047	7.4	5.8	42.92	510	17.99	11.88	0.42
	10	9.2	92	800	28.22	8.70	0.31
	11.1	10.5	116.55	960	33.86	8.24	0.29
11X7	7.4	5.8	42.92	510	17.99	11.88	0.42
	10	9.5	95	850	29.98	8.95	0.32
	11.1	10.9	120.99	1020	35.98	8.43	0.30
12X6	7.4	7.7	56.98	680	23.99	11.93	0.42
	10	12.1	121	1020	35.98	8.43	0.30
	11.1	13.8	153.18	1130	39.86	7.38	0.26

											SunnySky V2216-12 KV800 Brushless Motor Test Data		

Voltage (V)	Propeller (inch)	Throttle	Current (A)	Thrust (g)	RPM	Power (W)	Efficiency (g/w)	Temperature* (°C)	(°F)
11.1 3S	APC 10x3.8	50%	2.1	320	4131	23	13.7	47	117
		65%	3.5	440	4825	39	11.3		
		75%	5.9	600	5560	65	9.2		
		85%	7.8	690	5991	87	8.0		
		100%	10.6	830	6548	118	7.1		
	APC 11x4.7	50%	2.8	390	3840	31	12.5	50	122
		65%	4.5	500	4431	50	10.0		
		75%	7.4	700	5065	82	8.5		
		85%	9.9	820	5477	110	7.5		
		100%	12.4	960	5862	138	7.0		
	APC 12x3.8	50%	2.9	410		32	12.7	53	127
		60%	4.3	530		48	11.1		
		65%	5.7	590		63	9.3		
		75%	8.1	690		90	7.7		
		80%	10.1	800		112	7.1		
		85%	12	860		133	6.5		
		100%	14.5	980		161	6.1		
	ZX 12x3.8 Carbon Fiber	50%	2.4	360		27	13.5	48	118
		60%	3.5	470		39	12.1		
		65%	4.3	500		48	10.5		
		75%	6.1	620		68	9.2		
		80%	7.4	710		82	8.6		
		85%	9.3	800		103	7.7		
		100%	11.4	900		127	7.1		
14.8 4S	APC 9x4.7	50%	2.9	410		43	9.6	43	109
		60%	3.8	460		56	8.2		
		65%	4.4	530		65	8.1		
		75%	5.8	640		86	7.5		
		80%	6.9	710		102	7.0		
		85%	8.9	830		132	6.3		
		100%	10.5	930		155	6.0		
	APC 10x3.8	50%	3.3	480	5074	49	9.8	55	131
		65%	5.4	650	5837	80	8.1		
		75%	8.1	810	6514	120	6.8		
		85%	11.9	1030	7182	176	5.8		
		100%	15.2	1210	7750	225	5.4		
	ZX 10x3.8 Carbon Fiber	50%	3.2	430		47	9.1	51	124
		60%	4.3	550		64	8.6		
		65%	5.1	620		75	8.2		
		75%	7.2	760		107	7.1		
		80%	8.8	860		130	6.6		
		85%	10.9	970		161	6.0		
		100%	13.5	1120		200	5.6		
	ZX 11x4.7 Carbon Fiber	50%	3.9	530		58	9.2	85	185
		60%	5.5	680		81	8.4		
		65%	6.9	790		102	7.7		
		75%	9.5	910		141	6.5		
		80%	11	1020		163	6.3		
		85%	13.9	1150		206	5.6		
		100%	16.8	1320		249	5.3		

*Temperature was measured after 10 minutes full throttle load in a 25°C (77°F) environmen

Propeller APC 11×4.7

The propeller downloading from **UIUC Propeller Data Site**
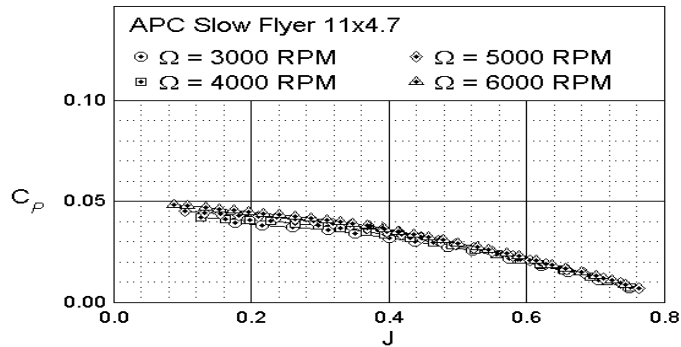
APC 11×4.7
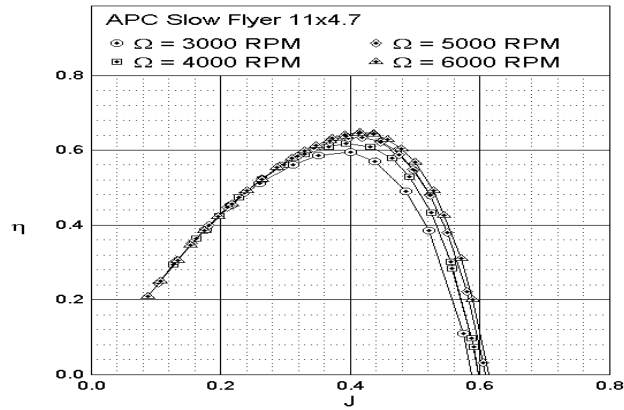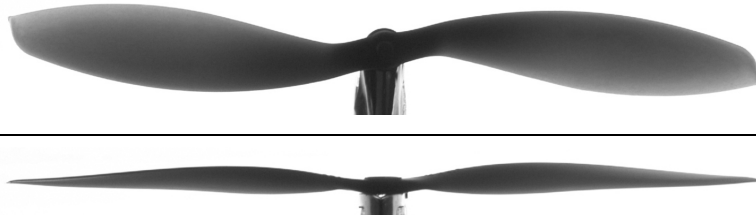
propeller 11×4.7 Efficiency curve vs advanced ratio
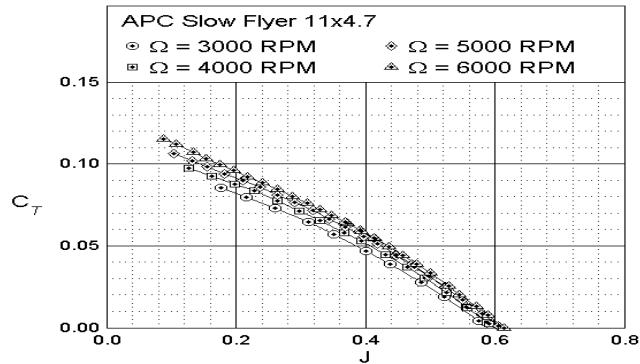
propeller 11×4.7 C_T curve vs advanced ratio

propeller 11×4.7 C_P curve vs advanced ratio

Electronic devices

	Part	Manufacturer	Ea	Type	Price/Ea ($)	Weight (grams)	Power consumption (Wh)
1	Rudder servo	Hitec	1	Mini	35	19	0.6
2	motor	Mini Motor	2	Sunny sky	~18	~75	~600
3	Controller	Jeti	1	Brushless	50	63.4	1.5
4	Elevator servo	Hitec	1	Mini	20	25	0.6
5	Aileron servo	Hitec	2	Flat	60	30	1.2
6	1200mA autopilot battery	E2TEK	1	Polymer	60	74	None
7	Thunder power battery (4s4p)	Thunder power	2	Polymer	600	1290	None
8	1000mW Video transmitter	Black widow AV	1	2.4GHz	250	50	30
9	Video transmitter antenna	customized	1	50ohm	5	7	None
10	Canon recorder & camera	Canon	1	500line progressive scan	600	300	2
11	CCD camera	Super circuit	1	400 line	200	61	1.2
12	Camera switching device	customized	1	Relay & Regulator	60	15	0.1
13	Krestel autopilot	Proceduer	1	Rabbit processor	565	55	3.6
14	GPS	Furuno	1	Micro	80	18	0.5
15	Regulator	Powerflite	1	6v	30	15	0.1
16	Video overlay device	UNAV	1	12v	120	33	0.8
17	Modem	Aeroccom	1	900Mhz	90	20	1.5
18	Modem antenna	customized	1	Dipole	10	9	None
19	Autopilot wire bundle	Proceduer	2	Micro	10	8	None
	Total				2863	2167.4	643.7

REFERENCES

[1]: Daniel P.Raymer "Aircraft design: A Conceptual Approach Fourth edition". AIAA Education Series by American Institute of Aeronautics & Astronautics 2006.

[2]: Mohammad H. Sadraey "AIRCRAFT DESIGN A Systems Engineering Approach". Daniel Webster College, New Hampshire, USA, Aerospace September 2012.

[3]: Memory: "Mini Unmanned Air Vehicle" Cairo university B.Sc graduation project 2008.

[4]: Memory: "Elaboration d'un modèle réduit en composite" IAES Blida.

[5]: K.P. Valavanis, G.J. Vachtsevanos (eds.) "Handbook of Unmanned Aerial Vehicles" Springer Science Business Media Dordrecht 2015.

[6]: John D. Anderson, Jr " Aircraft performance And design" University of Maryland 1999.

[7]: Kyuho Lee "Development Of Unmanned Aerial Vehicle (UAV) For Wildlife Surveillance "University of Florida 2004.

[8]: Memory: "Design in realization of a mini drone RB-50 for agriculture" IAES Blida (2012).

[9]: Eren Turanoğuz "Design of a Medium Range Tactical UAV and Improvement of its Performance by Using Winglets" Middle East Technical University (2015).

[10]: Memory: Abdulhakim Essari "Estimation of Component Design Weights in Conceptual Design Phase for Tactical UAVs" FACULTY OF MECHANICAL ENGINEERING, University of Belgrade 2015.

[11]: Memory: Chong Shao Ming "Unmanned Air Vehicle (UAV) Wing Design and Manufacture" Department of Mechanical Engineering, National University of Singapore.

[12]: Christopher A. Lyon, Andy P. Broeren, Philippe Giguere, "Summary of Low-Speed Airfoil Data". Ashok Gopalarathnam, and Michael S. Selig, Department of Aeronautical and Astronautically Engineering, University of Illinois at Urbana-Champaign, December 1997.

[13]: Theodore A.Talay "Introduction to the aerodynamics of flight" Langley Research Center, National Aeronautics and Space Administration, Washington, D.C. 1975.

Internet

[S1]: www.wikipédia.org

[S2]: UIUC airfoil data site

[S3]: www.hobbyking.com

[S4]: www.skywalker.com